

Hydrological
transport in the rock
formations
surrounding the host
rock

OPERA-PU-DLT621

Radioactive substances and ionizing radiation are used in medicine, industry, agriculture, research, education and electricity production. This generates radioactive waste. In the Netherlands, this waste is collected, treated and stored by COVRA (Centrale Organisatie Voor Radioactief Afval). After interim storage for a period of at least 100 years radioactive waste is intended for disposal. There is a world-wide scientific and technical consensus that geological disposal represents the safest long-term option for radioactive waste.

Geological disposal is emplacement of radioactive waste in deep underground formations. The goal of geological disposal is long-term isolation of radioactive waste from our living environment in order to avoid exposure of future generations to ionising radiation from the waste. OPERA (OnderzoeksProgramma Eindberging Radioactief Afval) is the Dutch research programme on geological disposal of radioactive waste.

Within OPERA, researchers of different organisations in different areas of expertise will cooperate on the initial, conditional Safety Cases for the host rocks Boom Clay and Zechstein rock salt. As the radioactive waste disposal process in the Netherlands is at an early, conceptual phase and the previous research programme has ended more than a decade ago, in OPERA a first preliminary or initial safety case will be developed to structure the research necessary for the eventual development of a repository in the Netherlands. The safety case is conditional since only the long-term safety of a generic repository will be assessed. OPERA is financed by the Dutch Ministry of Economic Affairs and the public limited liability company Electriciteits-Produktiemaatschappij Zuid-Nederland (EPZ) and coordinated by COVRA. Further details on OPERA and its outcomes can be accessed at www.covra.nl.

This report concerns a study conducted in the framework of OPERA. The conclusions and viewpoints presented in the report are those of the author(s). COVRA may draw modified conclusions, based on additional literature sources and expert opinions. A .pdf version of this document can be downloaded from www.covra.nl

OPERA-PU-DLT621

Title: Hydrological transport in the rock formations surrounding the host rock

Authors: J.R. Valstar & N. Goorden; Appendix 3 contributed by J.Hart & T.J. Schröder (NRG)

Date of publication: August 2017 (Revision 1)

Keywords: Groundwater model, travel time, repository, Boom Clay, geological scenarios

.....	1
Summary	1
Samenvatting	1
1. Introduction	2
1.1. Background	2
1.2. Objectives.....	2
1.3. Realization	2
1.4. Explanation contents	2
2. Geohydrological model	3
2.1. NHI model.....	3
2.2. Extensions of the groundwater model	4
2.2.1. Description of the geological formations in the range of the model extension	4
2.2.2. Conceptual model for transport routes	7
2.2.3. Model schematisation	8
2.2.4. Hydraulic conductivity	23
2.2.5. Faults.....	27
2.2.6. Boundary conditions.....	29
2.3. Results.....	29
2.3.1. Hydraulic heads.....	29
3. Pathline Analysis	32
3.1. Starting locations	32
3.2. Results.....	32
3.3. Selection of pathlines for transport calculations.....	36
3.4. Effect of transversal dispersion and transversal diffusion	37
4. Scenario calculations	40
4.1. Scenario descriptions.....	40
4.1.1. Normal evolution scenarios	40
4.1.2. Altered evolution scenarios	42
4.2. Model set up and results	43
4.2.1. Scenario 1: Moderate climate (present situation)	43
4.2.2. Scenario 2: Cold climate without ice cover (permafrost)	43
4.2.3. Scenario 3: Cold climate with ice cover (glaciation)	45
4.2.4. Scenario 4: Warm climate	46
4.2.5. Altered evaluation scenarios.....	49
4.3. Discussion	54
5. Parameter sensitivity scenarios	56
6. Conclusions and recommendations	60
6.1. Conclusions	60
6.2. Recommendations	61
7. References	62
8. Addendum	63
8.1. Introduction.....	63
8.2. Additional explanation and detailed output	63
8.2.1. Pathlines	63
8.2.2. Hydraulic conductivity Boom Clay	64
8.2.3. Interfaces Boom Clay - Overburden - Biosphere - Local well	67
8.2.4. Climate scenarios.....	71
8.3. Recommendations	73
8.4. Literature	73
Appendix 1: description of the geological formations near and below the base of the NHI model.....	74
Appendix 2: Method to calculate the horizontal and vertical hydraulic conductivity	79
Appendix 3: Conceptualization of the PA-model for the Overburden.....	83

A3.1 Introduction	83
A3.2 Elaboration of refinements of the current PA-model for the Overburden.....	83
A3.2.1 Pathlines	83
A3.2.2 Dispersion in the Overburden	84
A3.2.3 Flow rates.....	85
A3.2.4 Interface Boom Clay - Overburden.....	86
A3.2.5 Interface Overburden - Biosphere.....	86
A3.2.6 Climate scenarios.....	87
A3.3 Conclusions	88
A3.4 Literature	88

Summary

For research on the geological disposal of radioactive waste in the Boom Clay, the research program OPERA was set up. In this report, we describe the hydrological transport through the geological formations surrounding the Boom Clay up to the biosphere. The existing groundwater model NHI was extended in the vertical direction to include all relevant geological formations down to and even below the Boom Clay. The amount of nation-wide data for setting up the groundwater model was relatively limited and interpolation, extrapolation and simplifications were needed to obtain all model parameters. Therefore, all model results should be considered as a first estimate only.

Disposal of Dutch radioactive waste is not foreseen in the next decades and a preference for a host rock has not been made. As a start a geological disposal facility is assumed to be present at a depth of at least 500 metre within a Boom Clay formation of 100 metre in order to be able to make an assessment of a post-closure safety with this geological formation in a disposal concept. In order to make a representation of transport from such a facility, we calculated pathlines that started on locations where the Boom Clay has the following properties: thickness > 100 m and depth > 500 m. They were started at the top and bottom of the Boom Clay. The travel times of these pathlines vary between 1000 years to over 10 million years, with a majority of the travel times exceeding 100.000 years. Three pathlines (10, 50 and 90 percentile of the travel time distribution) were selected. Radionuclide migration along these pathlines is studied within another part of the OPERA program.

An uncertainty analysis with respect to the hydraulic conductivity of the Boom Clay and the future evolution (geological scenarios) is included.

Samenvatting

Voor onderzoek naar de geologische eindberging van nucleair afval in de Boomse Klei, is het onderzoeksprogramma OPERA opgezet. In dit rapport beschrijven we het hydrologische transport door de geologische formaties rondom de Boomse Klei tot aan de biosfeer. Het bestaande grondwatermodel NHI is in verticale richting uitgebreid met alle relevante geologische formaties tot aan en zelfs onder de Boomse Klei. De hoeveelheid data op landelijke schaal was relatief beperkt voor het opzetten van het grondwatermodel en interpolatie, extrapolatie en vereenvoudigingen waren nodig om alle modelparameters te verkrijgen. Daarom moeten alle modelresultaten vooral worden beschouwd als een eerste schatting.

De komende decennia wordt niet verwacht dat het Nederlands radioactief afval geborgen gaat worden en dat een keuze voor een gastgesteente wordt gemaakt. Om een veiligheidsberekening na het sluiten van de eindberging te kunnen maken is als start gekozen om de faciliteit te positioneren op 500 meter diepte in een kleilaag van 100 meter. Om een weergave van transport vanaf deze faciliteit voor de eindberging te verkrijgen, zijn stroombanen berekend vanaf locaties waar de Boomse Klei de volgende eigenschappen heeft dikte > 100 m en diepte > 500 m. Deze starten aan de boven- en onderkant van de Boomse Klei. De reistijden van deze stroombanen variëren van de 1000 jaar tot meer dan 10 miljoen jaar, met een meerderheid van de reistijden boven de 100.000 jaar. Drie van deze stroombanen (10, 50 en 90-percentiel van de reistijdenverdeling) zijn geselecteerd en in een ander deel van het OPERA-programma wordt het transport van radionucliden langs deze stroombanen doorgerekend.

Een onzekerheidsanalyse met betrekking tot de doorlatendheid van de Boomse Klei en de toekomstige evolutie (geologische scenario's) is uitgevoerd.

1. Introduction

1.1. Background

The five-year research programme for the geological disposal of radioactive waste - OPERA- started on 7 July 2011 with an open invitation for research proposals. In these proposals, research was proposed for the tasks described in the OPERA Research Plan.

1.2. Objectives

In this report, the approach and results of the research performed for task 6.2.1 with the following title in the Research Plan: “*Modelling approach for hydraulic transport processes*” are described.

The objective of this task is to describe the hydraulic transport starting at the interface of the potential host rock (i.e. the Boom Clay) towards the biosphere and to translate the hydraulic transport into a simplified transport model that is to be used for the radionuclide migration, task 6.2.2.

As no decision for the repository location has been made, we analysed transport starting on locations where the repository could be placed on a depth of at least 500 m with 50 m of Boom Clay both above and below the repository.

Moreover, the uncertainty with respect to future geological scenarios as described in task 4.1.2 has been considered.

1.3. Realization

The literature study and calculations presented in this report are performed by Deltares, with the exception of Appendix 3. Appendix 3 is written by NRG in consultation with Deltares.

1.4. Explanation contents

In chapter 2, the hydrological flow model is described, including the model input data and the model results. A pathline analysis for pathlines starting at the Boom Clay interfaces at potential repository locations is shown in chapter 3. Chapter 4 describes the impact of the geological scenarios on the transport calculations. Finally, conclusions are drawn and recommendations are given in chapter 5. In an addendum chapter, some additional results and explanations were added as they were needed to translate the results of this report into the work of the PA-model of Work Package 7.

2. Geohydrological model

The geohydrological model uses the existing national model NHI (Netherlands Hydrological Instrument) as a starting point. For most of the Netherlands, the depth of the NHI model does not reach the Boom Clay and its surrounding formations. Therefore the model has been extended in the vertical direction. The NHI model and the model extension are discussed in the next paragraphs.

2.1. NHI model

The NHI model is set up for addressing national water policy issues such as drought management, manure policy and climate variability. It combines saturated groundwater flow, unsaturated groundwater flow and surface water flow into a single model. The part of saturated groundwater flow of the model uses 7 model layers and has a horizontal resolution of 250 by 250 m. It can be run using daily time steps. The hydrological base of the NHI model is shown in Figure 2.1.

The new, extended model is a steady state model for the saturated groundwater only. Using the original NHI model, time-averaged boundary conditions for the new model have been obtained.

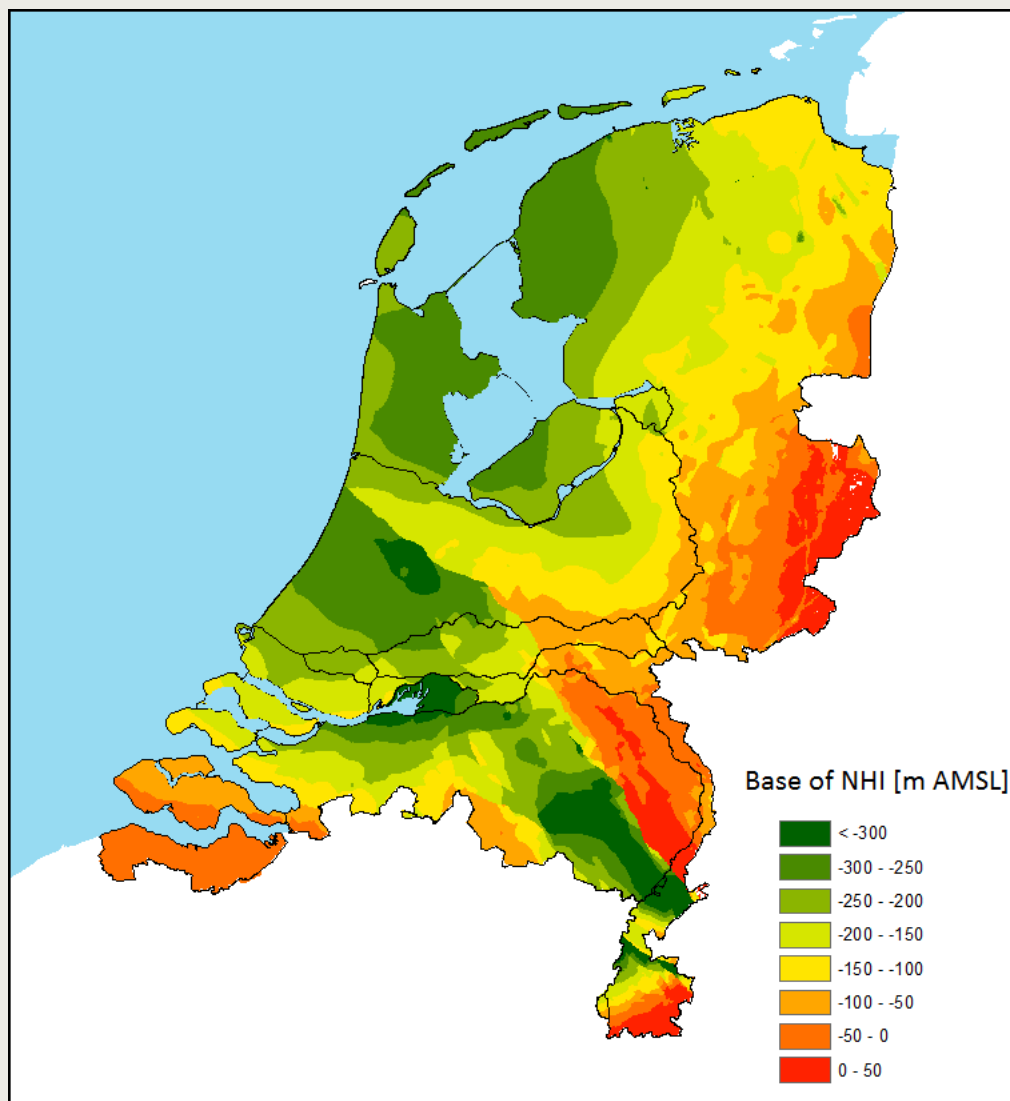


Figure 2.1 Base of the NHI model

The lowest model layer includes the Breda Formation in most of the Netherlands. For more information about the NHI, we refer to the documents that are available on <http://www.nhi.nu>.

2.2. Extensions of the groundwater model

In order to set up the deep groundwater flow model, information about position and properties of the geological formations is needed as well the boundary conditions that need to be supplied. The data about the deeper geological formations and the deeper groundwater is scarce. Therefore we provide an overview what data is directly available and motivate the choices we needed to make to set up the vertical extensions of the groundwater flow model.

TNO has several databases that provide gridded information about the geological formations.

1 DGM 1.3 (2009) (<http://www2.dinoloket.nl/nl/DINOMap.html>)

The Digital Geological Model contains the tops and bottoms of all geological formations in the Netherlands in the Quaternary and the Neogene.

2 REGIS II.1 (2008) (<http://www2.dinoloket.nl/nl/DINOMap.html>)

REGIS divides the geological formations into sandy and clayey layers and contains also hydrogeological properties such as hydraulic conductivity values. The most recent version covers fewer geological formations than DGM 1.3.

3 Oil and Gas portal (http://www.nlog.nl/en/pubs/maps/geologic_maps/NCP2.html)

The oil and gas portal contains for a number of deeper groups and formations information about the tops and the bottoms.

Finally, within the OPERA program, TNO has also collected information about the top and bottom of the Boom Clay and provides some information about the layers above and below the Boom Clay (Vis and Verweij, 2014). Together with a general description of the geological Formations and its members, we have been able to set up the groundwater flow model.

2.2.1. Description of the geological formations in the range of the model extension

The relevant geological formations for the model extensions are part of the North Sea Group. The North Sea Group is divided into the Upper North Sea Group, the Middle North Sea Group and the Lower North Sea Group. These groups are divided in several formations and some formations are subdivided in members. The most upper formation that is not fully present in the NHI model is the Maassluis Formation. Therefore the description of the geological layers relevant for the model extension starts with this formation.

Table 2.1 Relevant geological layers for the model extension

Group	Formation	Member
Upper North Sea Group	...	
	...	
	Maassluis	
	Oosterhout	
	Scheemda	
	Kieselooite	
	Breda	
	Inden	
	Ville	Heksenberg
Middel North Sea Group	Veldhoven	Someren
		Veldhoven Clay
		Voort
	Rupel	Steensel
		Rupel Clay ^a
		Vessem
	Tongeren	Goudsberg
		Klimmen
Lower North Sea Group	Dongen	Asse
		Brussel Sand
		Brussel Marl
		Ieper Clay
		Dongen Clay
		Basal Dongen Sand
		Basal Dongen Tuffite
	Landen	Reusel
		Landen Clay
		Gelinden
		Heers
		Swalmen

All formations are described in appendix A, using information available at the webpage <http://www.dinoloket.nl/nomenclator>.

Available grids

The following grids about the bases of some of these formations are available at present:

1 The bases of the Maassluis sand and Maassluis complex in some part of the country.

(source REGIS II.1)

2 The base of the Oosterhout Formation (source DGM1.3)

3 The base of the Kieselooite Formation (source DGM1.3)

4 The base of the Breda Formation (source DGM1.3)

5 The base of the Upper NorthSea Group (source :

http://www.nlog.nl/nl/pubs/maps/geologic_maps/NCP2.html)

^a The Rupel Clay Member is the official geological name for the Boom Clay

- 6 The base of the Lower NorthSea Group (source : http://www.nlog.nl/nl/pubs/maps/geologic_maps/NCP2.html)
- 7 The top of the Boom Clay (Opera Project WP 4: Vis and Verweij, 2014)
- 8 The Base of the Boom Clay (OPERA Project WP 4: Vis and Verweij, 2014)

Moreover, Vis and Verweij (2014) provide a map indicating which layers overlay the Boom Clay, see Figure 2.2 and a rough indication of the thickness of the Vessem Member that underlays the Boom Clay, see Figure 2.3.

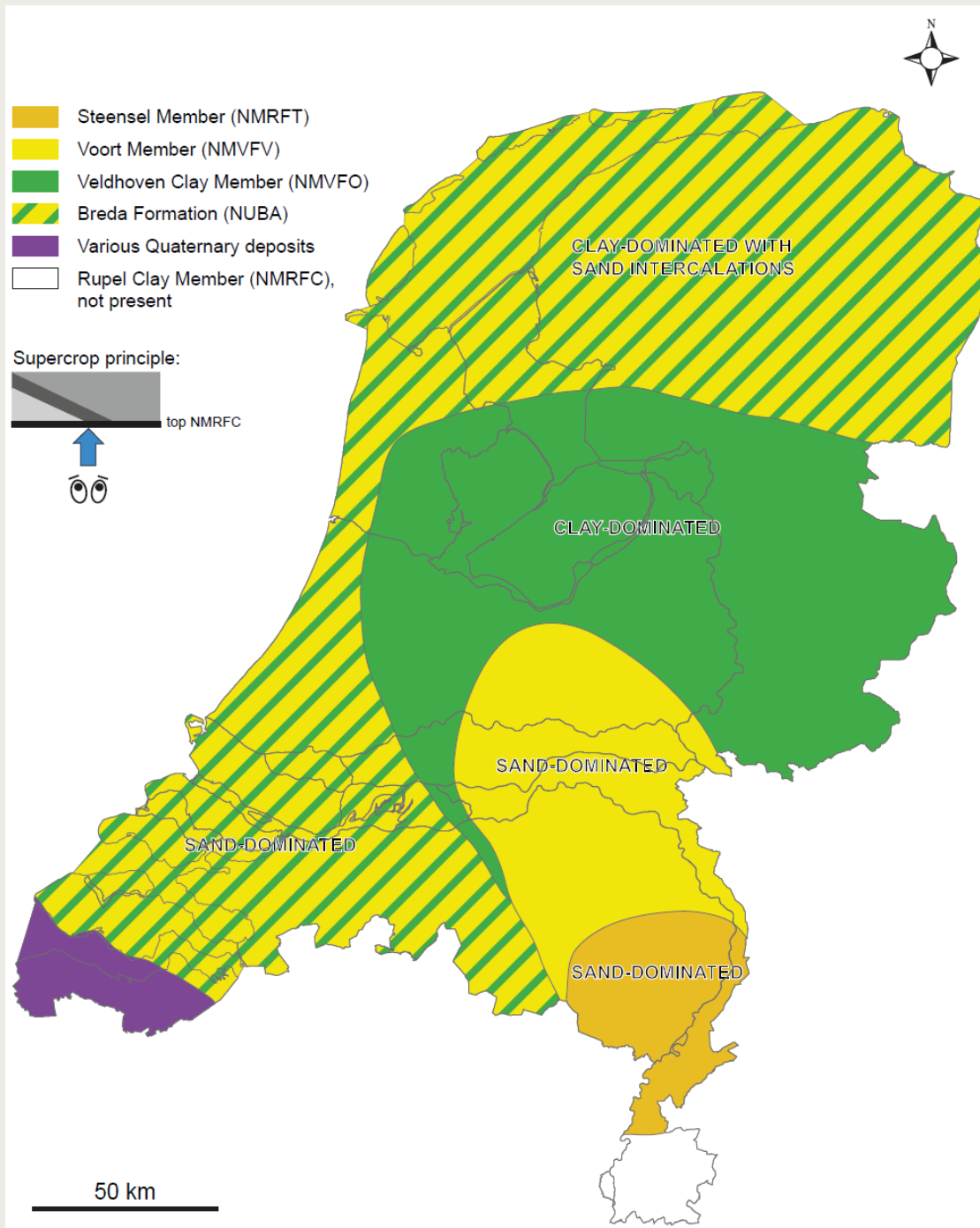


Figure 2.2 Information of layer overlaying the Boom Clay; after *Vis en Verweij(2014)*

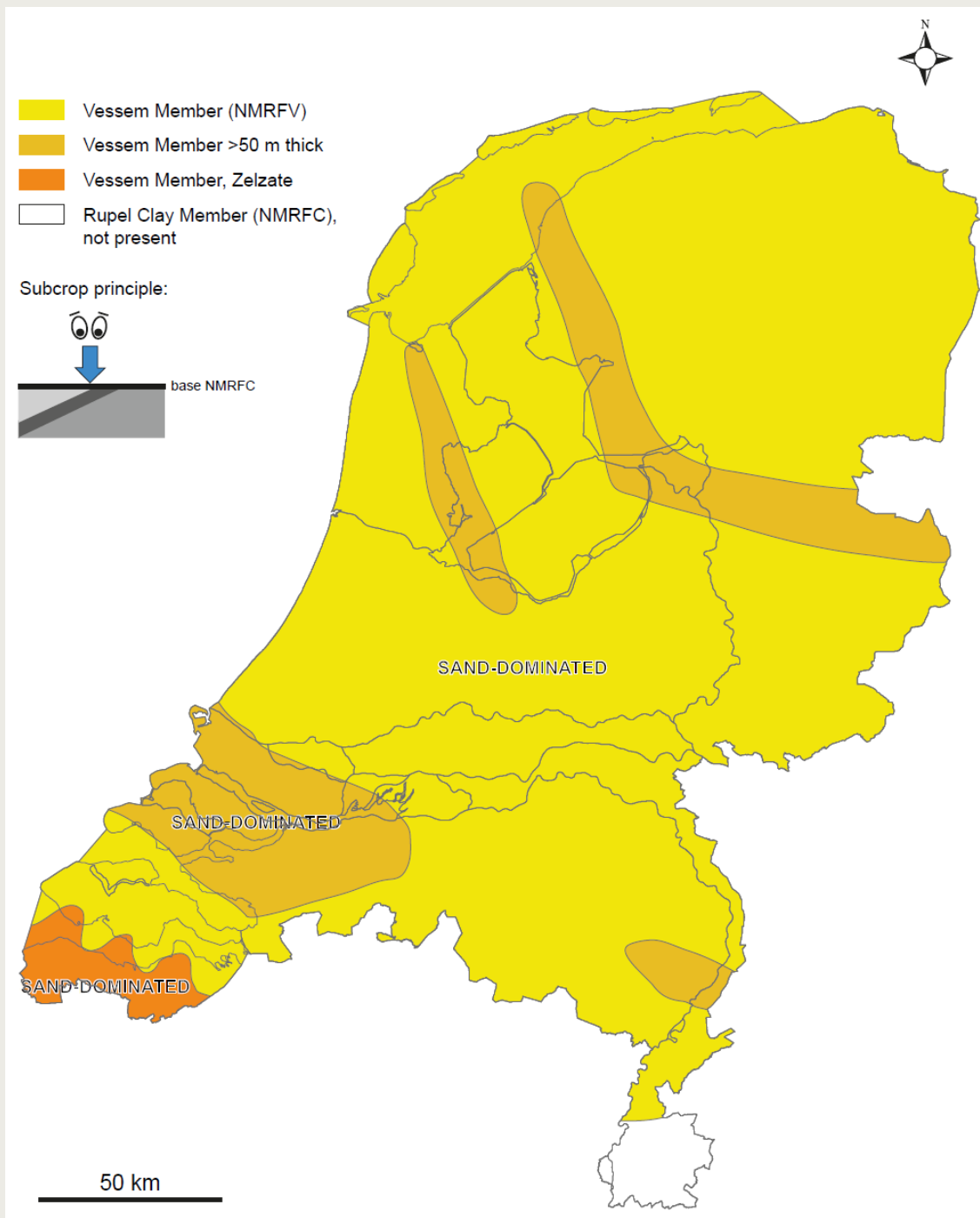


Figure 2.3 Rough indication of the thickness of the Vessem Member, directly underneath the Boom Clay; after *Vis en Verweij (2014)*

Altogether, it is clear that for many formations and formation members, information about the bases on the national scale is not available. Moreover, most of the various Formations and Formation members do not consist of a single lithology, but show sequences of more and less permeable layers.

In Section 2.2.3 it is described how the lack of data was dealt with in constructing the extension of the NHI model.

2.2.2. Conceptual model for transport routes

In order to make decisions how to set up the model discretization, it is important to have an idea about how the nuclides can migrate towards the surface, when they have diffused

out of the Boom Clay. Both the transport routes starting on top and underneath the Boom Clay are considered.

Flow routes starting underneath the Boom Clay

If the nuclides leave the Boom Clay at its base, it enters the sandy Vesseem Member. This member is present all over the Netherlands with the exception of South Limburg. This member crops out in Belgium and Germany, where groundwater recharge will directly feed this aquifer. Beneath the Vesseem Member, the clayey Ieper Member and the Dongen Clay Member are also present underneath almost all of the Netherlands and together they form a thick, relatively impermeable zone. In between the Vesseem Member and the Ieper and Dongen Clay Members, the Asse, Brussels Sand and Brussels Marl Member are present in part of the country. The Brussels sand Member is overlain mostly by the clayey Asse Member. Altogether, it is to be expected that main horizontal flow mechanism underneath the Boom Clay is within the Vesseem member. It is fed by groundwater recharge in the neighbouring countries, directly into that aquifer. Probably most of this recharge water is discharged into local surface water. The remaining part will flow underneath the Boom clay. Upward flow may occur, predominantly in regions where the Boom Clay is absent or less thick. In infiltration areas, the Vesseem Member can also be fed by downward flow through the Boom Clay.

Flow routes starting at the top of the Boom Clay

In the southern parts of the Netherlands, nuclides that exit the Boom Clay at its top will enter the sandy aquifers of the Steensel or Voort Members or the sandy part of the Breda Formation. Transport in these aquifers are probably also driven by direct groundwater recharge in this aquifers in Belgium and of Germany.

In the northern part of the country, the nuclides will enter the Veldhoven Clay Member of the clay deposits of the Breda Formations. Here, advection may still be an extremely slow process and upward diffusion may still be the most dominant process, until nuclides reach more permeable aquifers.

2.2.3. Model schematisation

Considering the described flow routes in the previous section and the availability of data it is decided to distinguish the following model layers in the extension of the groundwater flow model. From top to bottom:

- 1 Layers present in the original NHI model
- 2 Maassluis sand and Maassluis complex (if not present in NHI model)
- 3 Oosterhout (if not present in NHI model)
- 4 Breda Formation (from REGIS/ DGM and if not present in NHI model)
- 5 Veldhoven Formation: Someren Member
- 6 Veldhoven Formation: Veldhoven Clay Member
- 7 Veldhoven Formation: Voort Member
- 8 Rupel Formation: Steensel Member
- 9 Rupel Formation: Boom Clay
- 10 Rupel Formation: Vesseem Member
- 11 Lower North Sea group

The base and thickness of these formations are derived as follows:

- Maassluis sand, Maassluis Complex and Oosterhout. The top and bottoms of these formations and their horizontal and vertical hydraulic conductivity are obtained from REGIS II.1. Only where these formations are not fully represented by the NHI model, they are added to the model, otherwise their top and bottoms are set equal to the base of the NHI model.

- Breda Formation from REGIS if not present in NHI model
 Part of the Breda formation that is not included in NHI is present in REGIS II.1. The information in REGIS includes its top and bottom, lithology and hydraulic conductivity.
 Other parts of the Breda Formation are not described within REGIS II.1. The digital geological model DGM version 1.3 continues to the bottom of the Breda Formation. No direct description about the division in clay and sand layers is present in DGM. However, we presume that the choice of the base of REGIS II.1 is derived from a less permeable clay layer. Moreover, Vis and Verweij (2014), see also Figure 2.2, report that the layer on top of the Boom clay is the Breda formation for the northern and south-western part of the Netherlands, where the northern part is clay dominated and the south-western part is sand dominated. Based on this subdivision we make the assumption that the remaining part of the Breda Formation (i.e. the part not described in REGIS II.1) in the northern part of the Netherlands is clay dominated, whereas the remaining part in the southern part of the Netherlands is sand dominated for its lower half and clay dominated for its upper half. This information about the division of sand and clay layers within the Breda Formation is used during the upscaling of the hydraulic conductivity of the Breda Formation.
- Veldhoven Formation: Someren Member, Veldhoven Clay Member and Voort Member and the Rupel Formation: Steensel Member
 The locations where these members are present can be obtained from Figure 2.2. In the green-yellow striped area, i.e. where the Rupel Formation is overlain by the Breda Formation or Holocene layers, the members of the Veldhoven Formation and the Steensel Member are not present. Where the area is green, only the Veldhoven clay member is present, as the Someren Member that can be on top of the Veldhoven Clay Member is reported to be present in the Roer Valley Graben only, see Appendix A. The thickness of the Veldhoven Clay Member can be obtained by subtracting the base of the Upper North Sea Group from the top of the Boom Clay. For the remaining area, the same procedure gives the summed thickness of the Steensel member and the three Members of the Veldhoven Formation. The thickness of each member is estimated using interpolated values of the fraction of this member in the combined thicknesses. This interpolation is based on a) a number of well descriptions, available in the individual member description on webpage <http://www.dinoloket.nl/middle-north-sea-group-nm> and summarized in Table 2.2; their location is shown in Figure 2.4, b) the knowledge that the Steensel member is absent outside the orange region in Figure 2.2 and c) the knowledge that the Voort Member rapidly thins in Northern direction, see Appendix A.

Table 2.2 Thickness and fraction of thickness of the members in the Middle North Sea Group above the Boom Clay as used in the interpolation

well name	thickness (m)				Fraction			
	Someren	Veldhoven Clay	Voort	Steensel	Someren	Veldhoven Clay	Voort	Steensel
Asten-1	85	136	212	17	0.189	0.302	0.471	0.038
Veldhoven-1	75	112	56	19	0.286	0.427	0.214	0.073
Broekhuizenvorst 52E/114	21	2	164.5	5.5	0.109	0.010	0.852	0.028
Region								
northern edge of yellow region in Figure 2.2			0				0	
outside orange region in Figure 2.2				0				0



Figure 2.4 Locations of deep boreholes; data from boreholes Veldhoven-1, Asten-1 en Broekhuizenvorst 52E/114 are used in the interpolation (source: https://www.dinoloket.nl/sites/www.dinoloket.nl/files/file/Tertiary_Location_map.pdf).

Within the different regions of Figure 2.2, the fractions are interpolated using the point values in the table, while the northern edge of the yellow region is replaced by a number

of points in which the fraction of the Voort member is set to zero (simulating the abovementioned rapid thinning of the Voort member in the northern direction). After the interpolation of the fractions, the fraction of the Steensel Member outside the orange region is set to zero.

The remaining fractions are multiplied by a correction factor to make the sum of the fractions in each model cell equal to 1. Using the corrected fraction and the thickness of the sum of the four layers, the thickness of each of the four individual Members is obtained.

- Boom Clay
The grid data of the top and bottom of the Boom Clay is obtained digitally from the Work Package 4 of OPERA, which is reported in Vis and Verweij (2014).
- Vesseem member
In Figure 2.3, a rough indication of the thicknesses of the Vesseem Member is given. It is present in the entire onshore area of the Netherlands. The Vesseem Member is continuously present underneath the Boom Clay and it is considered well permeable so it provides a transport route for water underneath the Boom Clay. The model thickness of this layer is estimated from Figure 2.3 with values of 50 m in the light orange and values of 25 m elsewhere.
- Lower North Sea Group
The thickness of the Lower North Sea Group is obtained by subtracting the base of the Lower North Sea Group from the base of the Vesseem Member. As there is little direct information available on the thickness of the Dongen and the Landen Formation and their Members, it was decided to model these formations within one model layer.

The top, bottoms and thicknesses of all the layers in the model extension are given in Figure 2.5 to Figure 2.14.

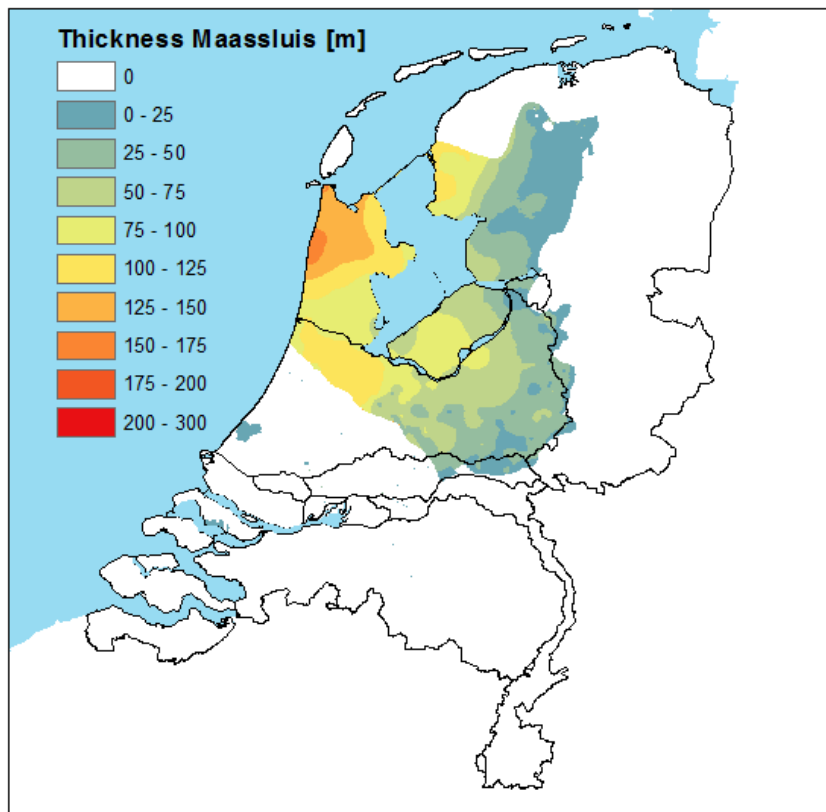
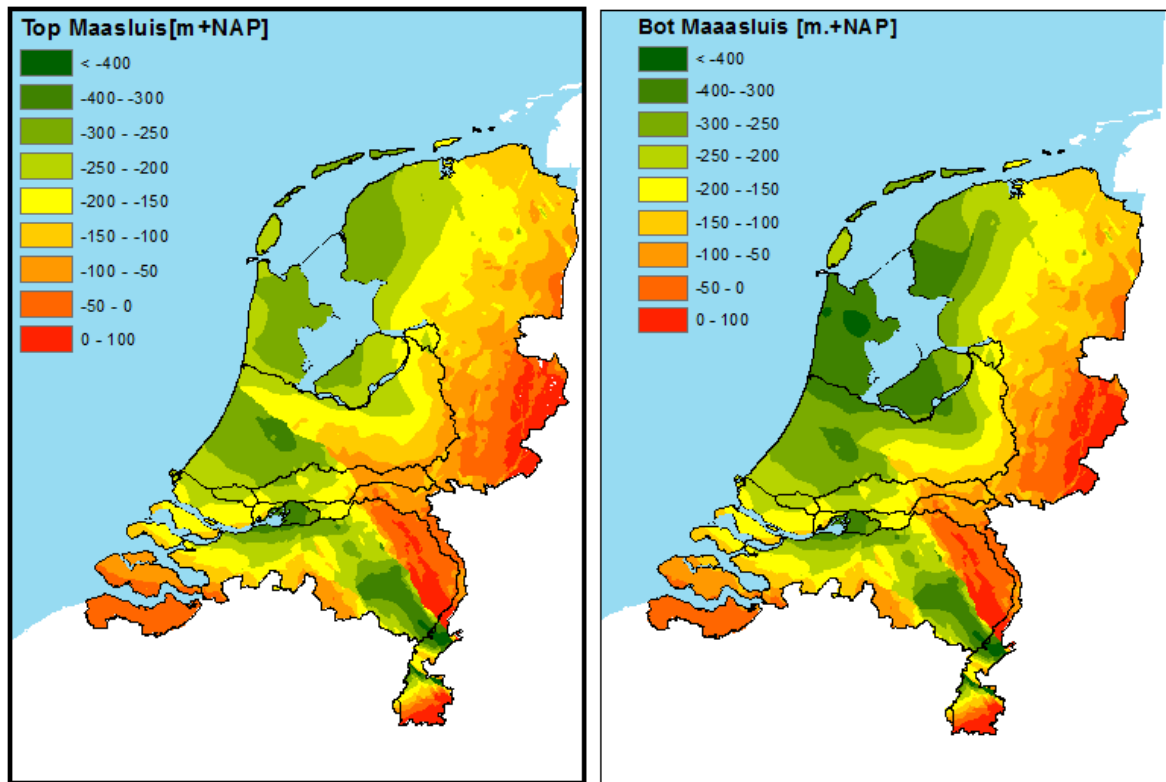


Figure 2.5 Top, bottom and thickness of the Maasvluis Formation within the model extension

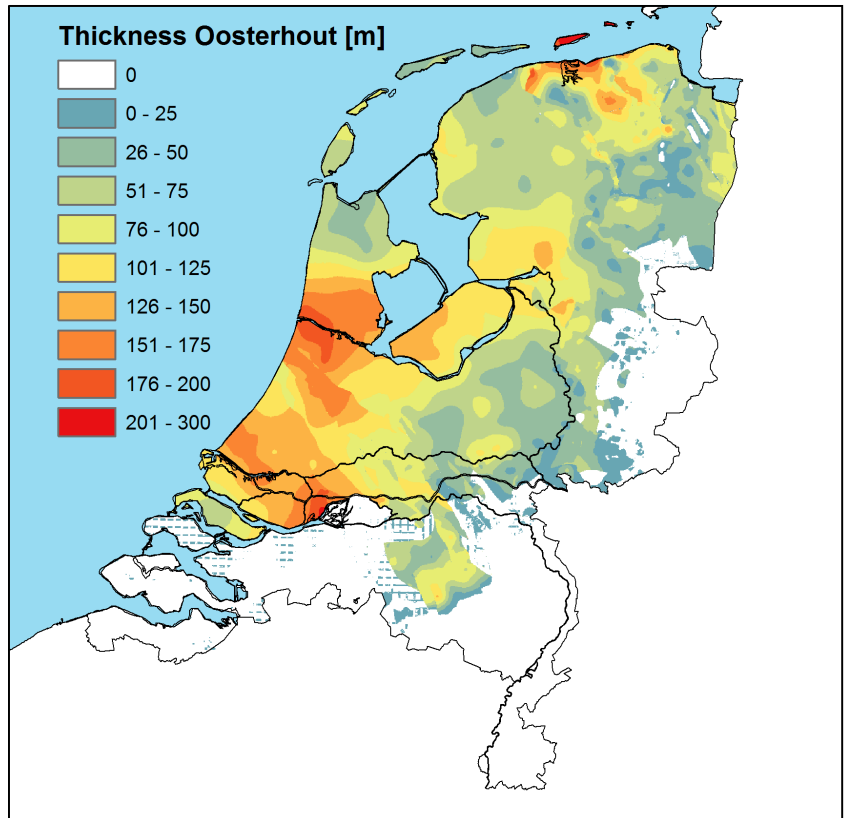
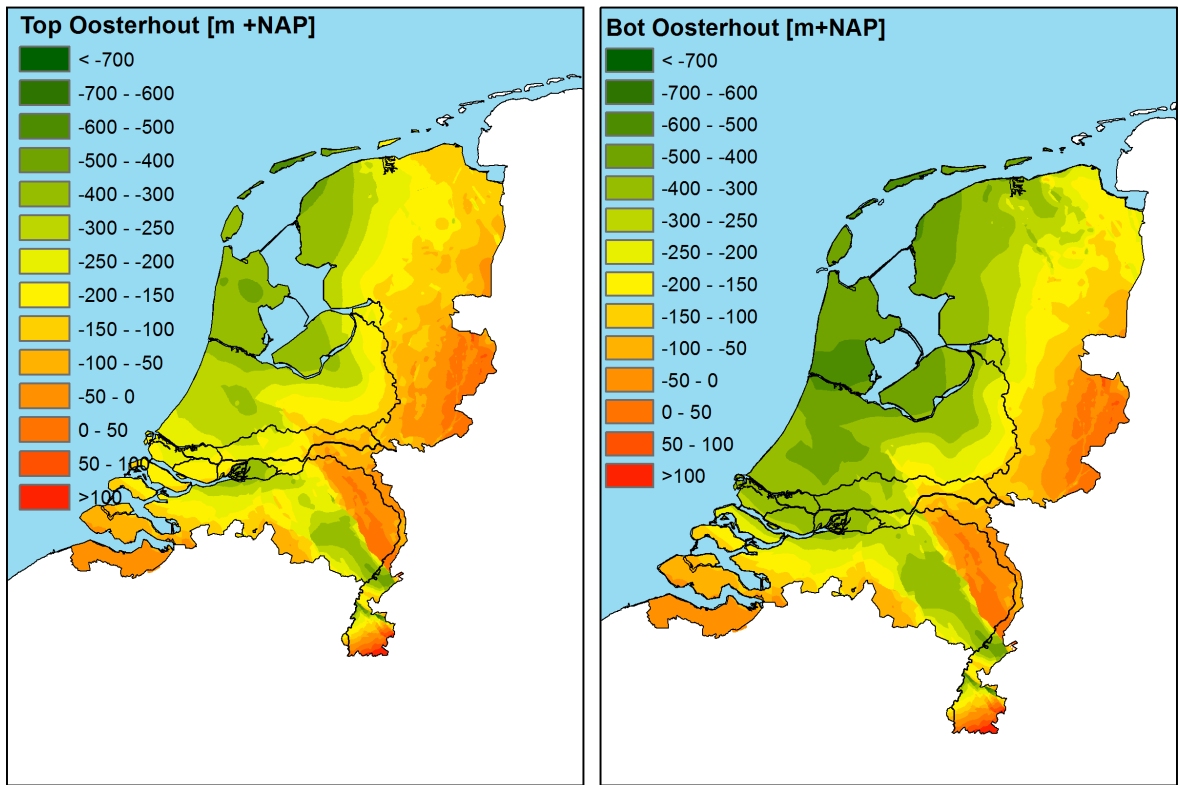


Figure 2.6 Top, bottom and thickness of the Oosterhout Formation within the model extension

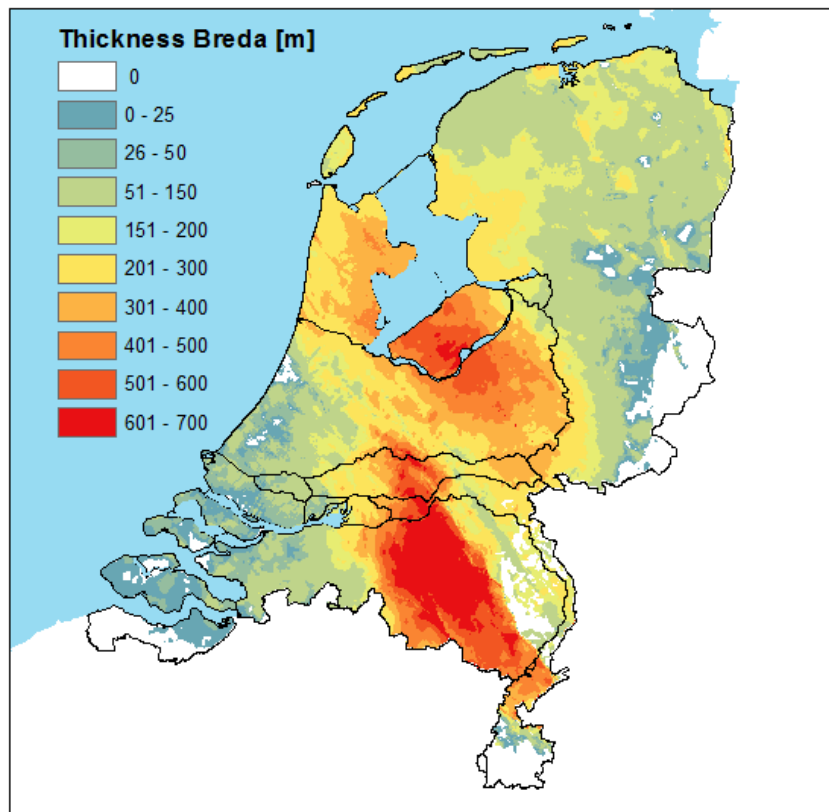
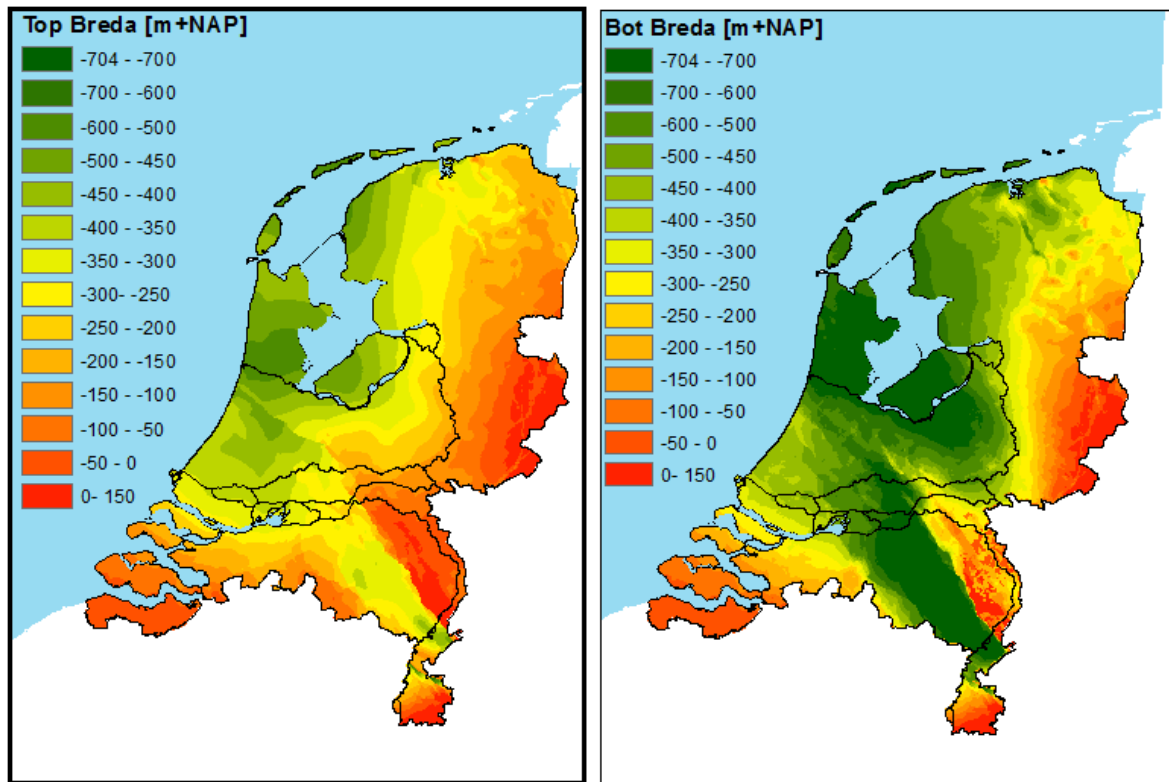


Figure 2.7 Top, bottom and thickness of the Breda Formation within the model extension

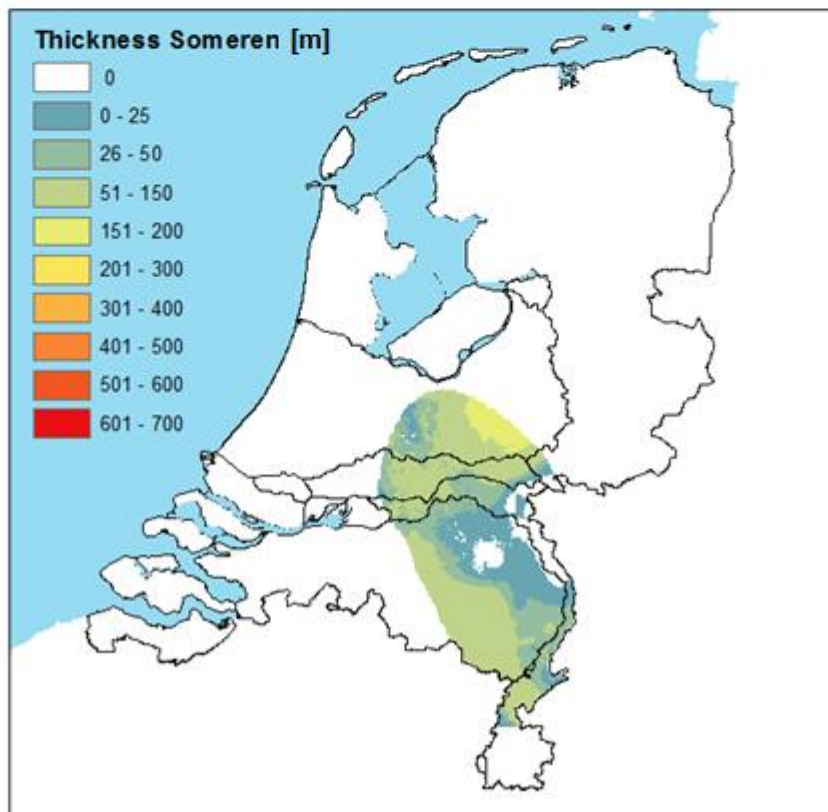
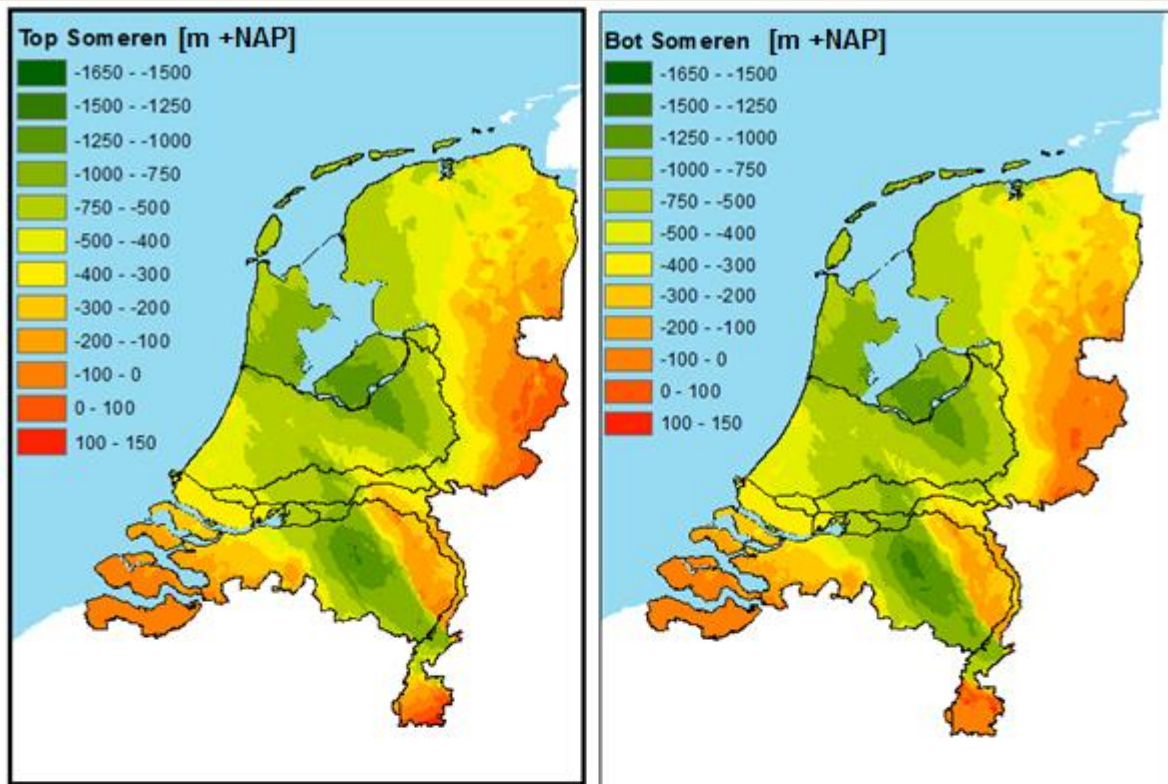


Figure 2.8 Top, Bottom and thickness of the Someren Member

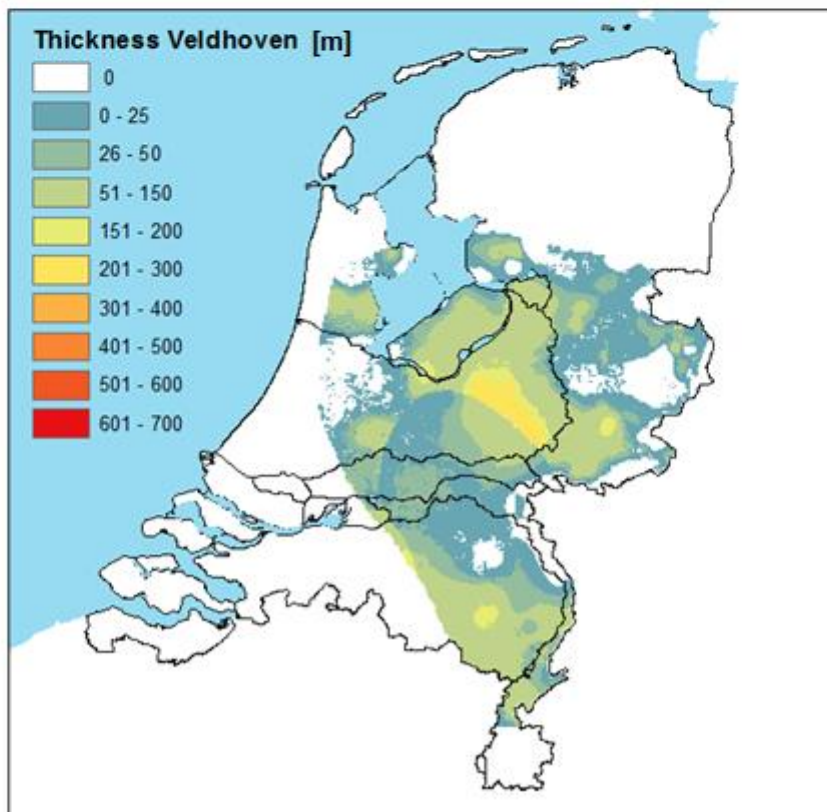
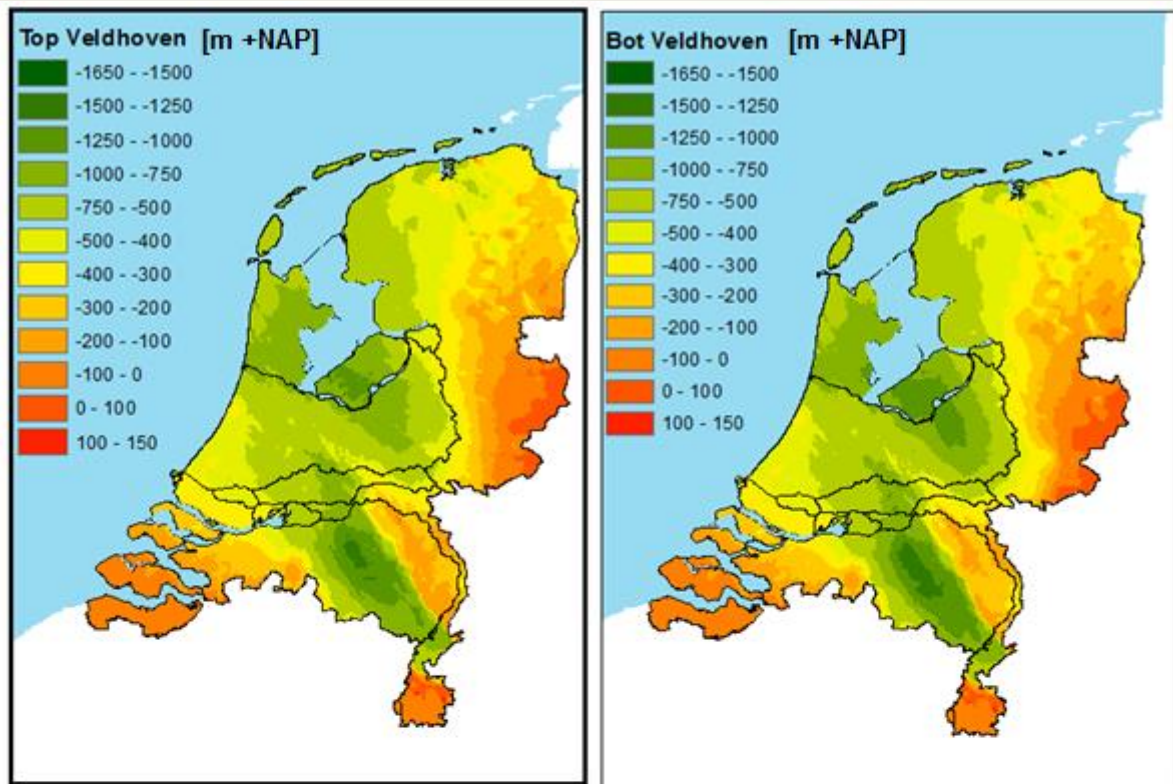


Figure 2.9 Top, bottom and thickness of the Veldhoven Clay Member

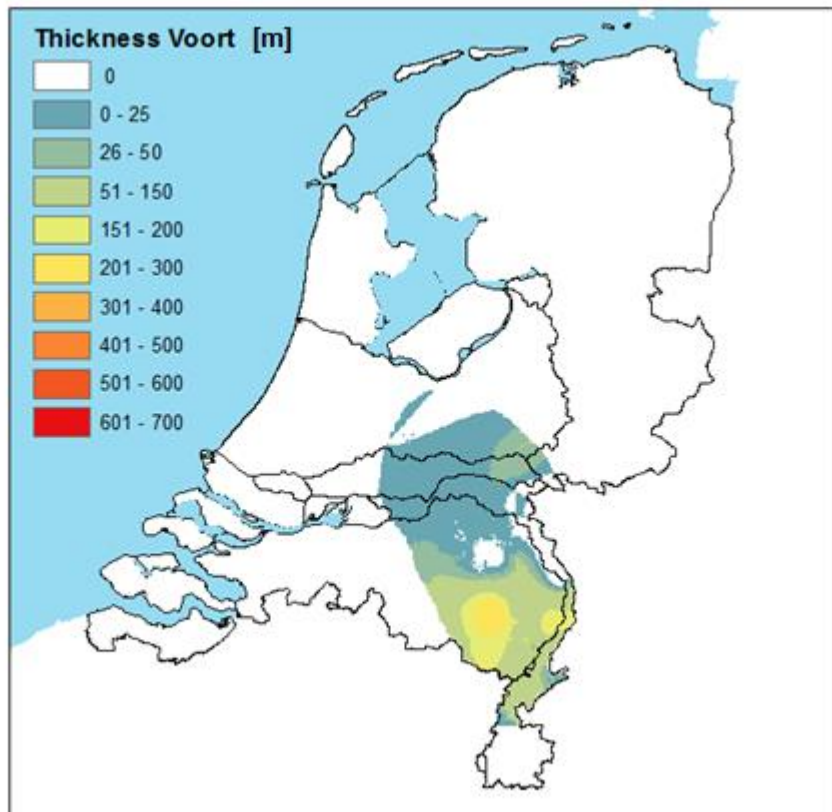
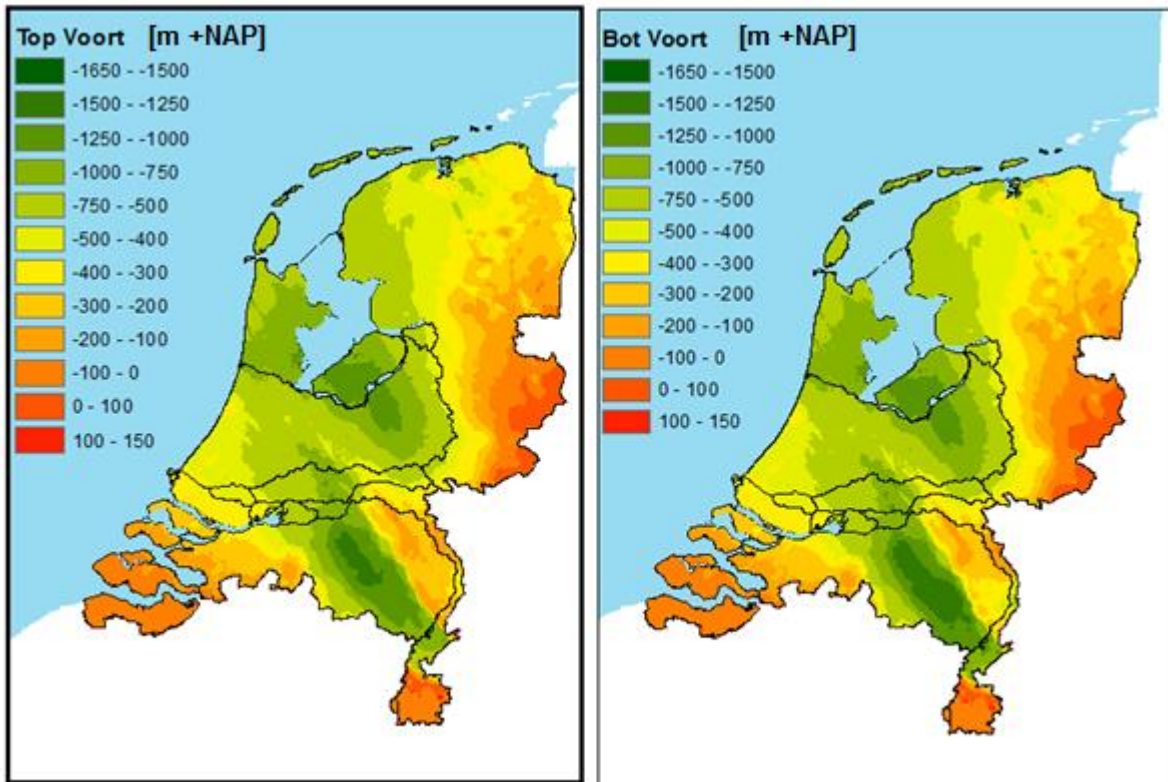


Figure 2.10 Top, bottom and thickness of the Voort Member

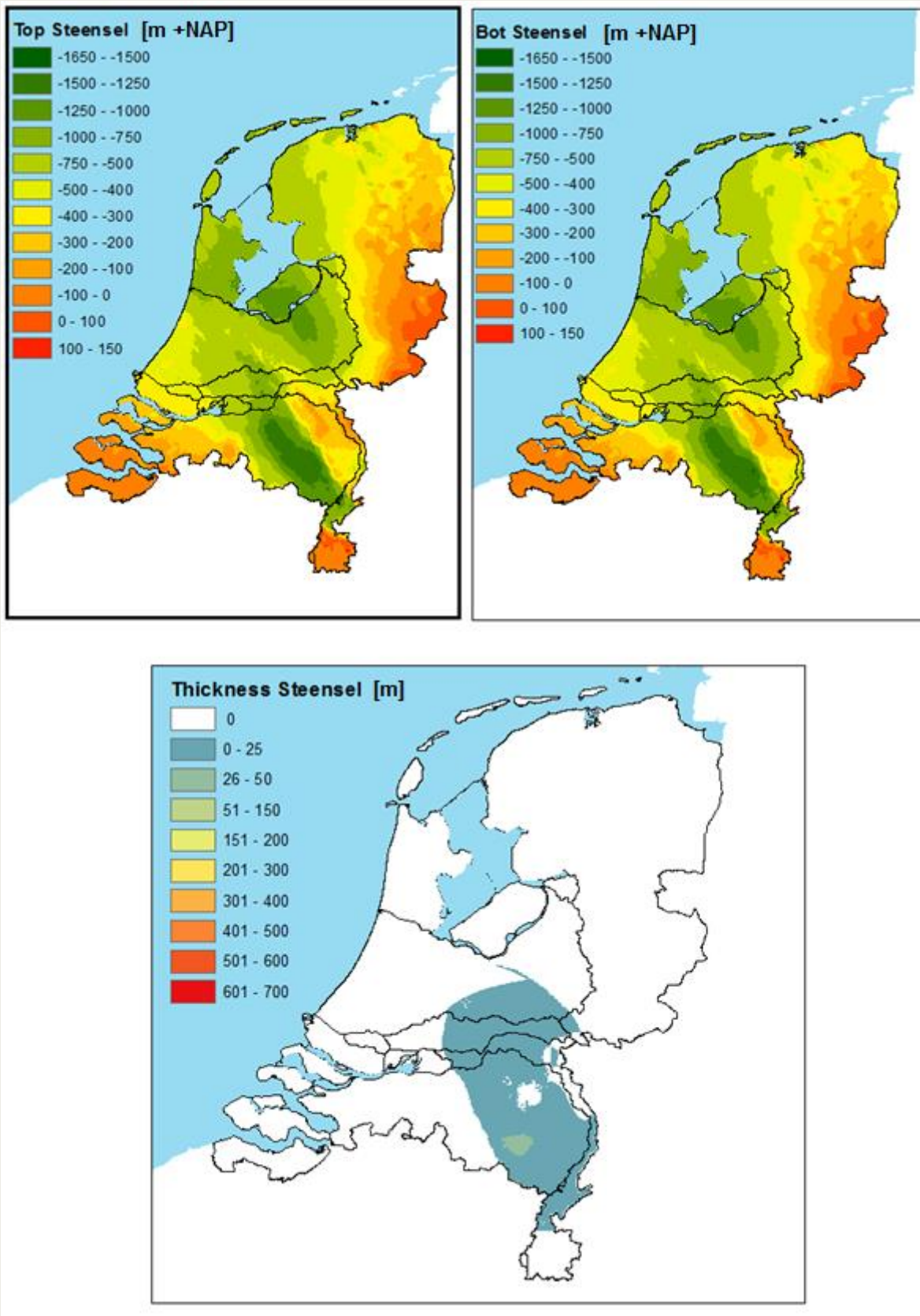


Figure 2.11 Top, bottom and thickness of the Steensel Member

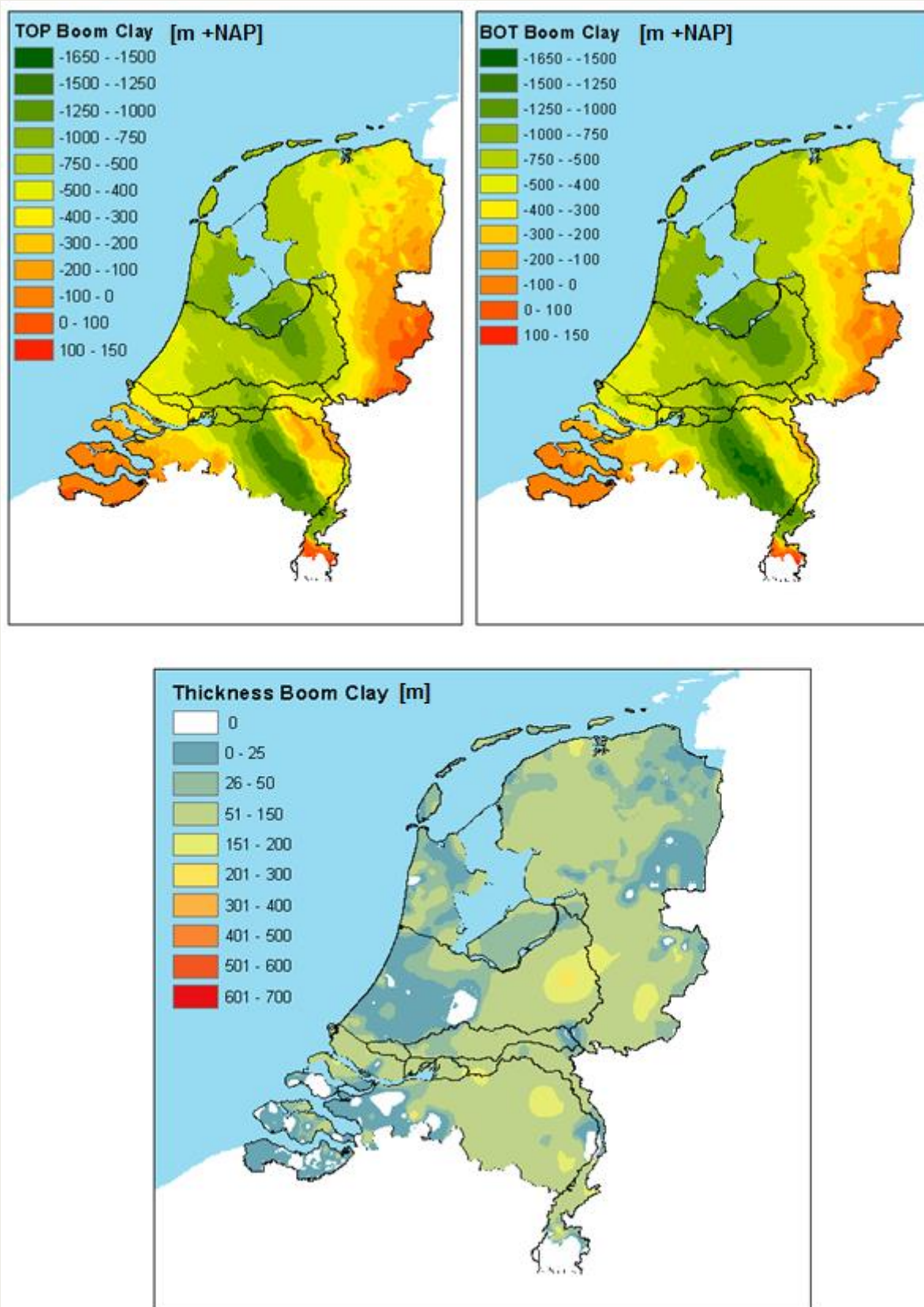


Figure 2.12 Top, bottom and thickness of the Boom Clay

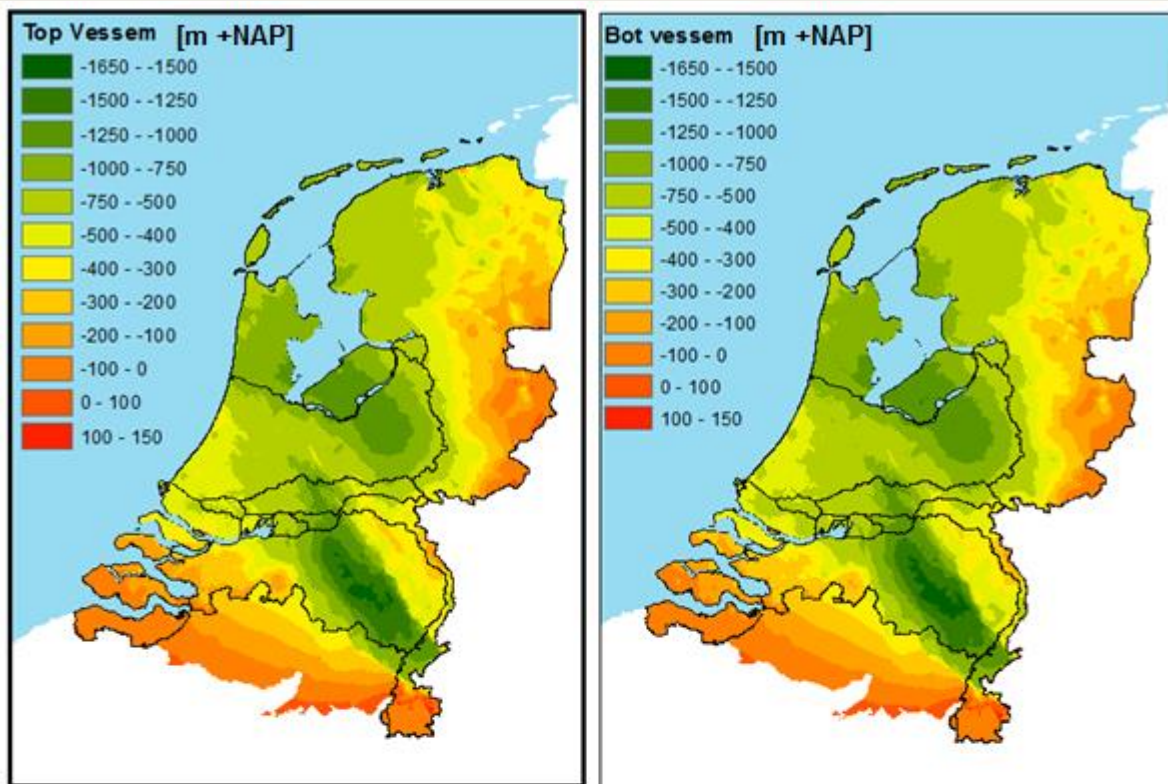


Figure 2.13 Top, bottom and thickness of the Vessem Member

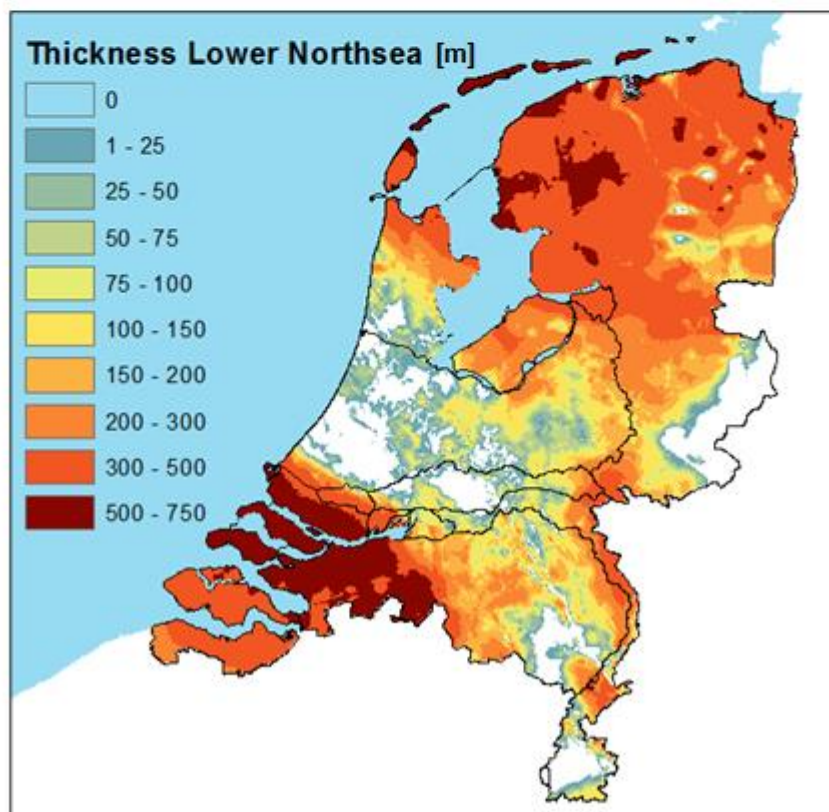
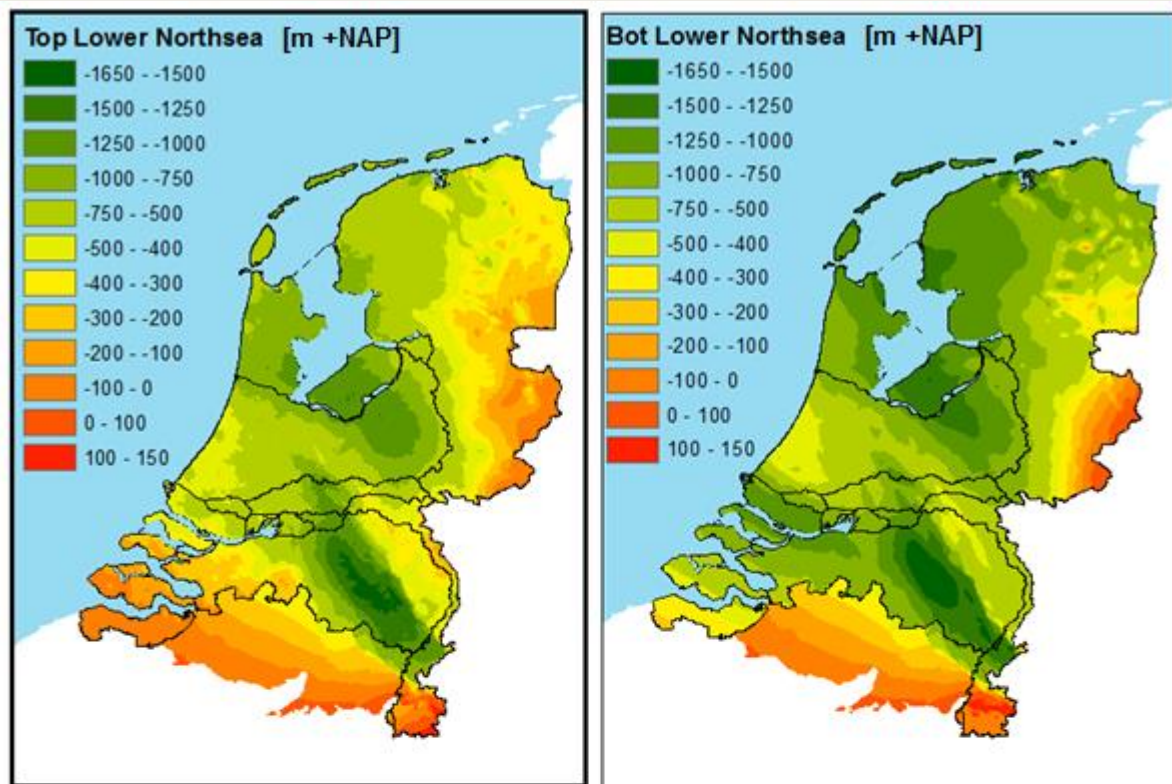


Figure 2.14 Top, bottom and thickness of the Lower North Sea Group

In Figure 2.15 and Figure 2.16, two profiles of the groundwater model are shown.

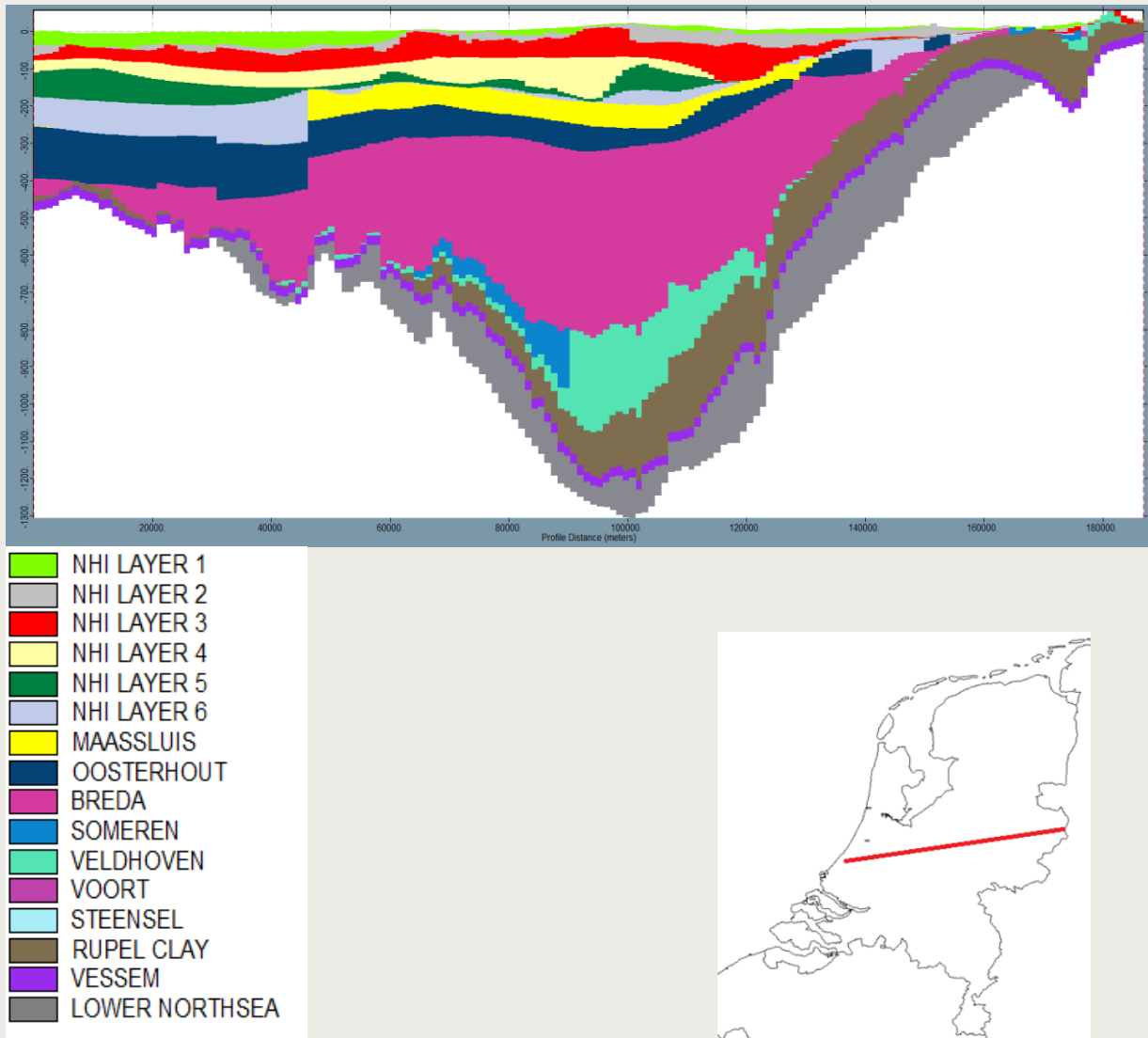
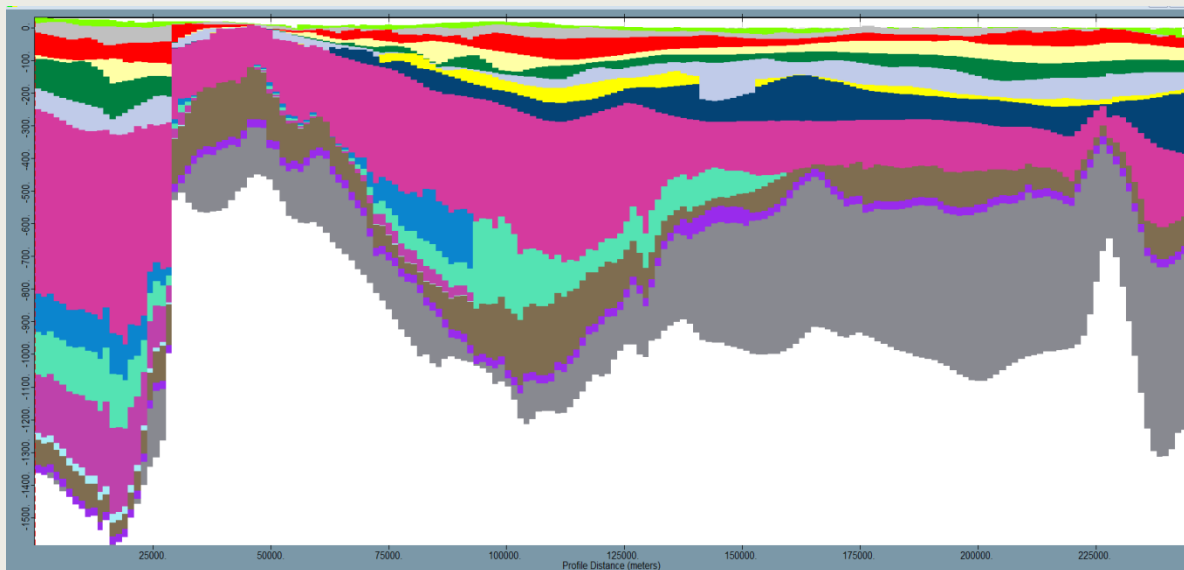


Figure 2.15 Cross-section 1 of the model layers



Profile model (NHI and OPERA)

- NHI LAYER 1
- NHI LAYER 2
- NHI LAYER 3
- NHI LAYER 4
- NHI LAYER 5
- NHI LAYER 6
- MAASSLUIS
- OOSTERHOUT
- BREDA
- SOMEREN
- VELDHOVEN
- VOORT
- STEENSEL
- RUPEL CLAY
- VESSEM
- LOWER NORTHSEA



Figure 2.16 Cross-section 2 of the model layers

2.2.4. Hydraulic conductivity

Values for the horizontal and vertical hydraulic conductivity are directly available in REGIS II.1 for the Maassluis and Oosterhout Formations and part of the Breda Formation that is characterized in REGIS II.1. For the part of the Breda Formation, for which no values are available in REGIS II.1, hydraulic conductivity values are estimated using the lithology (sand or clay) and hydraulic conductivity values for layers with similar lithology within the Breda Formation. Finally, these values of the various layers are scaled up into values for the horizontal and vertical conductivity.

For the other model layers, the horizontal and vertical hydraulic conductivity is derived with a methodology obtained from TNO. This methodology is described in Appendix 2.

Finally, Vis and Verweij (2013) report a large difference in Boom Clay hydraulic conductivity values between mud and non-mud samples. These values differ two orders of magnitude. The applied TNO-methodology is based on the non-mud members. Therefore a

model scenario is also run with hydraulic conductivity values 100 times lower, which is more representative of the Mud samples and more realistic for the northern part of the country in which the Boom Clay is known to consist of finer material.

The hydraulic conductivity values in both horizontal and vertical direction are shown in Figure 2.19 to Figure 2.26.

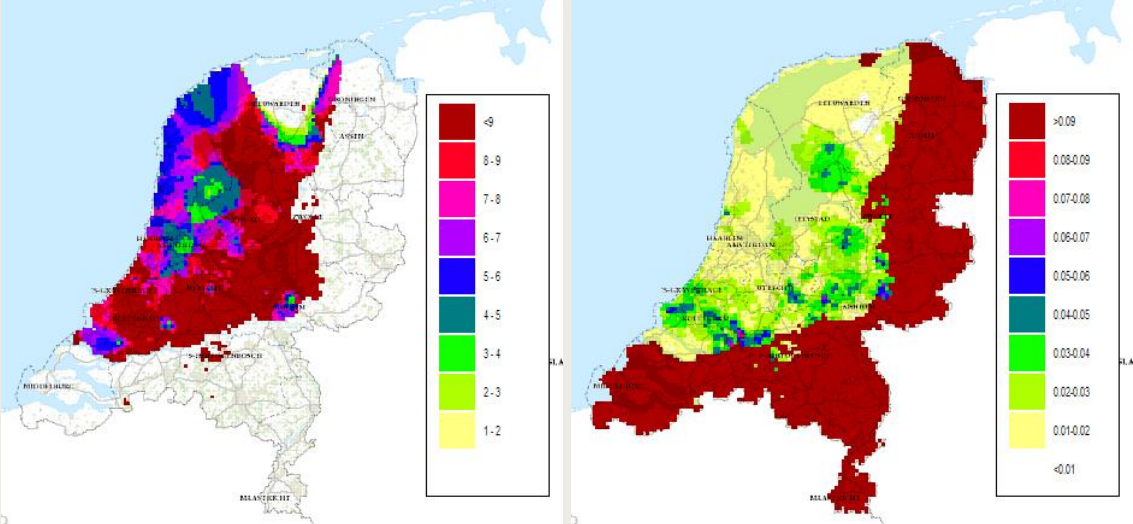


Figure 2.17 Horizontal (left) and vertical (right) hydraulic conductivity values (m/day) for the Maasluis Formation not represented by the NHI model

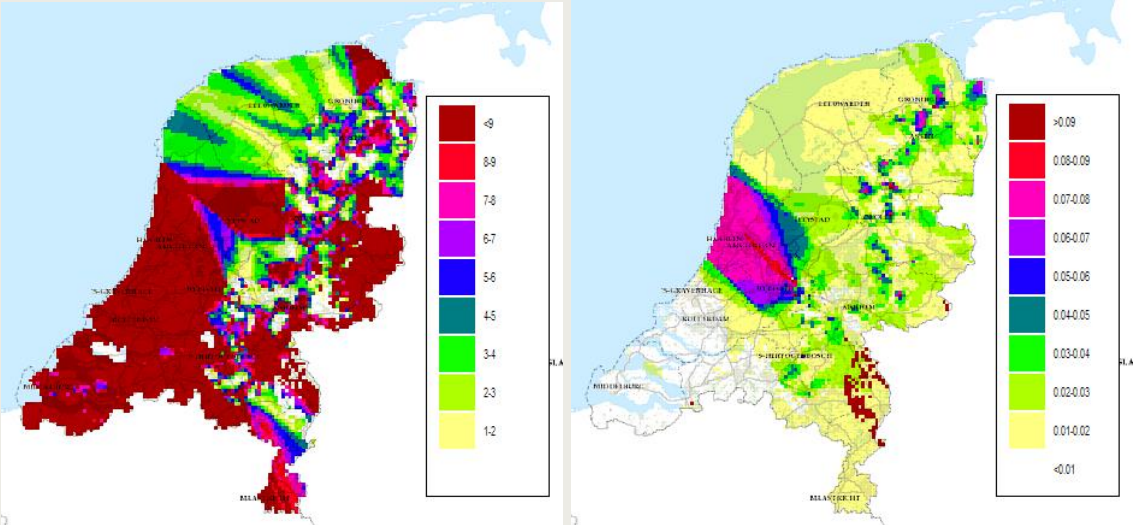


Figure 2.18 Horizontal (left) and vertical (right) hydraulic conductivity values (m/day) for the Oosterhout Formation not represented by the NHI model

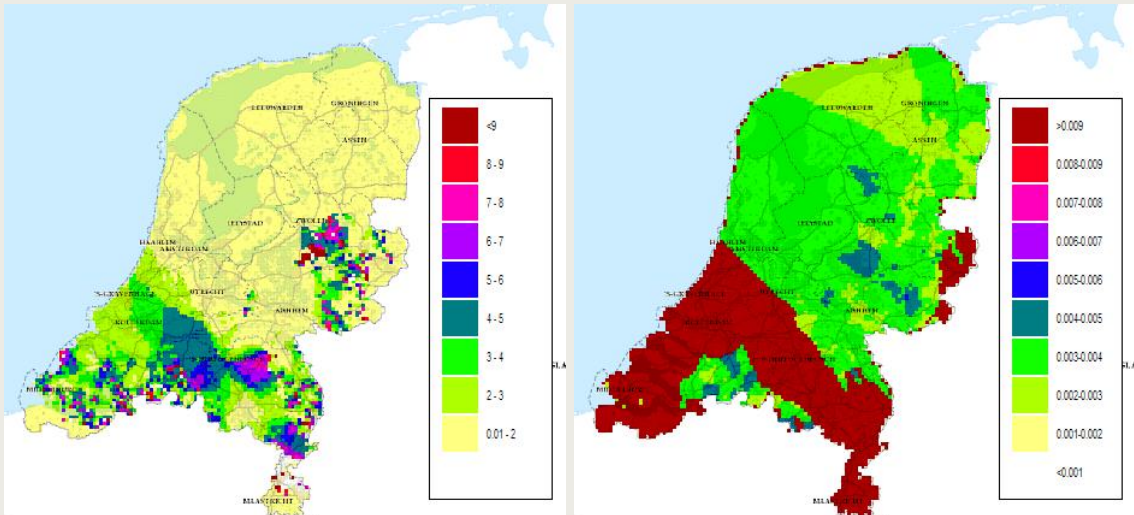


Figure 2.19 Horizontal (left) and vertical (right) hydraulic conductivity values (m/day) for the Breda Formation not represented by the NHI model

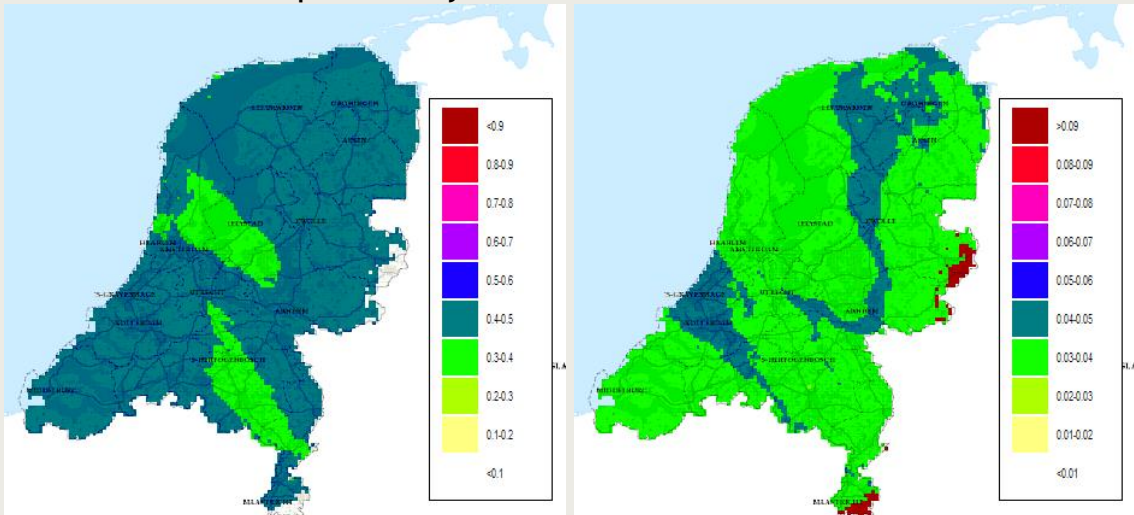


Figure 2.20 Horizontal (left) and vertical (right) hydraulic conductivity values (m/day) for the Someren Member

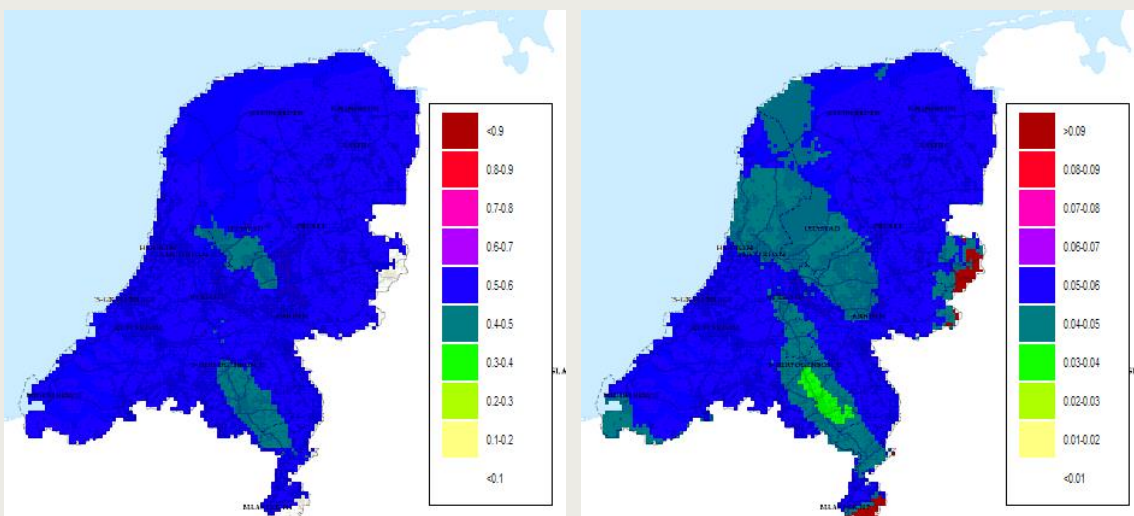


Figure 2.21 Horizontal (left) and vertical (right) hydraulic conductivity values (m/day) for the Veldhoven Member

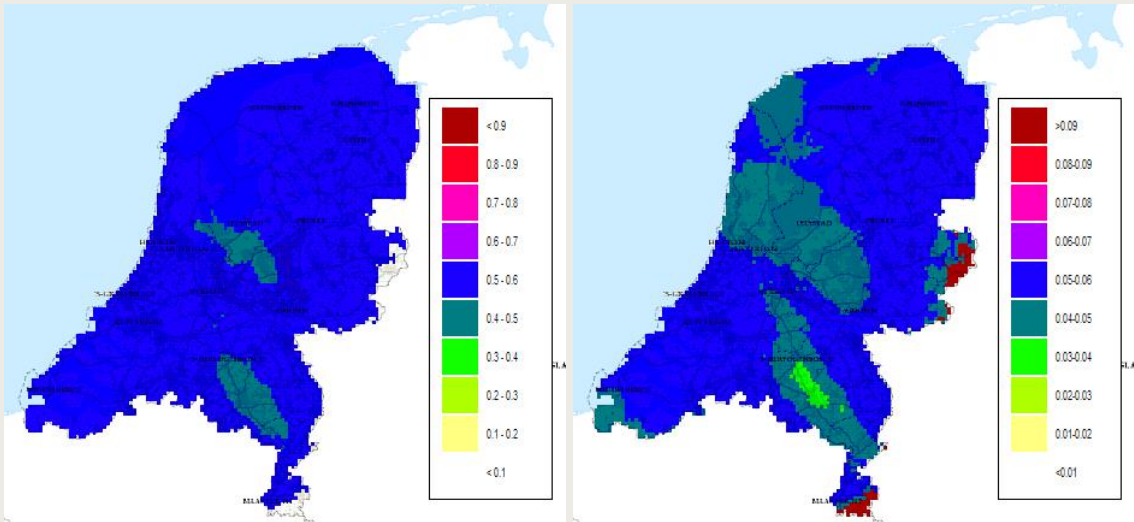


Figure 2.22 Horizontal (left) and vertical (right) hydraulic conductivity values (m/day) for the Voort Member

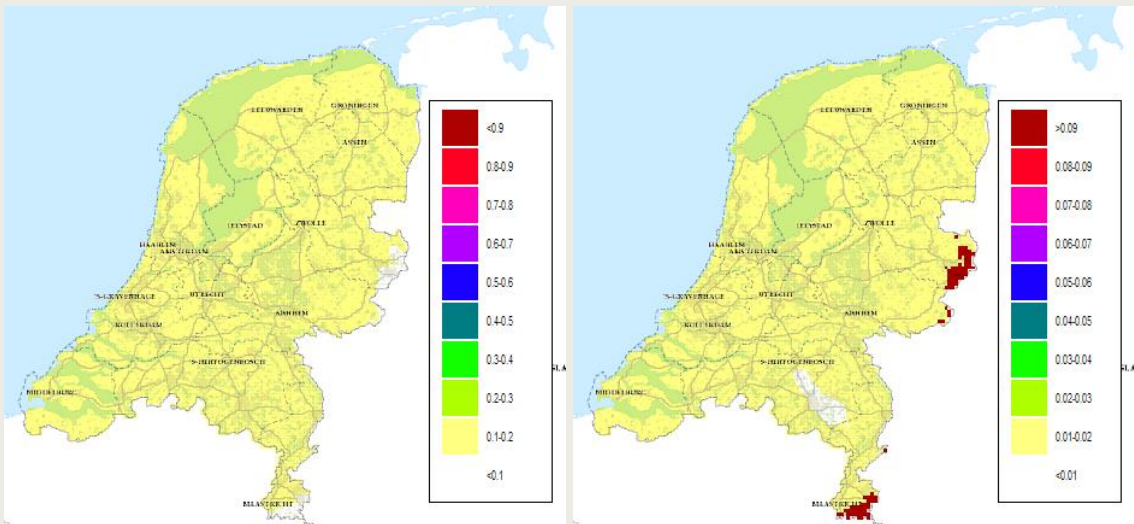


Figure 2.23 Horizontal (left) and vertical (right) hydraulic conductivity values (m/day) for the Steensel Member

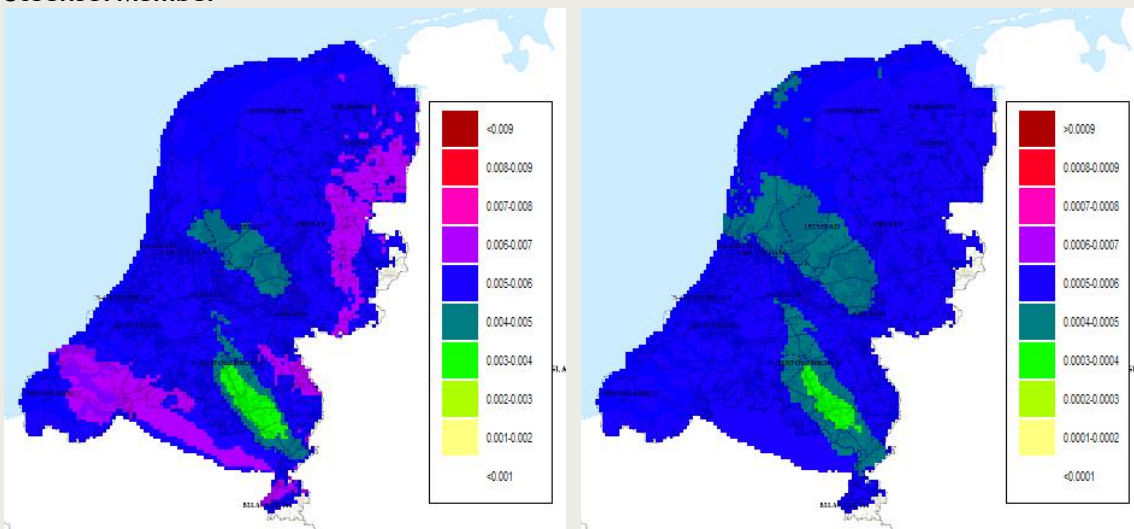


Figure 2.24 Horizontal (left) and vertical (right) hydraulic conductivity values (m/day) for the Boom Clay Member

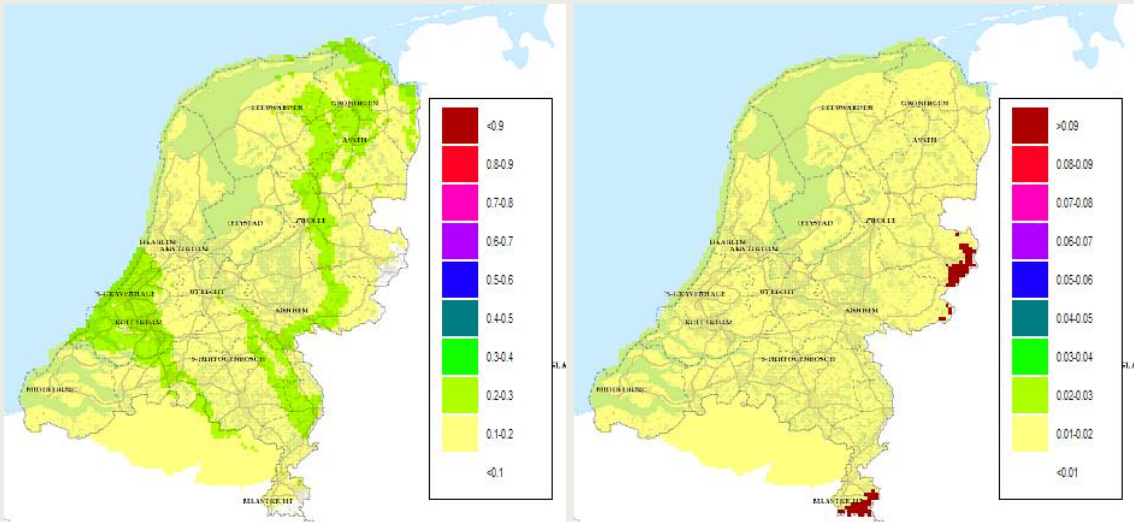


Figure 2.25 Horizontal (left) and vertical (right) hydraulic conductivity values (m/day) for the Vessem Member

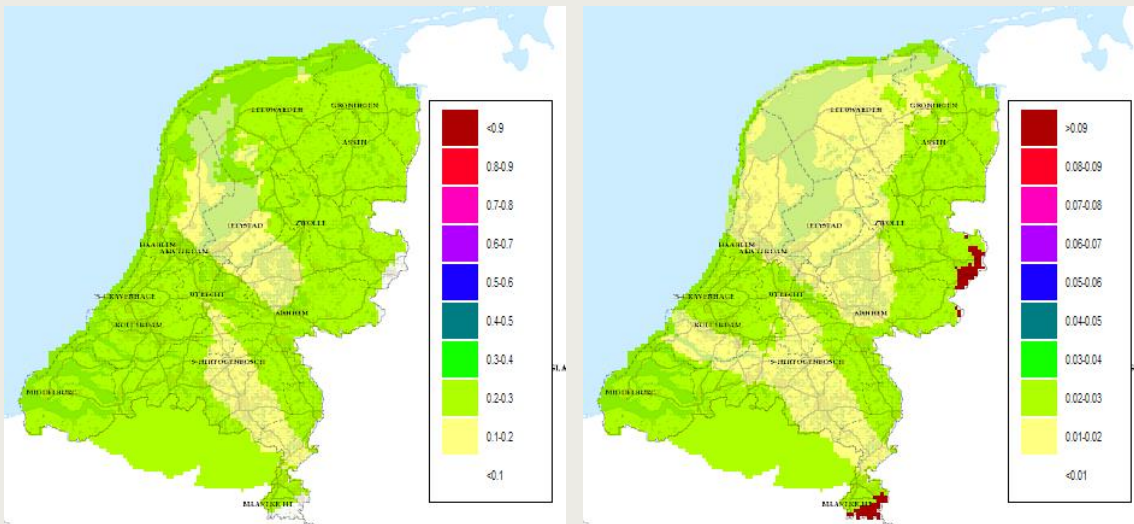


Figure 2.26 Horizontal (left) and vertical (right) hydraulic conductivity values (m/day) for the Lower North Sea Group

2.2.5. Faults

Faults are present in the subsurface in the Netherlands. Locations of faults that are known are given in Figure 2.27.

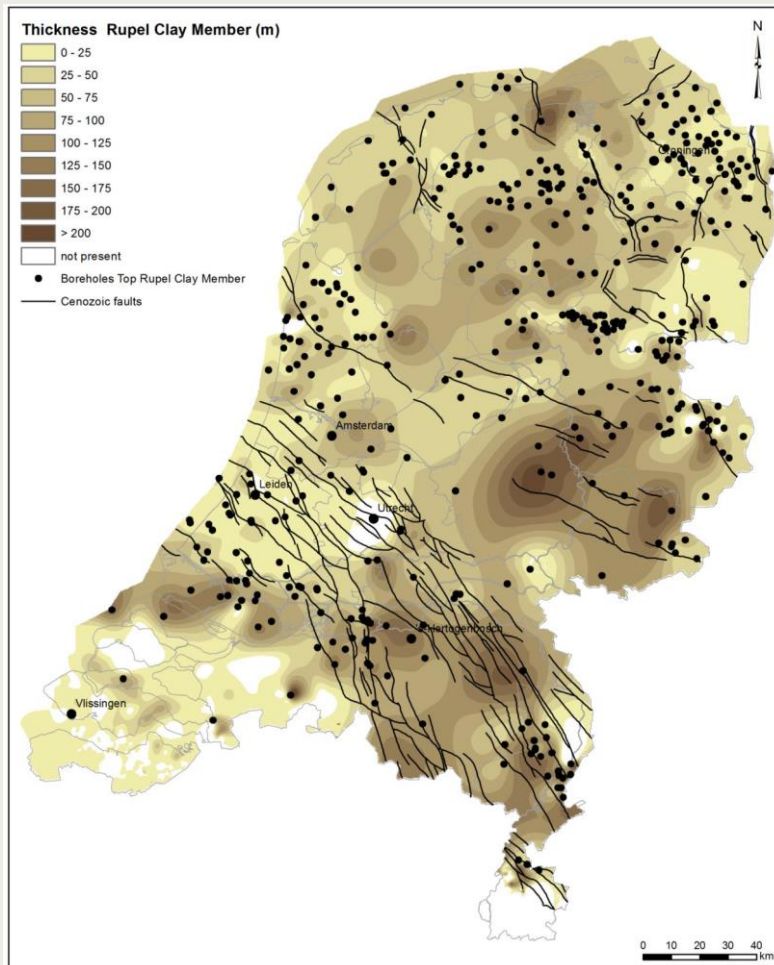


Figure 2.27 Location of faults (source: Vis and Verweij, 2014)

The potential effects of faults on the groundwater flow are:

1 Faults have shifted the position of the individual aquifers with the result that:

- aquifers from the same Formations/Member are not connected anymore or are only connected over a limited thickness.
- aquifers from different Formation/Members have become connected, causing preferential flow that bypasses less permeable layers in between.

2 Hydraulic conductivity values may have changed during vertical displacements of the fault blocks. In north Brabant examples are known in which strong jumps in hydraulic heads over faults are encountered.

Unfortunately, information on faults (such as the presence at which depth intervals, vertical displacement, sealing effect or possibility of vertical preferential flow paths through the faults) is limited. Therefore, the influence of faults is not explicitly taken into account in the groundwater model, other than jumps in the thicknesses of model layers known from the original grid data.

For potential repository locations near faults or if the pathlines starting at the potential repository location approach or even cross faults, it is recommended to study the effect of faults in more detail.

2.2.6. Boundary conditions

As mentioned before, the Formations/Members in the model extension outcrop over the border in Belgium and Germany. There, groundwater recharge will take place resulting in water tables that at maximum may get close to the surface elevation. One may expect that hydraulic heads in the aquifer at the model boundary are related to the level of surface waters that drain the areas where these formations outcrop in Belgium and Germany when no groundwater abstractions are present in these formations. Initial model runs, however, gave the impression that the hydraulic head distribution of the lower aquifer of the extended NHI model strongly resembles the hydraulic head distributions of the lower model layers of the original NHI model. Further analysis showed that the leakage factor^b of the deeper aquifers is often in the range of 1 to several kilometres only. Using the rule of thumb that the effect of fixed boundary conditions becomes negligible after 3 times the leakage factor, it can be concluded that the hydraulic head of the deeper aquifers at the model boundary would mostly be affected by the hydraulic heads of the layers above. Therefore, the boundary conditions of the deeper aquifers are chosen as fixed hydraulic heads with the same values as the deepest model of the NHI model.

No-flow boundaries at the coastal part of the model domain are chosen for the deeper model layers. This boundary condition is equal to the lower five model layers of the NHI model.

2.3. Results

2.3.1. Hydraulic heads

The calculated hydraulic heads are shown for the lowest model layer of the NHI model and the aquifers directly above and below the Boom Clay in Figure 2.28.

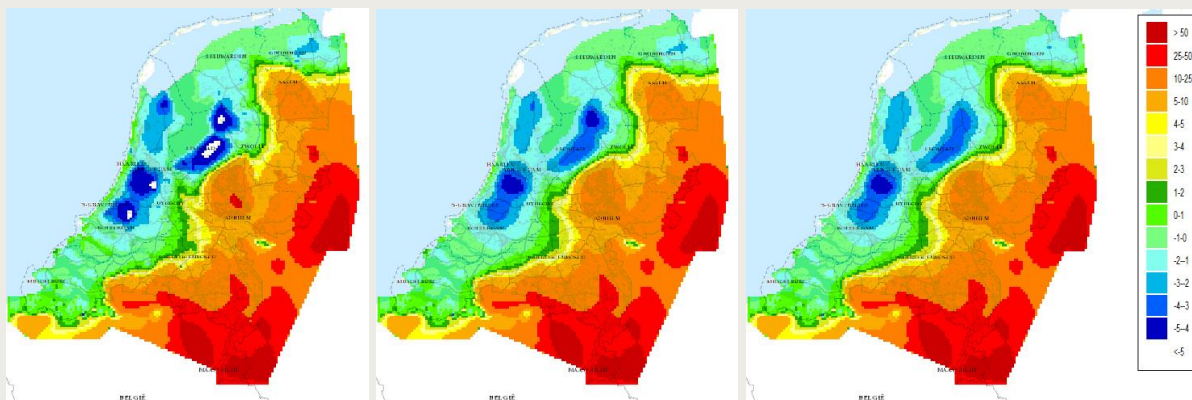


Figure 2.28 Hydraulic head distribution in lowest layer of the NHI model (left), and the layers above (middle) and below (Vessem) the Boom Clay

The pattern in the hydraulic head distribution are remarkably comparable for these three model layers. From these results, it can be concluded that the most important part of the flow resistance in the deeper aquifers is due to the flow resistances for horizontal flow in the deeper aquifers in combination with the long flow distances in these aquifers. Therefore, the vertical flow through the Boom clay and the other deeper model layers is small.

^b The leakage factor of an aquifer is the square root of the product of transmissivity (horizontal hydraulic conductivity times the thickness) of that aquifer and the hydraulic resistance (thickness divided by the vertical hydraulic conductivity) of the less permeable layer above

For comparison, the calculated hydraulic head values are compared with average measurement values in the period 1996-2006 from the lowest NHI model layer and all deeper layers, see Figure 2.29.

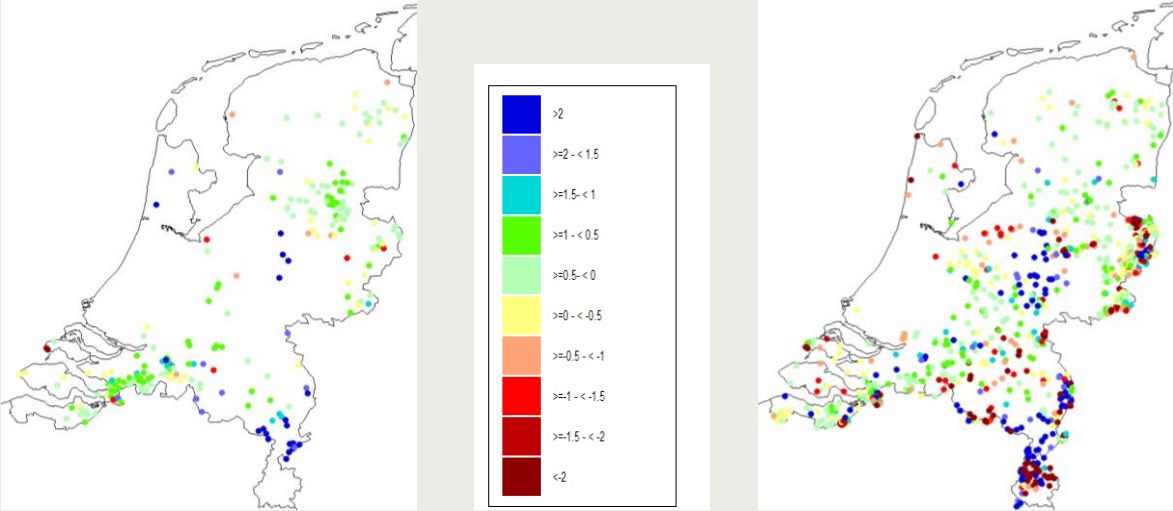


Figure 2.29 Difference in calculated and averaged measured heads (in meters) from 1996-2006 at the lowest NHI layer (left) and all layers below (right)

In general, the residuals in the layers below the original NHI model are on many locations comparable to the residuals in the lowest NHI-layers, such as the large positive residual in Limburg and on the Veluwe. The model predicted that the layers below the original NHI model show a head distribution pattern that is similar to that of the lowest NHI-layer. As the hydraulic head residuals of the lowest NHI-layers and the new model layers are comparable, it is hypothesized that head residuals in the layers below the lowest NHI-layer are for a considerable part due to errors that were already present in the original NHI model.

Finally, the flow direction in the Boom Clay is shown in Figure 2.30. It shows similar patterns as the infiltration and seepage area in shallow groundwater. Especially, locations where groundwater flow through the Boom Clay is downwards are expected to result in long travel times before that groundwater reaches the biosphere.

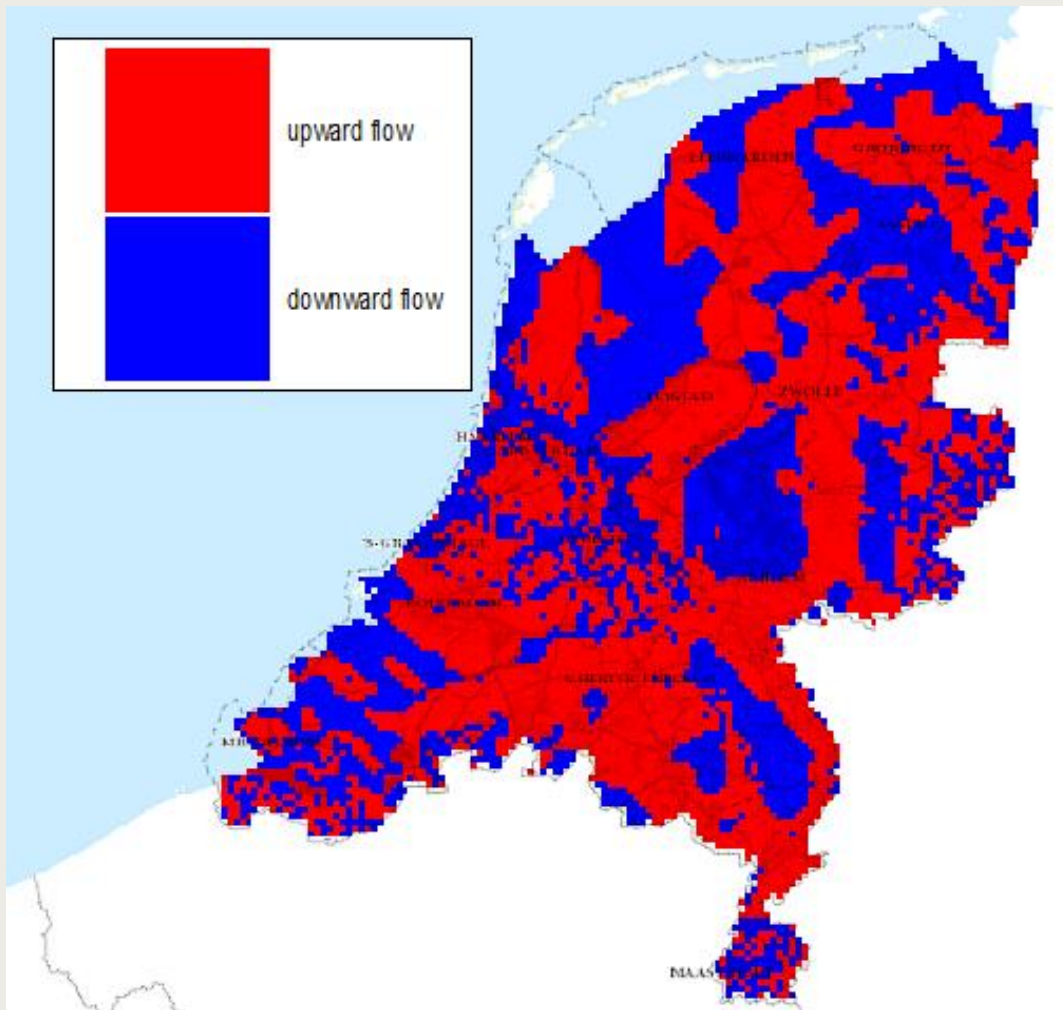


Figure 2.30 Vertical flow direction through the model layer representing the Boom Clay; in case the Boom clay is absent there is still a vertical flow calculated through this layer, but the thickness of the layer is zero.

3. Pathline Analysis

3.1. Starting locations

In order to make transport calculations with the disposal concept defined for OPERA, we selected locations using:

- 1 depth of repository ≥ 500 m
- 2 thickness of Boom Clay ≥ 100 m

Assuming that at least 50 m of clay should be present on top and below the repository, the bottom of the Boom Clay must be below 550 m and the thickness of the Boom Clay should exceed 100 m.

On all these locations starting points of the pathline calculations are located at the interfaces of the Boom Clay with the layers adjacent to the Boom Clay.

The starting locations of the pathlines are shown in Figure 3.1.

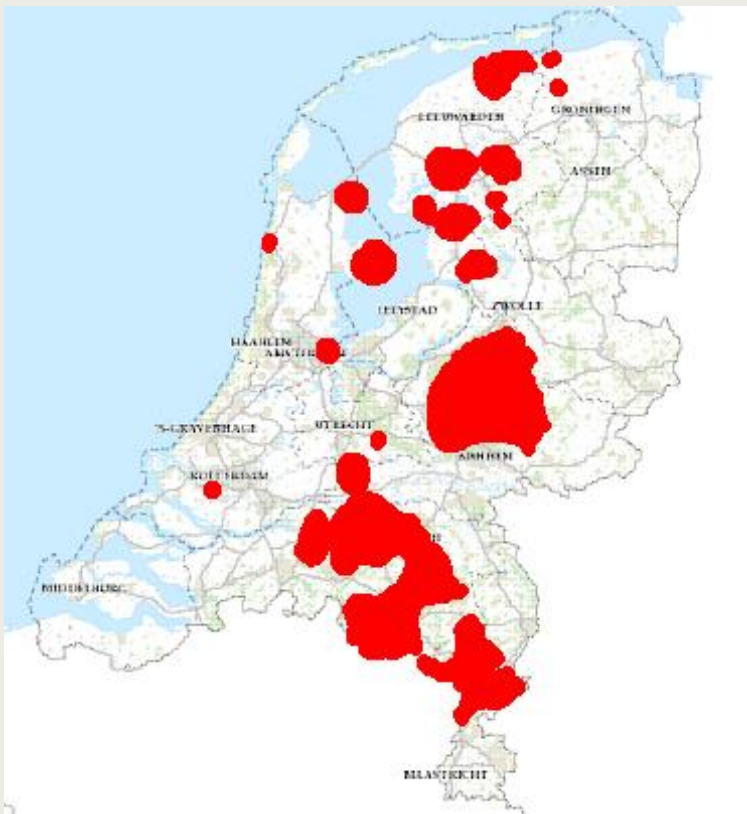


Figure 3.1 Starting locations of the pathlines for a geological disposal facility at 500 metre depth in Boom Clay

3.2. Results

The resulting pathlines are shown in Figure 3.2 and Figure 3.3. The colours indicate the conservative travel time along the pathline since its start. Be aware that many pathlines are plotted on top of each other. The flow patterns show that particles that start in infiltration areas such as the Veluwe and North-Brabant do flow over a large distance towards seepage areas, such as the polders in the western part of the country, the Wieringermeerpolder in the north-west and to the valleys of the IJssel and Rhine rivers in

Gelderland. In the Northern part of the country flow distances are relatively short and the pathlines end up in polder areas close to their starting locations.

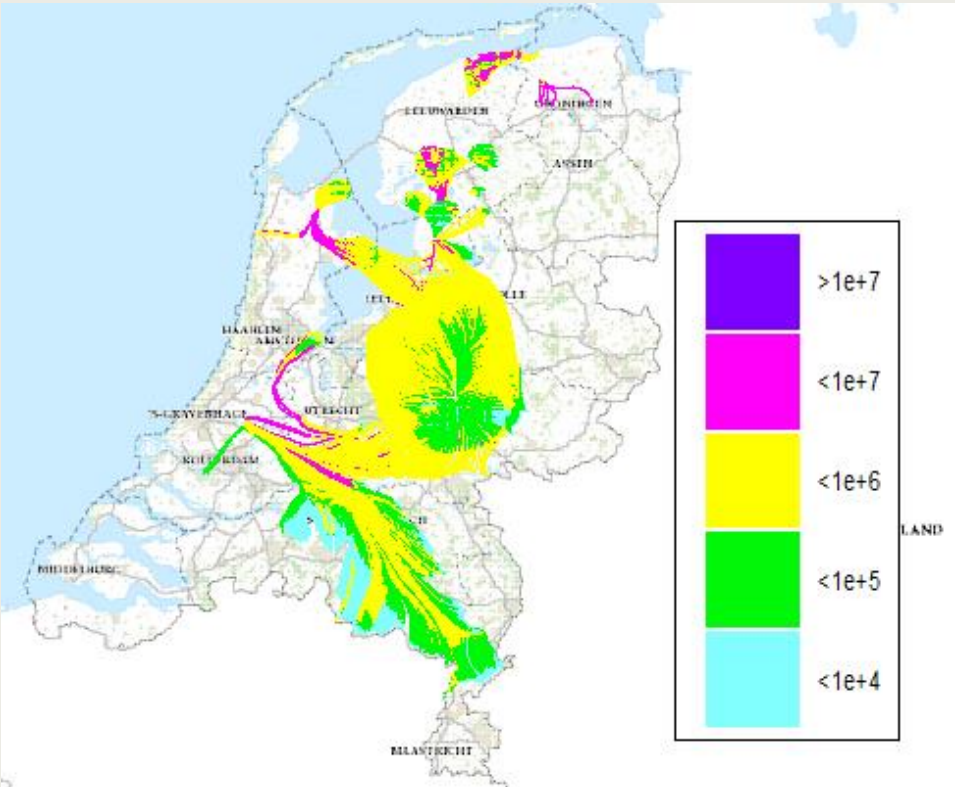


Figure 3.2 Pathlines with conservative travel times (in years) starting above the Boom Clay

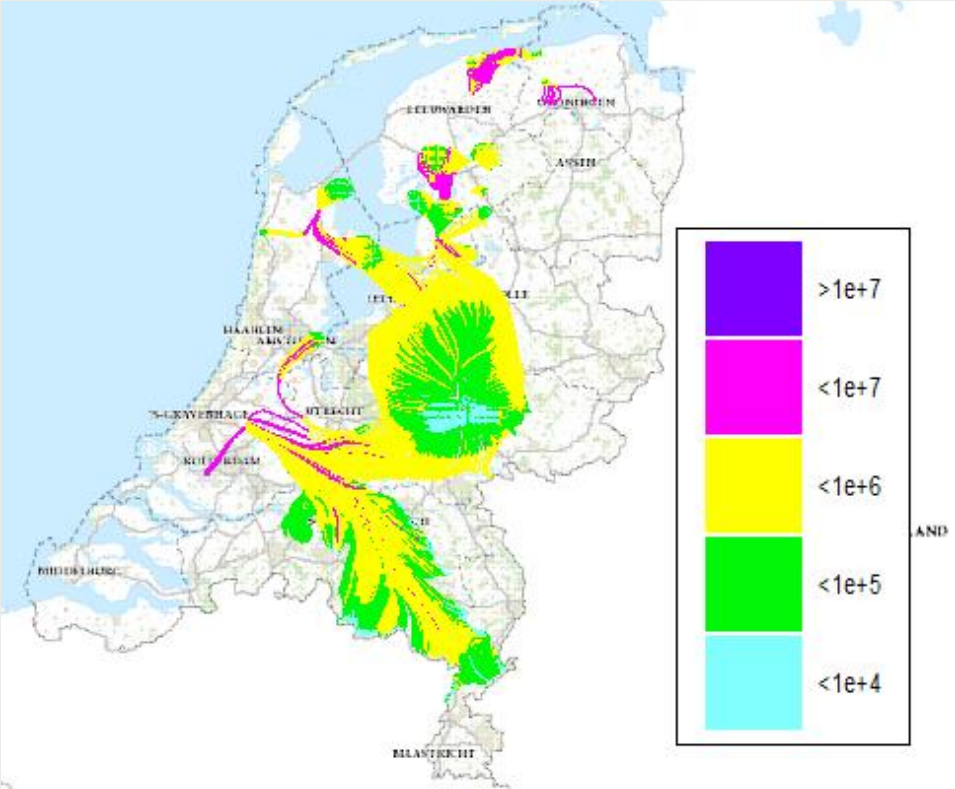


Figure 3.3 Pathlines with conservative travel times (in years) starting below the Boom Clay

Figure 3.4 shows the conservative residence times (Travel time of the pathline from starting location to final location) plotted on the starting locations

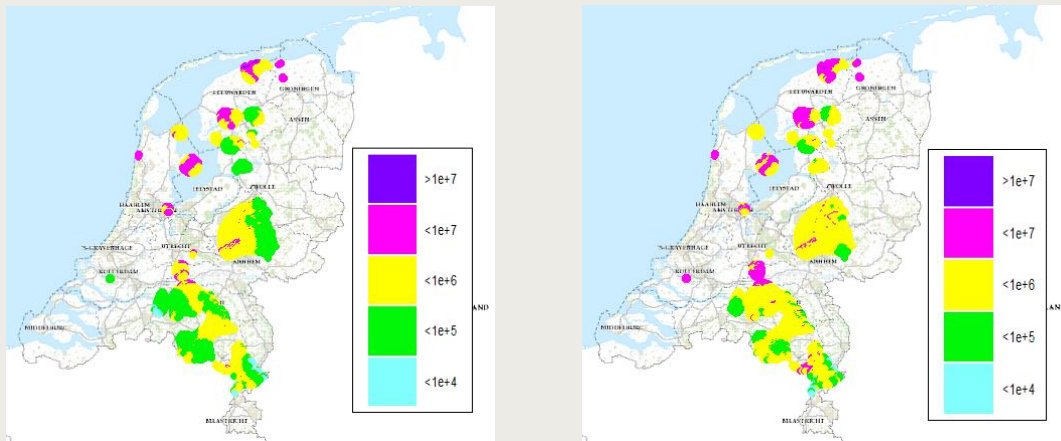


Figure 3.4 Residence times (in years) of pathlines starting at the top (left) or bottom (right) of the Boom Clay plotted on the starting locations

The distributions of conservative travel times for the pathlines starting above and below the Boom Clay are shown in Figure 3.5 and Figure 3.6.

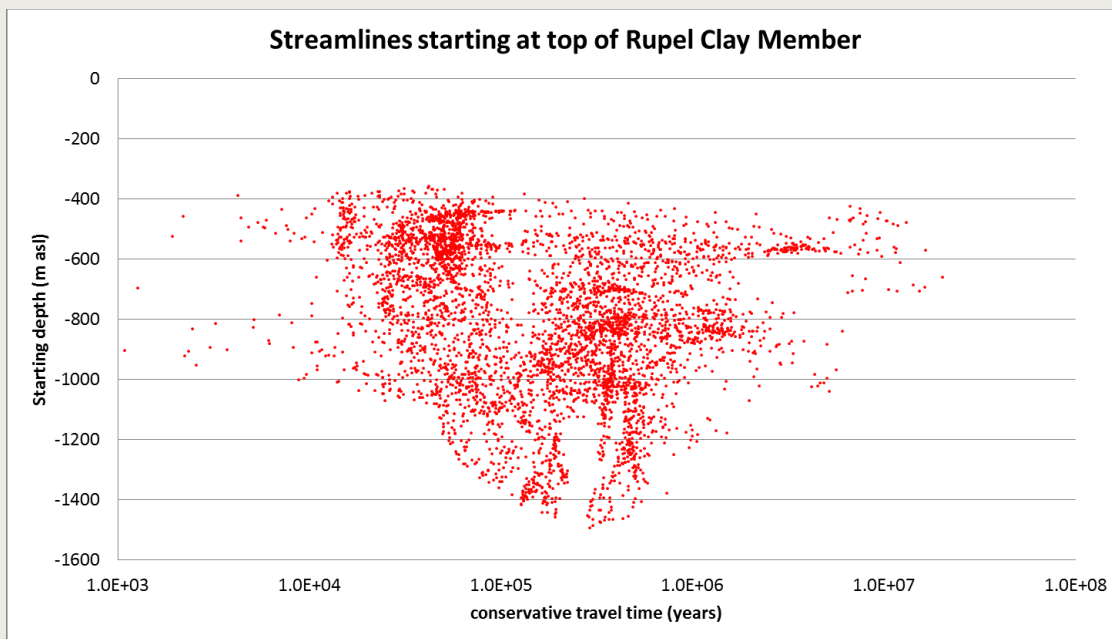


Figure 3.5 Travel times distributions of pathlines starting above the Boom clay

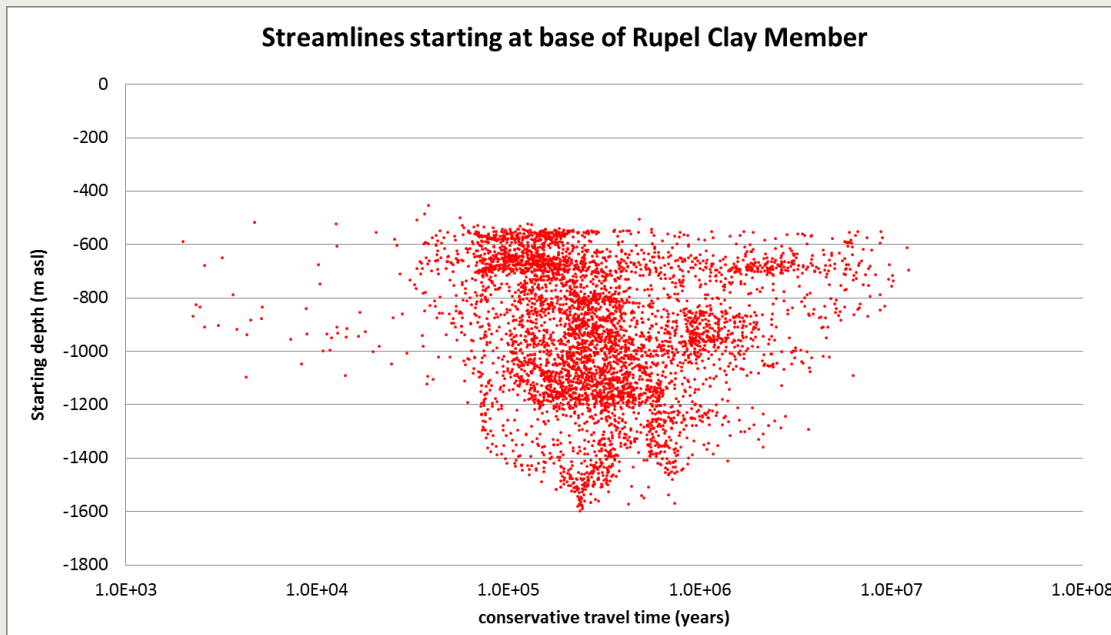


Figure 3.6 Travel times distributions of pathlines starting below the Boom clay

Also the residence time of water in the Boom Clay is calculated. These values are given in Figure 3.7. This figure also shows the result for the same analysis performed for the case the vertical hydraulic conductivity of the Boom clay is lowered by a factor of 100, giving values when using the analysis of the mud samples of the Boom Clay made in the framework of OPERA (Vis and Verweij, 2014) as input instead of the methodology described in Appendix 2.

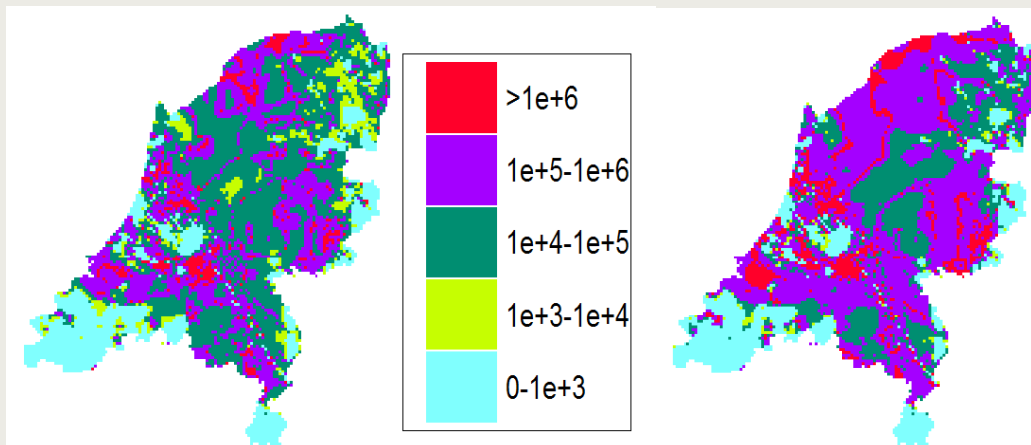


Figure 3.7 Distribution of conservative residence time in the Boom Clay: normal run (left) and scenario run with lower (100 times) vertical hydraulic conductivity for the Boom Clay based on the mud samples (right).

In areas where the Boom clay is not present, the residence time equals zero. For areas where the thickness of the Boom Clay exceeds 100 m the conservative residence time within the Boom Clay is in the range from 10.000 years to over 1.000.000 years. It is clear that in most areas, the model with the lower vertical conductivity of the Boom Clay has a longer residence time in the Boom Clay. The figures also show some small zones with very high residence times. These zones indicate a change in the flow direction through the Boom Clay resulting in a very small hydraulic head gradient over the Boom Clay and thus into long residence times within the Boom Clay.

3.3. Selection of pathlines for transport calculations

For the radionuclide migration calculations a selection of the pathlines needs to be made. This selection consists of a fast, a median and a slow pathline, which have been obtained using the following procedure. First, for the pathlines starting at the same xy-location, but either above or below the Boom Clay, the fastest pathline has been selected. From this selection, the cumulative distribution of the travel time from all xy-locations has been obtained, see Figure 3.8.

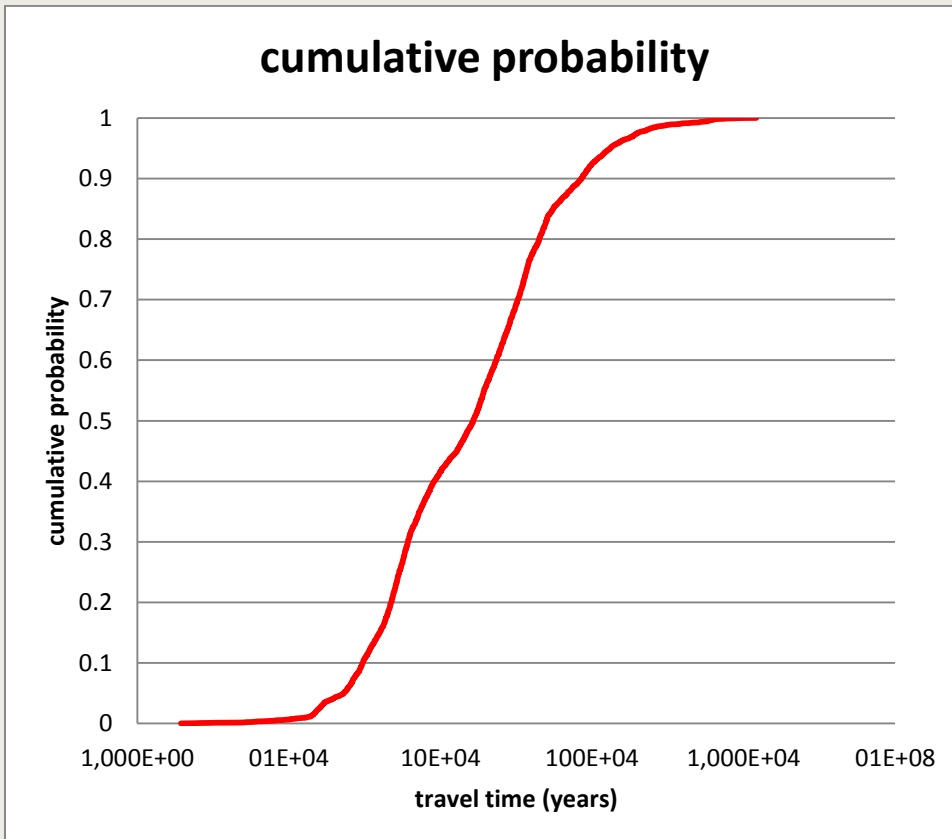


Figure 3.8 Cumulative distribution of conservative travel times from pathlines starting at the interface of Boom Clay at ≥ 500 metre towards the biosphere.

The fast, median and slow pathlines have been selected based on the 10, 50 and 90 percentiles of this distribution respectively. For the three pathlines, the residence time and travel distance in each model layer has been obtained and is used in the radionuclide migration calculations, see Table 3.1.

It is worth mentioning that, when dividing the distance in some formations by the residence time in the same formation, very low particle velocities, even lower than 0.1 m/year, are modelled in the deeper aquifers. This is much smaller than particle velocities often encountered in shallow aquifers in which particle velocities up to 100 m/year can be observed.

Table 3.1 Pathline trajectory data for three selected pathlines

layer name	fast				median				slow			
	residence time (years)	distance (m)	porosity	Formation	residence time (years)	distance (m)	porosity	Formation	residence time (years)	distance (m)	porosity	Formation
NHI_1	0	0	-	-	0	0	-	-	0	0	-	-
NHI_aquitard 1	0	0	-	-	0	0	-	-	5.00E+01	4.53E+00	0.3	Holocene Clay
NHI_2	0	0	-	-	0	0	-	-	1.00E+00	2.28E+01	0.3	Boxtel sand
NHI_aquitard 2	0	0	-	-	1.00E+00	3.27E+00	0.3	Kreftenheye - Zutphen Clay 1	0	0	-	-
NHI_3	0	0	-	-	1.00E+01	8.71E+01	0.3	Peize Waalre sand 4	2.00E+00	2.25E+01	0.3	Kreftenheye sand
NHI_aquitard 3	0	0	-	-	0	0	-	-	0	0	-	-
NHI_4	0	0	-	-	6.00E+00	4.81E+01	0.3	Peize Waalre sand 7	1.00E+01	6.67E+01	0.3	Urk sand
NHI_aquitard 4	0	0	-	-	0	0	-	-	1.70E+00	4.60E+00	-	-
NHI_5	2.00E+00	2.36E+02	0.3	Peize Waalre sand 4	2.00E+00	1.43E+01	0.3	Maassluis sand 2	3.00E+01	1.51E+02	0.3	Appelscha sand
NHI_aquitard 5	0	0	-	-	0	0	-	-	0	0	-	-
NHI_6	5.00E+00	3.29E+02	0.3	Peize Waalre sand 5	1.00E+01	1.78E+01	0.3	Maassluis sand 3	3.20E+02	2.19E+03	0.3	Peize Waalre sand 4, 5 and 6
NHI_aquitard 6	1.30E+01	2.20E+01	0.3	Peize Comple	0	0	-	-	2.40E+02	2.66E+01	0.3	Peize Complex
NHI_7	2.57E+02	1.48E+03	0.3	Peize Waalre sand 7	8.00E+01	5.96E+02	0.3	Oosterhout sand 1	8.00E+01	4.23E+02	0.3	Peize Waalre sand 7
Maassluis	0	0	-	-	0	0	-	-	2.78E+03	1.96E+03	0.37	Maassluis
Oosterhout	4.71E+03	4.58E+03	0.4	Oosterhout	4.10E+02	2.82E+02	0.4	Oosterhout	7.25E+03	7.37E+03	0.35	Oosterhout
Breda	1.50E+04	1.36E+04	0.4	Breda	9.33E+03	1.07E+03	0.4	Breda	2.33E+05	2.99E+03	0.32	Breda
Someren	0	0	-	Someren	0	0	-	Someren	0	0	-	Someren
Veldhoven	1.07E+04	3.09E+03	0.35	Veldhoven	1.92E+04	1.04E+03	0.35	Veldhoven	9.42E+04	5.33E+03	0.3	Veldhoven
Voort	0	0	-	Voort	0	0	-	Voort	0	0	-	Voort
Steensel	0	0	-	Steensel	0	0	-	Steensel	0	0	-	Steensel
Rupel Clay	0	0	-	Boom Clay	3.17E+04	1.07E+02	0.37	Boom Clay	9.82E+04	8.16E+01	0.3	Boom Clay
Vessem	0	0	-	Vessem	1.26E+04	7.79E+02	0.3	Vessem	1.06E+05	1.48E+03	0.29	Vessem
Lower North Sea Group	0	0	-	Lower North Sea Group	9.11E+04	9.94E+03	0.25	Lower North Sea Group	3.11E+05	6.11E+03	0.23	Lower North Sea Group
total	3.07E+04	2.33E+04			1.64E+05	1.40E+04			8.53E+05	2.82E+04		

3.4. Effect of transversal dispersion and transversal diffusion

When simplifying the transport of the radionuclide into a 1D transport model, the effect of dilution due to mixing in the transversal direction is neglected. The radionuclides that will leave the Boom Clay and after some time will reach an aquifer with a higher flow velocity will likely form a thin plume initially due to the relatively large horizontal flux in the receiving formation compared to the small vertical water flux out of the Boom Clay. In each next aquifer the thickness of the plume can be different. A schematic representation is given in Figure 3.9.

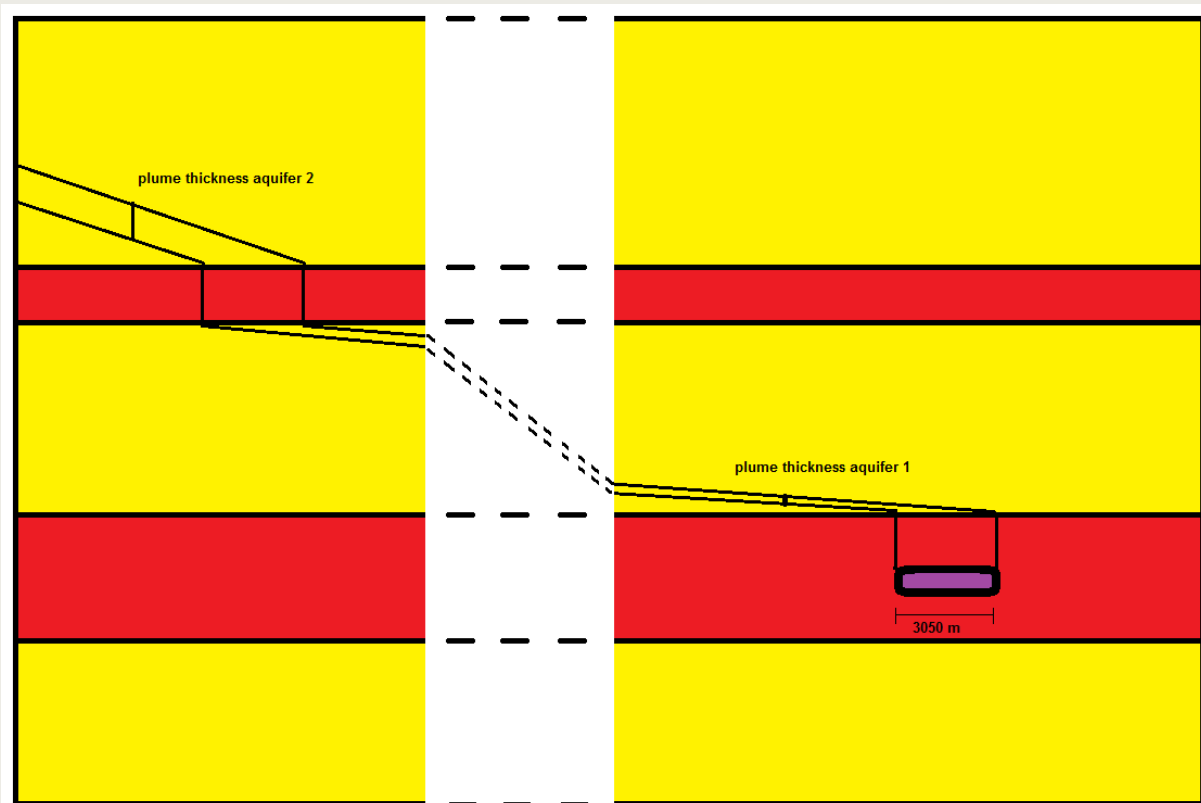


Figure 3.9 Schematic representation of the plume thicknesses in the different aquifers

The thickness of the non-transversally-mixed plume in each aquifer is estimated based on the pathline's distance with the interface with the Boom Clay after a horizontal flow distance of 3050 m (which is equal to the maximum horizontal extent of the repository (figure 5.2 in Verhoef et al. 2011^c) and the ratio of the horizontal flow velocity in each aquifer with the horizontal flow velocity in the aquifer adjacent to the Boom Clay. In case the horizontal flow distance in the aquifer adjacent to the Boom Clay, is smaller than or approximately equal to the 3050 m than the interface with the next geological layer is used in the analysis. If we assume that this plume has a constant concentration over its thickness and a concentration of zero outside, then after a certain distance, the plume gets a Gaussian shape that can be described by the following equation:

$$C(x, z) = \frac{C(0)D}{(\pi x \alpha_t)^{0.5}} \exp\left(-\frac{z^2}{4x\alpha_t}\right)$$

Where D is the plume thickness and α_t is the transversal dispersivity, x and z are horizontal and vertical coordinates.

This equation is valid for a homogeneous aquifer. In reality, the plume does not stay in a single aquifer with constant flow velocity, but flows from one aquifer into another. The thickness of the plume is inversely related to its flow velocity. In order to apply the equation above, the x coordinate is rescaled according to the following relation:

$$x^* = x * \left(\frac{v(1)}{v(max)}\right)^2 \quad \text{aquifer 1}$$

^c The disposal volume of conditioned waste was reduced after a concrete recipe was defined for depleted uranium. The maximum horizontal extent of the disposal facility was reduced to 2450 m (Verhoef et al. 2014)

$$x^* = x^*_{end}(1) + (x - x_{begin}(2)) * \left(\frac{v(2)}{v(max)}\right)^2 \quad \text{aquifer 2}$$

$$x^* = x^*_{end}(n - 1) + (x - x_{begin}(n)) * \left(\frac{v(n)}{v(max)}\right)^2 \quad \text{aquifer n}$$

In this equation, $v(max)$ is the maximum velocity that each pathline encounters. For D, the plume thickness in the aquifer with the maximum velocity should be used. For the three pathlines described in Table 3.1, the calculations have been performed. The plume thicknesses in the aquifers with the highest velocities of these three pathlines are: 3.7 cm, 1.08 m and 2.4 cm respectively in the NHI Layer 5, 3 and 2 respectively. The rescaled travel distances x^* for these pathlines equal 343 m, 578m and 278 m for the three pathlines respectively.

Field scale values for the transversal dispersivity have been obtained in several tracer tests. For field tests with a scale in the range of 100 m, Gelhar et al. (1992) give values for the vertical transversal dispersivity of approximately 2 mm to 7 cm for the most reliable tracer tests (Cape Cod and Borden). In this analysis, we use the lower value as that is the most conservative.

For the first path line, the concentration profile as function of a number of rescaled travel distances is shown in Figure 3.10.

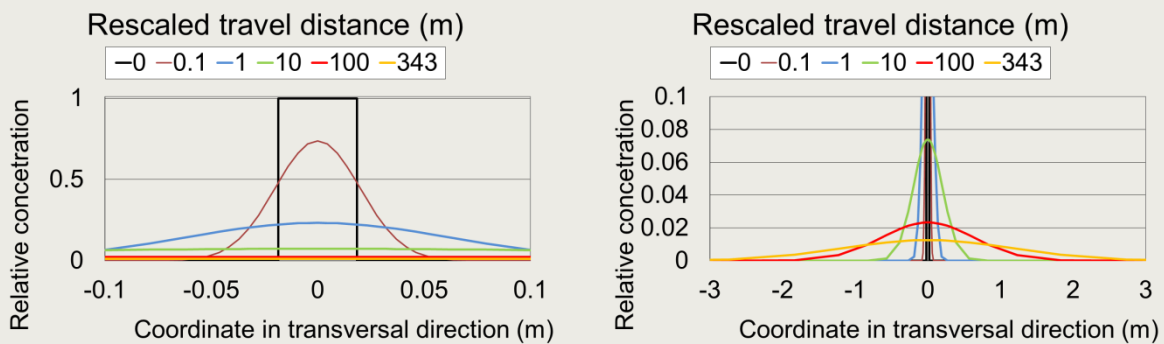


Figure 3.10 Relative concentration profile in transversal direction as function of rescaled travel distances for the first selected path line; Right figure has a rescaled x- and y-axes.

The concentration at the center of the profile after the rescaled distance of 343 m was reduced to 1.3% of its initial value due to the transverse spreading. The total mass flux is not reduced due to transversal mixing as the plume has become thicker. For pathline 2, the maximum concentration after a rescaled travel distance of 578 m is reduced to 28% of its initial value. For pathline 3, the maximum concentration after a rescaled travel distance of 278 m is reduced to 0.9% of its initial value.

4. Scenario calculations

4.1. Scenario descriptions

Within OPERA a normal evolution scenario and altered evolution scenarios have been defined (e.g. ten Veen et al. 2015). The impact of these scenarios on the hydrogeological system in a general sense is discussed briefly in this section. The translation of these scenarios into the hydrogeological model is discussed in the next section.

4.1.1. Normal evolution scenarios

The normal evolution scenarios are defined as a sequence of the following different climate conditions:

- 1 moderate climate (present day),
- 2 cold climate without ice cover (permafrost),
- 3 cold climate with ice cover (glaciation),
- 4 warm climate.

Moderate climate:

For this climate, the existing hydrogeological situation with the present human impact is used.

Cold climate without ice cover (permafrost)

In the permafrost climate, the moisture in the soil and subsoil freezes to a considerable depth. It may thaw in summer but only for a few surface feet at maximum (ten Veen et al., 2015). In general, precipitation will not be able to reach the deeper groundwater and will be discharged as overland flow to reach a surface water.

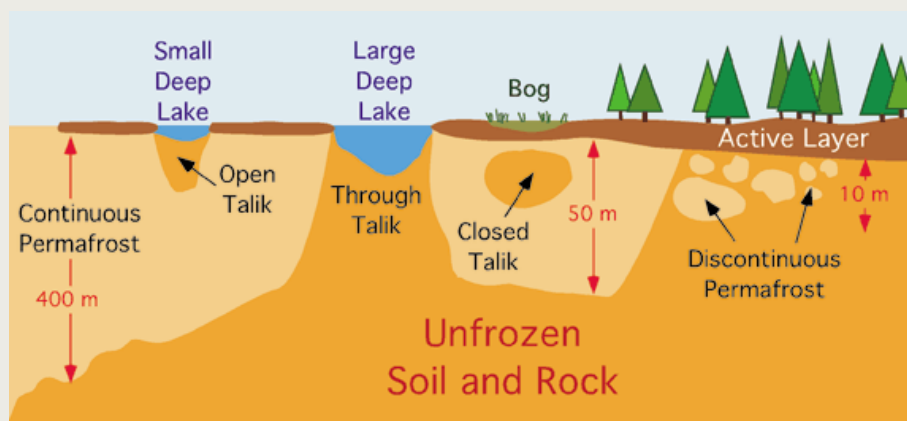


Figure 4.1 Hydrogeological schematization during permafrost. From (ten Veen et al., 2015) and (<http://www.physicalgeography.net/fundamentals/10ag.html>).

A potential connection between the biosphere and the deeper groundwater may be present in active river systems with considerable seepage whose heat flux prevents the soil to get frozen. If this potential connection is not present, the groundwater flow can be expected to be much lower as it is driven from higher groundwater tables in areas without permafrost (far away in the hinterland) towards the lowered sea level or towards active river systems.

Hence, on a larger scale the groundwater flow is expected to be dominated by recharge somewhere in the hinterland, where no permafrost conditions exist. Hydraulic heads in the hinterland are possibly also influenced by draining surface water streams, resulting in a water table in the hinterland that is close to the drainage levels of the surface water. Through the subsurface, the hinterland is hydrogeologically connected with the Netherlands. Seepage can only take place into open river systems or eventually into the sea.

The sea level can drop more than 120 m during an intense glacial cycle (Ten Veen et al., 2015; chapter 6). The sea would retreat far away from the present coast line. The hydraulic heads will drop by far less than this 120m at the present coast line (i.e. at the boundary of the groundwater model). Ten Veen et al. (2015) also report that the range of expected fluvial incision over Dutch territory does not exceed 20 m in the Southern North Sea Delta. It is assumed that river stages would drop by a few of tens of meters at most and groundwater heads near these river systems can be expected to drop by the same amount. Hydraulic heads along the present coast line will drop as well, but also not with the same amount as the drop of the sea level. When no groundwater recharge is present, the hydraulic gradient in the deeper aquifers in the direction towards the river system is likely to be small and the deeper groundwater will flow into the same direction as the active river systems.

During permafrost conditions without ice cover in the Netherlands a forebulge can develop in the Netherlands due to an ice sheet loading north of the Netherlands. A maximum forebulge uplift of 12 m is assumed for an assumed ice sheet thickness of 1500 m (proposal for the maximum ice sheet thickness in Scandinavia by Follestad and Fredin, 2011; Figure 4-3 in ten Veen et al., 2015). River systems can incise to a greater depth below ground surface due to this forebulge uplift.

Permafrost depth model calculations by Govaerts et al. (2015) indicate that the average permafrost front would reach depths of 140 and 180 m below ground surface for Weichselian temperature conditions.

Cold climate with ice cover (glaciation)

During a period with ice cover, additional water fluxes are expected to be present. When air temperatures are above zero, the ice will melt at its surface. Surface melting rates in the ablation area of the ice sheet are reported to be in the order of 1000 to 10,000 mm/year (Boulton and Curle, 1997). These authors also report that this surface meltwater can flow into the glacier through moulins but that this meltwater is discharged as surface water at the glacial surface of the ice further downstream, with the exception for a narrow marginal zone.

At the base of the glacier, water also melts due to the geothermal heat flux and by shear heating at the ice-bed interface. The rate of this basal meltwater is unlikely to exceed the range of 1 - 100 mm/year (Boulton and Curle, 1997). This water may infiltrate into the subsurface if the transmissivity in the subsurface is enough to drain this water. Otherwise, it may flow in a thin layer between the ice bed interface or through channels. The assumption in model calculations in Boulton and Curle (1997) is 25 mm/year.

Another flux is caused by consolidation of the subsurface due to the load of the ice sheet. The porosity will decrease and a volume of water equal to the decrease in the porosity is squeezed out. Depending on the soil type and the extent to which the groundwater will find its way out, this consolidation process can act as a fast or slow process. This process will cease when the soil matrix becomes able to withstand the glacial load and a new equilibrium is reached. During the retreat of the ice cap, the subsurface will rebound

partially. Although this process is described in (Boulton and Curle, 1997) it has been neglected in the modeling in their chapter. The locations of the ice cover during the last Elsterian, Saalian and Weichselian periods are shown in Figure 4.2.

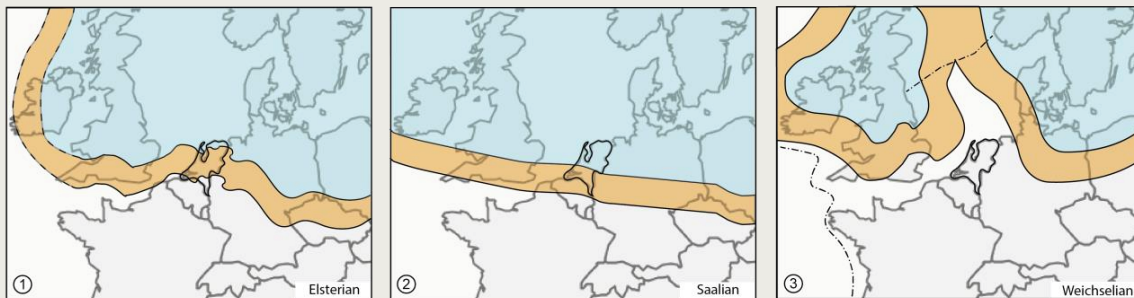


Figure 4.2 Location of the ice cover (blue) and the forebulge (orange) for three different ice-advance scenarios with analogy to the Elsterian, Saalian and Weichselian ice-sheet configurations (from Ten Veen et al., 2015)

Ten Veen et al., (2015) report in table 4.2, third scenario, a maximum ice cover thickness of 195 m for an ice cover in the northern half of the Netherlands.

In front of the ice cover, permafrost conditions can be present resulting in an impermeable upper part of the subsurface in the permafrost regions and permeable upper part related to active surface water systems.

Warm climate

For a warm scenario, different predictions for different time scale have been made:

1 For the climate change due to CO₂ increase in the atmosphere, KNMI (http://www.climatescenarios.nl/images/Brochure_KNMI14_EN.pdf) made 4 different scenarios for the periods around 2050 (between 2036 and 2065) and around 2085 (between 2071 and 2100). In the most extreme scenario W_H (warm with a large change in air circulation pattern), the average temperature increases with 3.7 °C; the sea level rises with 45 to 80 cm, the average rainfall increases with 7% (from 851 to 911 mm/year) and the potential evaporation (Makkink) increases with 10% (from 559 to 615 mm/year).

2 On the longer term climate change can even be more severe. In ten Veen et al. (2015; Chapter 12) sea level rises of a few meters to 10 m are reported for a Mediterranean type of climate and up to 60 m as an extreme case if all ice on earth will melt. In ten Veen et al. (2015) an analogue for the Mediterranean climate is given: south of Porto in Portugal with an average annual precipitation of 1236 mm/year. In <http://www.stadtklima.de/cities/europe/pt/porto/porto.htm> an annual average potential evapotranspiration of 716 mm/year is given for Porto, which is probably close to the value for the region south of Porto.

In the second scenario, it seems unlikely that the present coast line in the Netherlands will still be present and large parts of the Netherlands will have been reclaimed by the sea.

4.1.2. Altered evolution scenarios

Deep well

A deep well can influence the water fluxes near the interface of the Rupel Clay as well as increase the hydraulic gradient over the Rupel Clay. This deep well could be anywhere in

the country at depth where an attractive aquifer is present. The effect of such well is expected to be highest close to the well location.

Glacial valley

During a period of deglaciation, melt water may erode the subsurface below the ice coverage locally. In a later stage these valleys are filled up with new deposits. Tunnel valleys created during the Elsterian ice age reach depths of about 500 m below the present land surface in the Northern part of the Netherlands (ten Veen et al., 2015). Tunnel valleys can have lengths of up to more than a hundred kilometers and width of a few kilometers (ten Veen et al., 2015).

Fault

Bense et al. (2003) describe fault properties for faults in the Roer Valley Graben. They report a fault width of 5 m, a reduction in horizontal hydraulic conductivity of more than 2 orders of magnitude for a fault zone crossing a sandy aquifer, and an increase in vertical hydraulic conductivity in the fault zone. They also report that effects of clay smearing or juxtaposition of aquitards and aquifers may be an important reason for increased flow resistance. Although not mentioned in Bense et al. (2003), it seems likely that for clayey layers no increase in the vertical hydraulic conductivity takes place.

4.2. Model set up and results

The above scenarios were translated into the subsurface flow model. The model of the present day situation was already described in chapters 2 and 3. For each scenario, all adaptations from the model and the model results are described in the following sections.

4.2.1. Scenario 1: Moderate climate (present situation)

This scenario was already modeled in chapters 2 and 3.

4.2.2. Scenario 2: Cold climate without ice cover (permafrost)

River stages and bottom elevations

In the permafrost groundwater model, a drop of hydraulic heads of 30 m is assumed at the fixed model boundaries at the North Sea and at the river stages of the main river systems (Rhine and Meuse and Scheldt systems). The hydraulic head drop of 30 m is an assumption for the fluvial incision due to sea level drop and the forebulge uplift.

All other surface water and drainage systems that are active in the moderate climate model are inactive in this scenario.

Groundwater recharge

In areas with permafrost all precipitation is drained by surface runoff and groundwater recharge is zero. In areas with active rivers the groundwater flow is dominated by the river levels and not by recharge which thus is also assumed to be zero.

Hydraulic heads at model boundary with Germany and Belgium

During permafrost conditions hydraulic heads in Belgium and Germany are likely to drop as well but it is hard to make an estimate how large this drop will be. It is probably controlled by the river levels (that have may have declined as well) and by the groundwater levels somewhere in a far hinterland where no permafrost conditions are present.

As a worst case assumption, the boundary heads in all model layers are set equal to heads that mimic best the larger scale flow systems with minimal influences of present recharge based on present data. For the Belgium and German borders south of the entrance of the river Rhine, a fixed head boundary is set, with a hydraulic head that is 30m lower than the present hydraulic head of the lowest layer of the model in the present situation. At the German border north of the entrance of the Rhine, a no flow boundary has been implemented. In that region the hydraulic boundary heads in the present model are strongly affected by recharge and implying a similar boundary condition as for the other borders did result in unrealistic groundwater flow patterns.

Hydraulic conductivity

The hydraulic conductivity in the upper 160 m (average of the permafrost front (140-180 m) in the permafrost model) are set to zero for the entire model with an exception below river systems of the Rhine, Meuse and Scheldt.

Abstractions:

All groundwater abstractions in the present model are not present in this model scenario.

Results

For the same starting locations as in the reference model, pathline calculations were performed for this scenario. For each xy-location, pathlines were started at the top and bottom of the Boom Clay and the one with the shortest travel time was considered as the critical pathline. The critical travel time for a single xy-location is compared with the model results for the present situation that was reported in chapter 3. A limited number of pathlines that ended at a lateral outflow model boundary was excluded from the analysis. The same procedure was repeated for all geological scenario calculations. The comparison in travel times is shown in Figure 4.3.

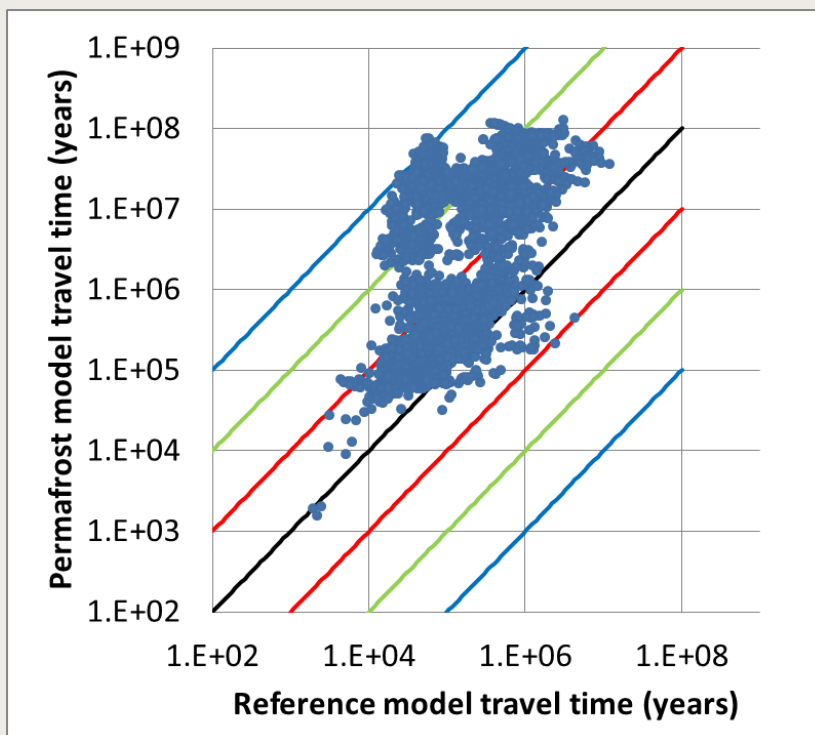


Figure 4.3 Comparison of the critical travel times for the permafrost scenario and the model for the present situation

The black line in this figure denotes equal travel time in both models. For circles on the lower-right side of this line, it means that the travel time is shorter in the geological scenario and in the upper left side the travel time is larger. The red green and blue lines denote a travel time ratio of 10, 100 and 1000 or 0.1, 0.01 and 0.001. In this scenario, the maximum reduction factor of the travel time is approximately 11, but for most of the starting locations the travel time is increased considerably. This outcome is to be expected as hydraulic gradients in the subsurface have decreased in general due to the absence of groundwater recharge, abstraction wells and anthropogenic drainage levels. Locally, the flow over the Boom Clay has become upwards which can result in a lower travel time towards the surface for pathlines starting in these areas. The regions where the flux over the Boom Clay has become upward are related to the locations of the active river systems.

4.2.3. Scenario 3: Cold climate with ice cover (glaciation)

Ice cover

The glacial extent in the model is set north of the present Rhine, Nether Rhine and Lek rivers and the maximum ice cover thickness is set to 195 m (see ten Veen et al., 2015, table 4.2: third scenario) at the northern edge of the Netherlands diminishing to zero at the ice sheet margin, see Figure 4.4. Its melt water flux is 25 mm/year for the entire area and this flux is forced into the upper layer as long as the groundwater pressure does not exceed the ice pressure.

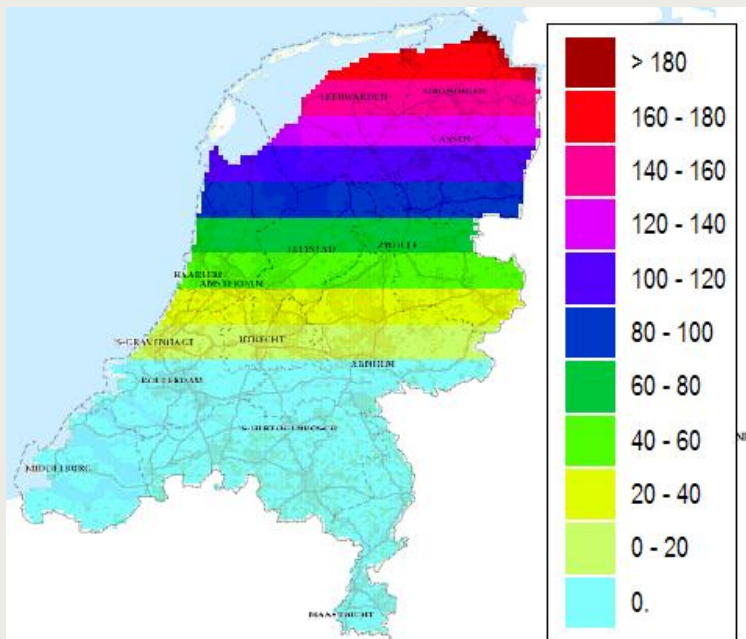


Figure 4.4 Ice thickness (m) in scenario model

The boundary conditions in the part with the ice cover are not known beforehand and depend on how well the melt water is drained by the subsurface. It is to be expected that part of the meltwater from the area north of the Netherlands enters the subsurface and flows south toward the Netherlands. As a worst case the hydraulic heads at the northern boundary are set equal to the pressure of the ice cover for all model layers. The eastern and western boundaries in the area with the ice cover are set to no flow boundaries. These boundary conditions are based on a north-south flow direction that can be expected for the Saalian analogy in Figure 4.2.

The pressure of the ice cover forces a flux of groundwater out of the pores. The amount of water that is replaced during a period with ice coverage is calculated using the porosity-depth relationships described in section 2.2.4. This amount is translated into a source flux of each individual model cell, by dividing this amount of water with an assumed period of the ice coverage of 20,000 year. The porosities and hydraulic conductivities in this region are also updated using the relationships given in section 2.2.4.

Permafrost region

The other part of the model domain is assumed to be a permafrost region with the exception of the Rhine (without the IJssel), Maas and Scheldt river systems. This region of the model has the same changes as the permafrost model.

Results

The comparison of the critical travel time between this scenario and the present day model is shown in Figure 4.5.

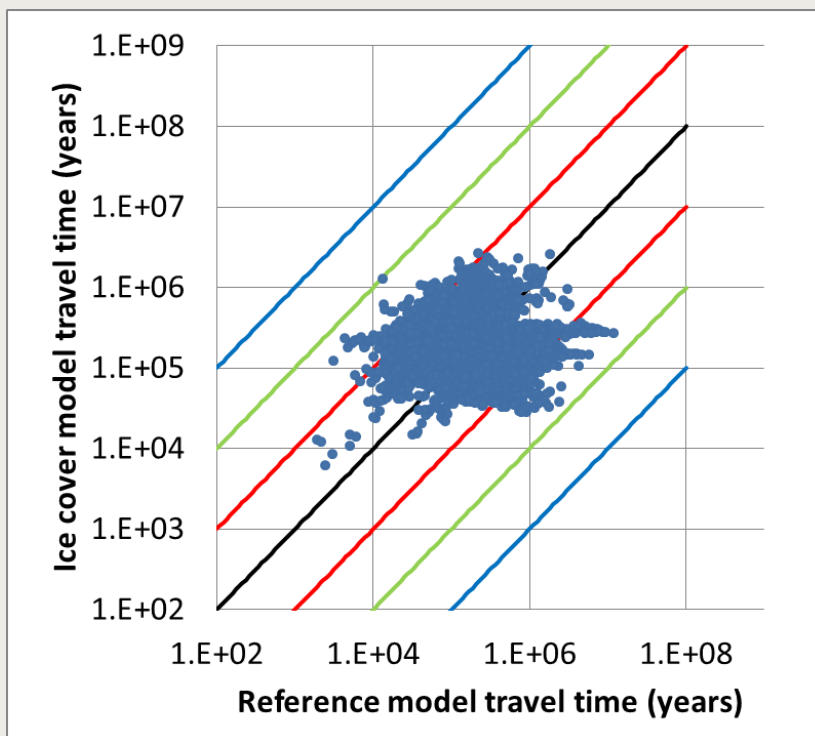


Figure 4.5 Comparison of the critical travel times for the ice cover scenario and the model for the present situation

Also in this scenario the travel time for various pathlines can either increase or decrease in comparison with the model for the present situation. The maximum reduction factor of the travel times is approximately 63. It should be remarked that most of the modeled travel times exceed the period of 20,000 years of the assumed ice cover period and for which the water flux from the consolidation of the Boom clay was based on. This also holds for all pathlines in which the travel time for the ice cover scenario is at least ten times smaller than the model for the present day situation.

4.2.4. Scenario 4: Warm climate

Both warm climate scenarios are modeled:

Scenario 4a: Climate Change prediction W_H of KNMI

In this scenario, the sea level is assumed to increase with 0.80 m, the groundwater recharge is assumed to increase with 4 mm/year (based on the increase in precipitation minus the increase in the potential evaporation). River levels in the major river systems (Rhine, Meuse, Scheldt) as well as in the IJssel lake are increased with 0.8 m. The other surface water levels are not changed. All other model input is not changed.

Results

The comparison of the critical travel time between this scenario and the present day model is shown in Figure 4.6.

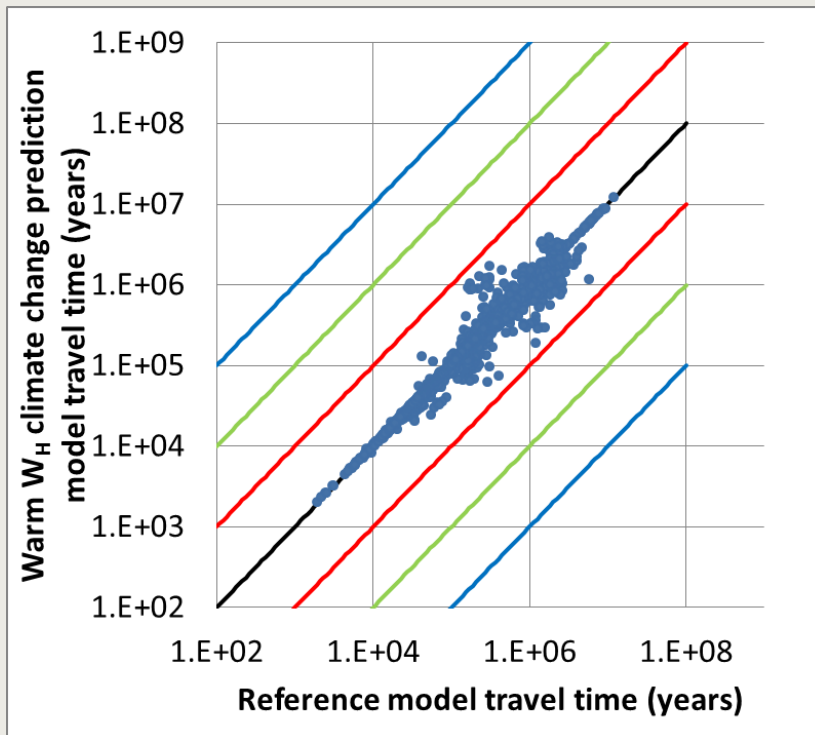


Figure 4.6 Comparison of the critical travel times for the warm scenario with the climate change prediction W_H of KNMI and the model for the present situation

In this scenario, the modeled travel times for the various pathlines have also increased or decreased compared to the model for the present day situation. The maximum reduction factor of travel times is approximately 6.5 for this scenario.

Scenario 4b: Mediterranean Climate

In this scenario, the sea level rise is assumed to be 10 m, based on the upper margin for the Mediterranean Climate. The part of the model domain with an elevation below 10 m above the present mean sea level is modeled with a constant head boundary of 10 m above the present mean sea level in the upper layer of the model. This area is shown in Figure 4.7. River and drain stages in all layers which were lower than 10 m in the present day model are set equal to 10 m. All groundwater abstractions in the flooded area are turned off.

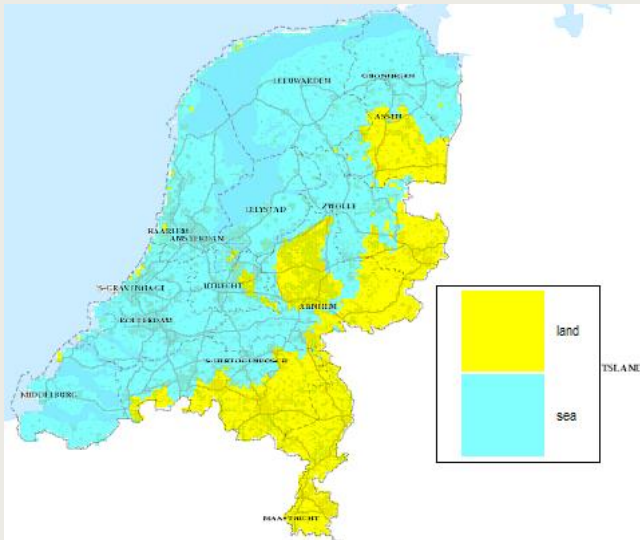


Figure 4.7 Area reclaimed by the scenario in the warm, Mediterranean scenario

For groundwater recharge, we assume a value of 520 mm/year based on an average annual precipitation of 1236 mm/year and an actual evaporation that is equal to the potential evapotranspiration of 716 mm/year.

The boundary condition in Germany and Belgium are set equal to 10 m above the present mean sea level in case the value in the reference model was lower; otherwise the boundary head remains unchanged.

Other input parameters remain unchanged.

Results

The comparison of the critical travel time between this scenario and the present day model is shown in Figure 4.8.

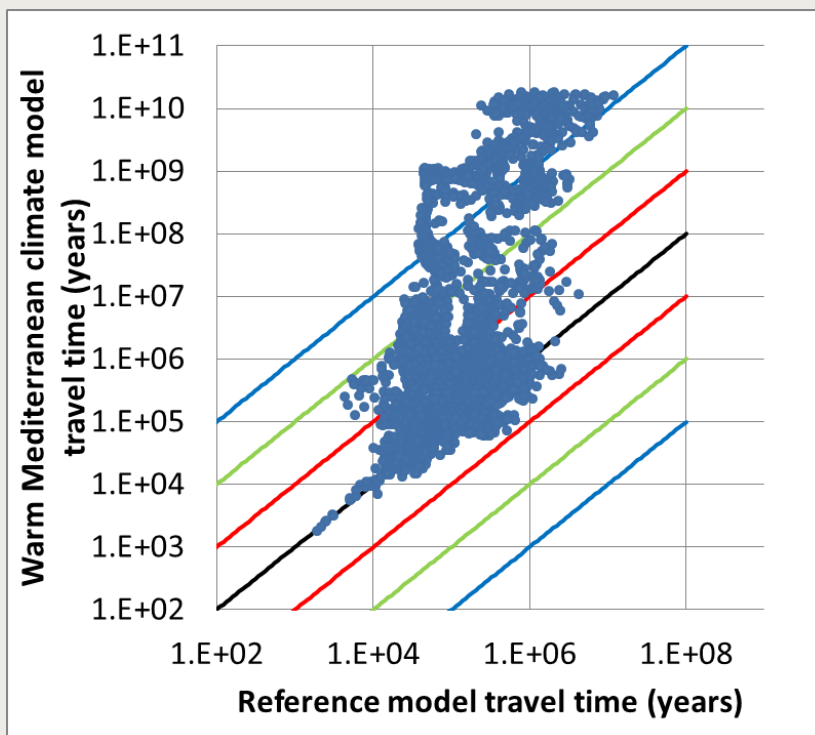


Figure 4.8 Comparison of the critical travel times for the warm, Mediterranean climate scenario and the model for the present situation

In this scenario, most of the modeled travel times for the various pathlines have also increased compared to the model for the present day situation. This is due to the severe reduction in hydraulic gradients for the part of the Netherlands that was reclaimed by the sea due to the 10 m sea level rise. The maximum reduction factor of the travel times is approximately 7.3 for this scenario.

4.2.5. Altered evaluation scenarios

Deep well

This scenario includes a well in the center of the country at a depth of 500 m with a maximum drawdown in the model of 10 m. The well location is selected in a region where pathline calculations are started and thus the effect on travel times of pathlines starting near such a well is expected to be large. The deep well location is shown in Figure 4.9.



Figure 4.9 Location of the well in the deep well scenario

Results

The comparison of the critical travel time between this scenario and the present day model is shown in Figure 4.10.

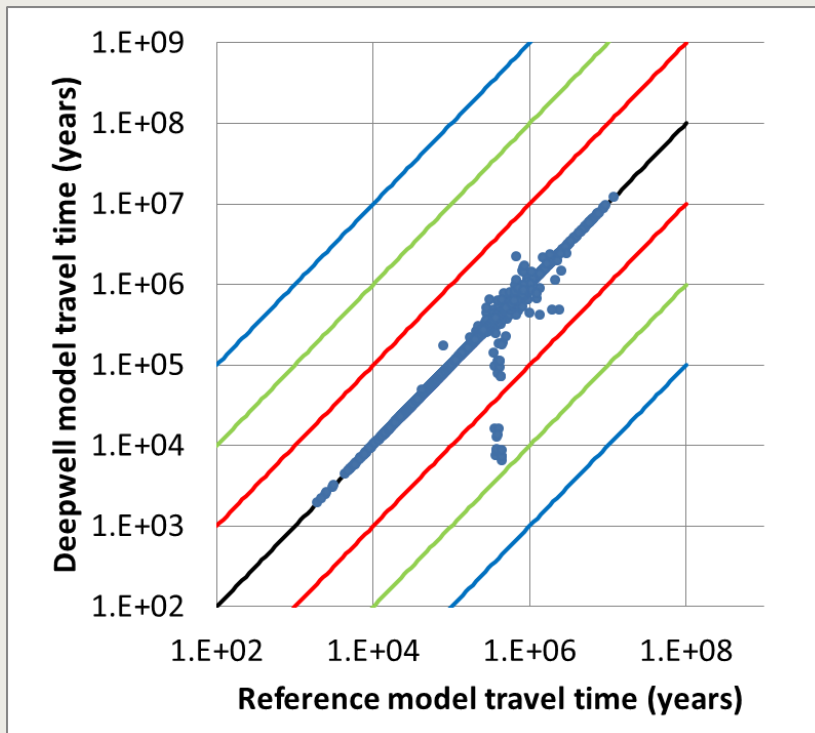


Figure 4.10 Comparison of the critical travel times for the ice cover scenario and the model for the present situation

In this scenario, most of the travel times are approximately equal to the travel times of the present day situation. Only pathlines with starting locations near the deep well are impacted significantly. The maximum reduction factor in travel time is approximately 72.

Glacial valley

In this model scenario, a glacial valley of 500 m depth, 5 km wide, 50 km long oriented north to south in the Northern part of the Netherlands is added. Two different scenarios for this glacial valley are modeled: (a) the valley is filled up with coarse sand and other conditions are similar to the present day moderate climate model and (b) the valley is filled up with ice with a melt water rate of 25 mm/year and other conditions similar as in the glacial scenario. The location of the modeled glacial valley is shown in Figure 4.11.



Figure 4.11 Location of glacial valley in the model scenario

Results

The comparison of the critical travel time between these scenarios and the present day model is shown in Figure 4.12 for the glacial valley filled up with sand and in Figure 4.13 for the glacial valley with ice cover.

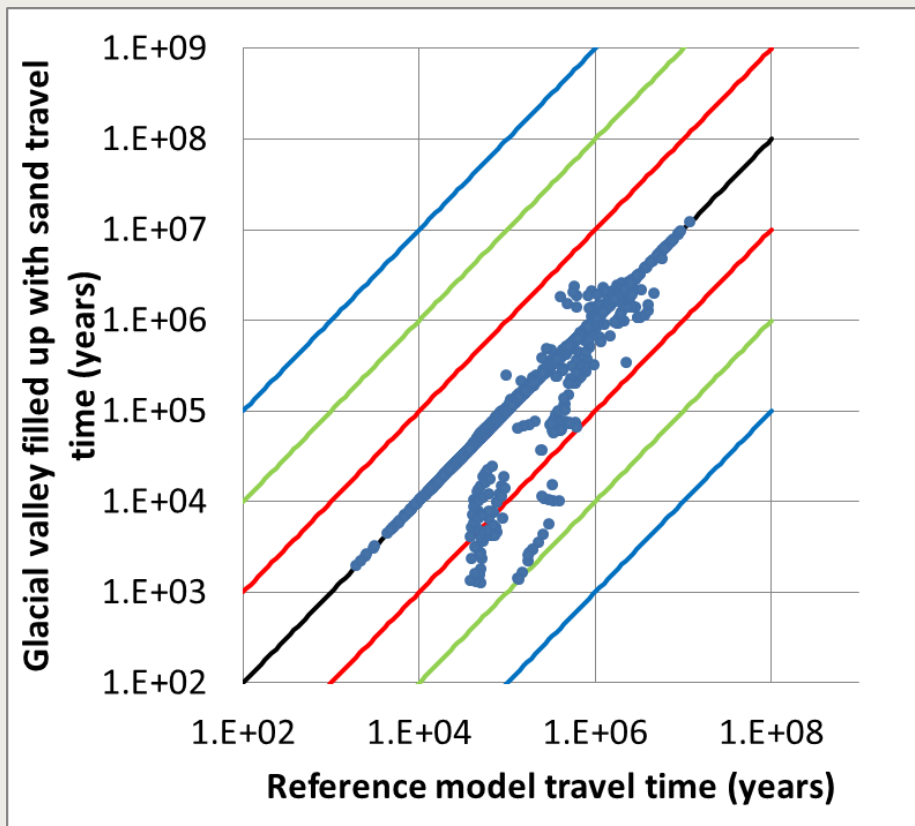


Figure 4.12 Comparison of the critical travel times for the glacial valley filled up with sand scenario and the model for the present situation

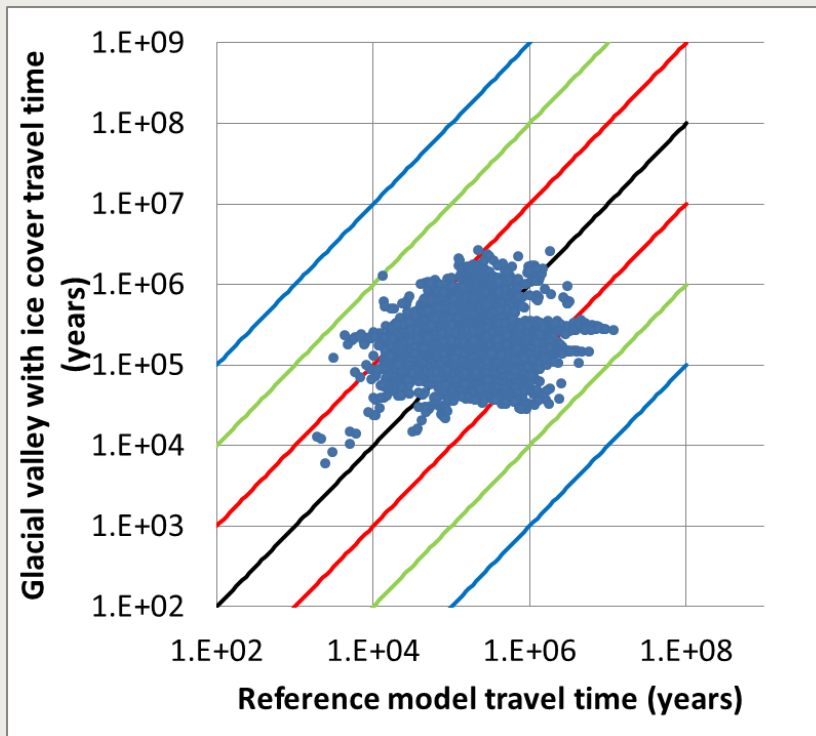


Figure 4.13 Comparison of the critical travel times for the glacial valley with ice cover scenario and the model for the present situation

In the scenario with the glacial valley filled up with sand, only pathlines close to the glacial valley are affected. The chosen location of the glacial value here too has a dominant impact which pathlines are strongly affected. The maximum travel time reduction factor for the scenario glacial valley filled up with sand is approximately 94. For the glacial valley scenario with ice cover, the results are very similar as for the ice cover scenario that was shown in Figure 4.5. The maximum travel time reduction factor is 63.

Fault

One fault was added to the model. The width of the fault is assumed to be 5 m, which is smaller than the resolution of the model grid. The location of the simulated fault is shown in Figure 4.14.



Figure 4.14 Location of the simulated fault

The horizontal hydraulic conductivity in the fault $k_{h,fault}$ is decreased by a factor 100 compared to its original value $k_{h,original}$. The effective horizontal conductivity $k_{h,eff}$ is obtained with the upscaling equation for serial flow:

$$\frac{250m}{k_{h,eff}} = \frac{5m}{k_{h,fault}} + \frac{245m}{k_{h,original}}$$

Using a reduction factor for the fault hydraulic conductivity of a factor 100, the effective horizontal hydraulic conductivity perpendicular to the fault becomes approximately 33% of its original value.

The vertical hydraulic conductivity at the fault is set at 10 times its original value for all layers except for clayey layers (Veldhoven Clay Member and Rupel Clay). The effective vertical hydraulic conductivity is obtained with the upscaling equation for parallel flow:

$$k_{v,effective} = \frac{5m}{250m} k_{v,fault} + \frac{245m}{250m} k_{v,original}$$

The effective value for the vertical hydraulic conductivity in the model cells with the fault is 18% larger than its original value.

Preferential flow in the vertical direction is expected to take place as the hydraulic conductivity in the fault is assumed to be 10 times larger than its original value. However due to the model grid resolution of 250 m this effect cannot be modeled directly, but applying a worst-case assumption that a pathline would remain in the more permeable part of the fault as long as it is in a model cell with a fault an indirect approximate approach can be used by applying a smaller porosity for these model cells.

Within each model cell with a fault the vertical flow contributions are obtained:

$$q_{v,fault} = \frac{5m \cdot k_{v,fault}}{245m \cdot k_{v,original} + 5m \cdot k_{v,fault}} q_{v,total}$$

$$q_{v,non-fault} = \frac{245m \cdot k_{v,original}}{245m \cdot k_{v,original} + 5m \cdot k_{v,fault}} q_{v,total}$$

Applying the assumption that the vertical conductivity through the fault is 10 times its original value makes that 17% of the vertical flux in the model cell flows through the fault and 83% flows through the remaining part of the model cell. As the fault contributes only 2 % of the cell area makes that the flow velocity in the fault is approximately 8.5 higher than it would be in a homogeneous model cell. By reducing the porosity in the model cells that contains the fault with a factor 8.5, an increase in the vertical velocity of a factor 8.5 is also obtained. This approach will underestimate the travel time slightly as in a more detailed resolution, the pathline would also go through the non-fault part of the model cell.

Results

The comparison of the critical travel time between this scenario and the present day model is shown in Figure 4.15.

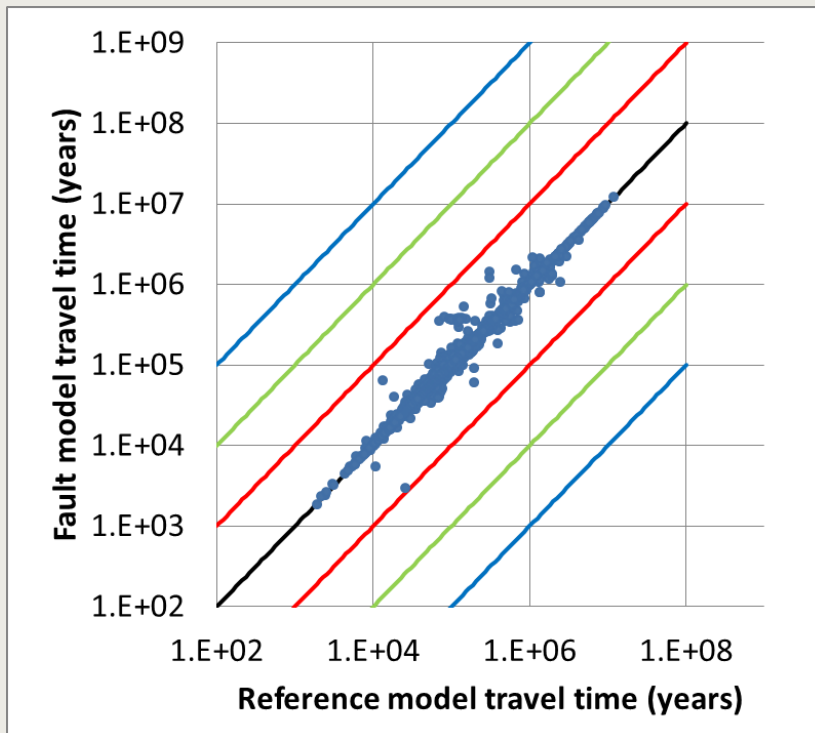


Figure 4.15 Comparison of the critical travel times for the fault scenario and the model for the present situation

Also for this scenario, only the pathlines close to the fault are affected and most of the pathlines' travel times are not affected. The maximum reduction factor in travel time in this scenario is approximately 8.7.

4.3. Discussion

For these calculations, the following remarks are made:

1. In many geological scenarios, the location of the new or adapted feature is chosen arbitrarily, such as the locations of the active river systems under permafrost or ice cover conditions, the deep well, the fault, the glacial valley, etc. The pathlines for which the calculated critical travel times changed significantly also depend on the chosen locations for these geological features. Therefore, no relation between the calculated changes in travel time and the starting location of the pathlines are presented here. The relevant model outcome here is to give a first estimate of the potential effect of each of the geological scenarios.
2. Moreover, most of the calculated travel times are longer than the feature is likely to exist, such as the duration of the ice cover or the life span of a deep well. For future calculations, it is recommended to incorporate this temporal variation.
3. Some of the scenario results strongly depend on the boundary conditions, such as the hydraulic heads in the various model layers in Germany, Belgium and at the present coast line. A model with an extended model domain would help to obtain more realistic head pressures near the present model boundaries.
4. The translation from geological scenarios to hydrogeological models required many subjective choices. These choices required insight from many different disciplines. In this study, these choices were made from the viewpoint of the hydrogeological modeling after gaining some insight into the other disciplines and agreed upon by

partners from other work packages within the OPERA program. Some of these choices needed to be adjusted by analyzing intermediate model results. For the future, a thorough review of the required and relevant model assumptions as well as the intermediate and final results by experts from the different disciplines is recommended.

5. Parameter sensitivity scenarios

Unfortunately, no uncertainty bounds for the model parameters such as the hydraulic conductivity could have been obtained. As mentioned in Chapter 2, a difference in Boom Clay vertical hydraulic conductivity values of two orders of magnitude was observed between mud and non-mud samples. For other formations, no comparison with more detailed information is readily available. Therefore, it was decided to perform a sensitivity analysis on the hydraulic conductivity which is commonly considered as the parameter that gives most uncertainty on model results in geohydrological models. For all hydraulic conductivities that were derived from the depths and the lithology, which were not available in the database REGIS, the hydraulic conductivity values in horizontal and vertical direction were multiplied with a factor 10 and the residence time of each pathline was compared with the base model. The results are shown in Figure 5.1 for horizontal hydraulic conductivities and in Figure 5.2 for vertical hydraulic conductivities.

Also some statistical values of the sensitivity are given. In order to give an increasing and decreasing factor of the travel time an equal impact, $^{10}\log$ values of the relative travel times (travel time in the sensitivity model run, divided by the travel time of the reference model run) were calculated and statistically analysed. The results are shown in Table 5.1.

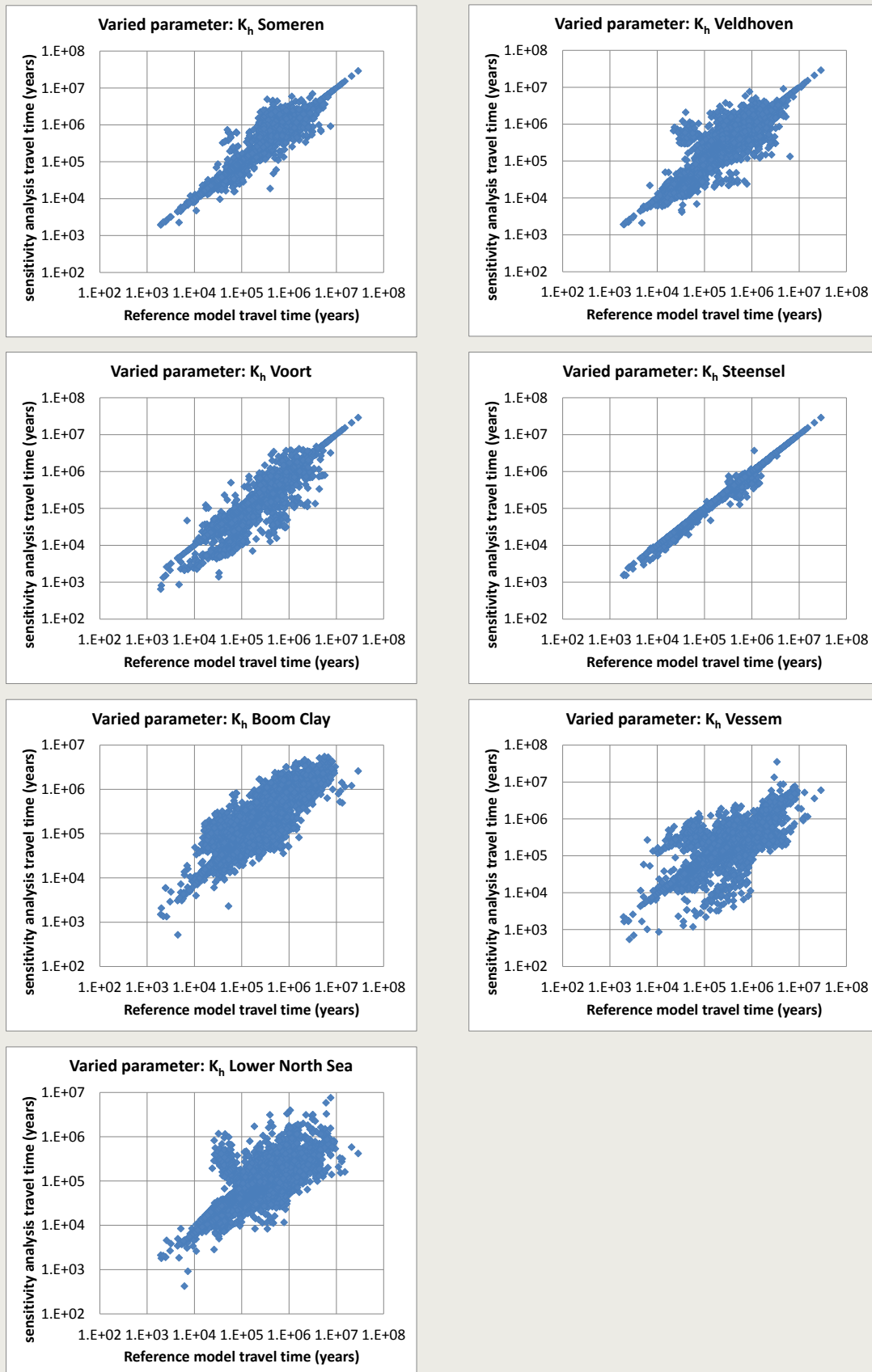


Figure 5.1 Comparison of total travel time for sensitivity model runs with the reference model for the horizontal hydraulic conductivity

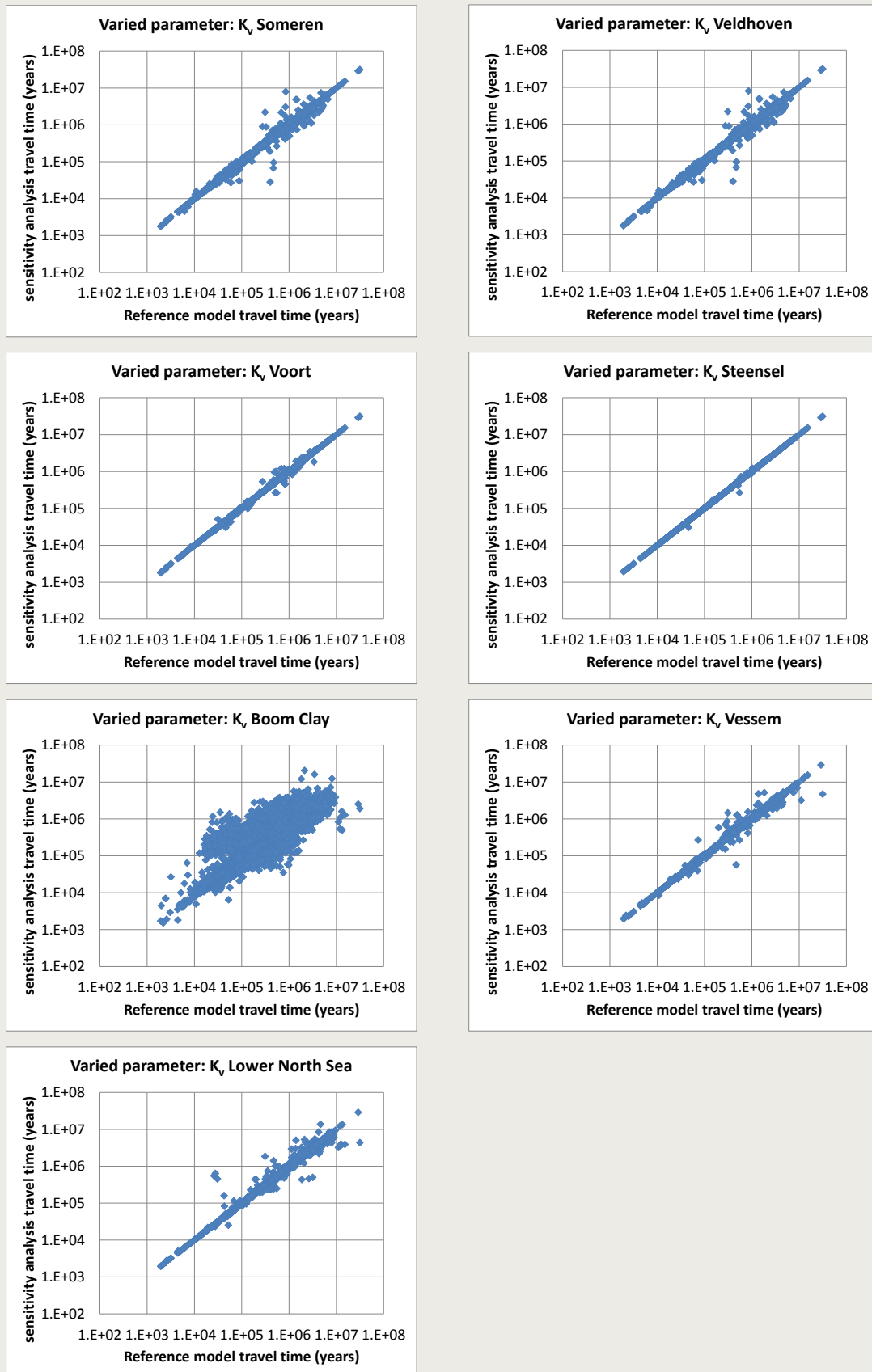


Figure 5.2 Comparison of total travel time for sensitivity model runs with the reference model for the vertical hydraulic conductivity

Table 5.1 Statistical values of sensitivity: $^{10}\log$ values of relative travel time of individual pathlines (travel time in adapted model divided by the reference travel time) to horizontal (k_h) and vertical (k_v) hydraulic conductivity (parameters were increased by a factor 10).

Formation	k_h		k_v	
	mean	standard deviation	mean	standard deviation
Someren	0.000	0.016	-0.001	0.001
Veldhoven	-0.003	0.055	-0.001	0.001
Voort	-0.073	0.035	0.000	0.000
Steensel	-0.008	0.002	0.000	0.000
Boom	-0.093	0.062	-0.027	0.067
Vessem	-0.200	0.072	0.000	0.001
Lower North Sea	-0.445	0.095	0.000	0.002

The sensitivity of the travel time of the individual pathlines is hard to predict beforehand. When changing one of the hydraulic conductivity values, the flow velocities are adapted. Although the overall flow resistance in the subsurface is decreased when increasing the hydraulic conductivity, flow velocities may decrease in some part of the model domain resulting in larger travel times of some of the pathlines and also pathline trajectories of individual particles may go through regions with a lower flow velocity.

From the sensitivity analysis, it follows that on average the travel time is more sensitive to the horizontal hydraulic conductivity in comparison with the vertical hydraulic conductivity. For the vertical hydraulic conductivity, the Boom Clay has the largest sensitivity by far. The negative values of the mean $^{10}\log$ values of the relative travel times in indicates that on average the travel time decreases when increasing the hydraulic conductivity .

In general, the travel times are more sensitive to the hydraulic values of the Boom Clay and the layers below in comparison with the model layers above. At first sight the sensitivity of the travel times to the horizontal hydraulic conductivity of the Boom Clay is surprising as the pathline mainly go vertical through the Boom Clay. However, after the multiplication of the horizontal hydraulic conductivity of the Boom Clay by a factor 10, that transmissivity (horizontal conductivity times the thickness) of the Boom Clay becomes of the same order as the values of the layers below (Vessem en Lower North Sea), which can be seen by combining the information from the figures of the thicknesses in Figure 2.12 to Figure 2.14 and the hydraulic conductivity of these layers in Figure 2.24 to Figure 2.26. It results in a change in the flow pattern in these lower three layers and consequently also in the travel times. As a check the same procedure was done when decreasing the horizontal hydraulic conductivity of the Boom clay by a factor 10. The mean and standard deviation of the $^{10}\log$ values of relative travel time of individual pathlines then became: 0.009 and 0.007. The large sensitivity of the travel time to the horizontal hydraulic conductivity of the Lower North Sea Group indicates that it is to be recommended to characterize the formation and Formation Members in this group in more detail.

6. Conclusions and recommendations

6.1. Conclusions

With the present model analysis, the following conclusions can be drawn:

1. The availability of data in the deeper subsurface on the scale of the entire country is relatively limited. Many simplifications and assumptions needed to be made in order to build a numerical model. A model simplification that is expected to have a considerable influence on the model output is the negligence of heterogeneity within the deeper formations, due to a lack of nationwide data.
2. Nevertheless, it has been possible to build a groundwater flow model of the entire Netherlands that extends in depth beyond the Boom Clay.
3. Good data for model validation is lacking, especially if one considers that transport of the time scale of the order of 100.000 years is the purpose of the model.
4. The conservative travel times of particles starting at the interface between the Boom Clay and surrounded aquifers, as on locations that meet the present requirements of the repository, range from 1000 to over 10 million years, with the majority of the travel times of these pathlines exceeding 100.000 years. Due to the uncertainty in the model's set-up, these values should be considered as a first, order of magnitude, estimate for conservative travel times only.
5. In the present model, the groundwater flow in the deeper aquifers is small, with velocities sometimes lower than 0.1 m/year.
6. Boundary conditions in Germany and Belgium seem to have a negligible impact on the hydraulic head distribution in the deeper aquifers in the model for the present situation.
7. When using hydraulic conductivity values that are based on the mud samples (about 100 times lower than hydraulic conductivity values of the reference model), the residence time in the Boom Clay increases significantly.
8. The effects of existing faults and density effects due to the present distribution of fresh and saline water, sea water intrusion as well as dissolution at salt domes are not incorporated in the model due to a lack of data. These processes are expected to have an important effect on the groundwater flow.
9. Transversal dispersion will cause mixing of the radionuclide plume and decrease the maximum concentration at the arrival location, but it will not decrease the total nuclide mass flux. The concentration at arrival at the biosphere for the three pathlines analysed decreased 0.9%, 1.3% and 28% as compared to the starting concentration at the interface with the Boom Clay due to transversal mixing only.
10. Geological scenarios have been analysed using stationary flow assumptions. In reality, the travel time of the radionuclides will often be larger than the expected duration of the geological scenario such as an ice age. Nevertheless it gives insight which conditions can have a strong impact on the nuclide residence times. For all scenarios, it holds that the travel time could both decrease or increase depending on the starting location of the pathlines and the location of geological features such

as ice cover, incised rivers, deep well, glacial valleys or faults. The scenarios with ice cover (maximum reduction factor of the travel time (MRF) = 63), deep well (MRF=72), glacial valley without ice cover (MRF = 94) and glacial valley with ice cover (MRF=63) resulted in a larger potential negative impact than the scenarios permafrost (MRF = 11), warm, KNMI W_H scenario (MRF =6.5) , warm Mediterranean climate (MRF = 7.3) and fault (MRF = 8.7). Scenarios with a single local feature such as the deep well, the glacial valley without ice cover or fault resulted only in affected pathlines close to this single feature, but similar effects could be expected on other locations if these single features would have been located around there.

11. The sensitivity analysis of the hydraulic conductivity data showed that the travel time is more sensitive to the horizontal hydraulic conductivities than to the vertical hydraulic conductivities. Only for the boom Clay the vertical hydraulic conductivity is also sensitive. The Lower North Sea Group showed the largest sensitivity for the horizontal hydraulic conductivity.

6.2. Recommendations

1. As the availability of data in the deeper subsurface on the scale of the entire country is relatively limited, it is recommended to put more emphasis on analyzing existing available data and on acquisition of new data. Especially, more data about the formations within the Lower North Sea Group could improve the geological model.
2. The impact of heterogeneity within the geological formations should in some way be taken into account. As it will be unlikely that it will be possible to collect all data to build a full deterministic model, data collection and analysis should also focus on stochastic modelling. Questions that arise are: What is the size of relevant features within a formation that need to be analysed^d? What are the extensions and probability of these relevant features and how do we upscale these feature in a model of the national scale.
3. The hydraulic conductivity of all model layers that were added to the NHI model, are derived using the lithology-depths relations supplied by TNO. For the vertical hydraulic conductivity of the Boom Clay, estimates presented in Vis and Verwey (2014) varied by approximately 2 order of magnitude for the ‘mud’ and ‘non-mud’ samples. Validation of these numerical values including comparison with values used in Belgian and German model studies is recommended.
4. Model validation could be done using groundwater age data. It would, however, require a model which takes into account the time varying human and climate interference with the hydrology. Another option would be to validate the hydraulic head difference over the Boom Clay in combination with groundwater flow velocity data in or underneath the Boom Clay.
5. For some geological scenarios, water fluxes over the boundaries of the present model are very important and they ideally should be obtained from a model with a larger domain in future studies. An example is the cold climate without ice cover (permafrost) scenario in which the effect of rivers beyond the present model boundary such as the Ems in Germany and a river system north and west of the

^d Long and thin, more permeable layers may have no effect due the transversal exchange with less permeable layers and thick

Netherlands over the present bottom of the North Sea is expected to influence the water flow near the present model boundaries considerably.

6. The effect of the interplay between the different geological conditions and their temporal variability should be analyzed in more detail. An example is the depth of the permafrost in front of a slowly backward and forward moving ice cap. Moreover the pathline calculations should be adapted to deal with different flow fields during the time of interest for nuclide transport, including the dealing with the uncertainty on the arrival time of the nuclides at the interface of the Boom clay and the effect of different sorption characteristics on nuclide transport.
7. The translation from geological scenarios to hydrogeological models required many subjective choices. These choices required insight from many different disciplines. In this study, these choices were made from the viewpoint of the hydrogeologic modeling after gaining some insight into the other disciplines and these choices were summarized in a short memo and agreed upon by partners from other work packages within the OPERA program. Some of these choices needed to be adjusted by analyzing intermediate model results. For the future, a thorough review of the required and relevant model assumptions as well as the intermediate and final results by experts from the different disciplines is recommended.

7. References

Bense V., van Balen R., de Vries J., 2003. The impact of faults on the hydrogeological conditions in the Roer Valley Rift System: an overview, *Netherlands Journal of Geosciences / Geologie en Mijnbouw* 82 (1): 41-54.

Boulton G., Curle F., 1997. Simulation of the effects of long-term climate change on groundwater flow and the safety of geological disposal sites, Final report, contract no F12W-CT90-0046, EUR 17793 EN, 308 pages.

Follestad, B., Fredin. O., 2011. Geometry and vertical extent of the late Weichselian ice sheet in northwestern Oppland County, Norway. *Norges geologiske undersøkelse Bulletin*, 451: 1-19.

Appendix of OPERA-PU-TNO421: Govaerts J., Beerten K., Ten Veen J., 2015. Numerical simulation of Permafrost Depth in the Netherlands, SCK•CEN-R-5848, 44 pages.

Ten Veen J., Govaerts J., Beerten K., Ventra D., Vis G., 2015. Future evolution of the geological and geohydrological properties of the geosphere, OPERA-PU-TNO412 2015-07-17, 121 pages.

Verhoef, E. Neeft, E., Grupa, J. and Poley, A., 2011. Outline of a disposal concept in clay, OPERA-PG-COV008, 17 pages, first revision from 2014 published

Vis G, Verwey H, 2014, Geological and geohydrological characterisation of the Boom Clay and its overburden OPERA-PU-TNO-411, 86 pages

8. Addendum

8.1. Introduction

In chapter 2 - 6 of this report, the hydrological transport in the rock formations surrounding the host rock has been described. The results from these chapters have been used in Work Package 7 (WP 7) within the OPERA project. The translation from the detailed hydrogeological model to the more simplified model of WP 7 does sometimes require some more insight and detailed output of the calculations that were not been reported in chapters 2 - 6.

Moreover, the connection with the interfacing compartments, the host rock as well as the biosphere, did require some explanation on how the results in chapters 2-6 were acquired and how they should be interpreted. These aspects are addressed in this addendum chapter. The translation of the relevant data from this addendum chapter to the PA model of WP 7 is included in this report in Appendix 3.

8.2. Additional explanation and detailed output

8.2.1. Pathlines

In section 3.3, three pathlines were selected to be used in the performance assessment (PA) calculations in WP 7. The pathlines represent a typical fast, median and slow flow path. The latter two pathlines have a significant, but not predominant, part of their residence time in the Boom Clay (Table 3.1). This is contradictionary as the conservative, advective transport of the nuclides was modelled starting when the nuclides have left the Boom Clay. Diffusive transport including any retardation of radionuclides through the Boom Clay from the repository to the interface of the Boom Clay with the overburden has been reported in OPERA-PU-NRG6131 and is conceptualized in the 'Host Rock' compartment of the OPERA PA model.

The explanation of the median and slow flow paths modeled in the 'Overburden' compartment re-entering the Boom Clay is that the median and slow pathlines have their origin at the bottom of the Boom Clay. The pathlines first go through the layers underneath the Boom Clay and further downstream they flow upwards through the Boom Clay at a location where the thickness of the Boom Clay may be less than 100 m. Pathlines starting at the top of the Boom Clay on the same horizontal starting locations have a longer travel time. Due to a downward flow through the Boom Clay at the starting location, the pathline starting at the top of the Boom Clay, directly dives into the Boom Clay and almost goes straight down to the bottom of the Boom Clay. From there on, the flow path is approximately equal to the flow path that directly starts at the bottom of the Boom Clay, but it has an additional residence time due to the transport through the Boom Clay.

An analysis of the critical travel times of all pathlines showed that some calculated pathlines starting at the interface at the top of the Boom Clay at other horizontal locations have travel times comparable to the travel times of the selected median and slow pathlines. Therefore, the total travel times for the selected fast, median and slow pathlines are also realistic values in case one would exclude pathlines that intersect through the Boom Clay somewhere downstream of the repository.

For the representation of advective radionuclide transport through the overburden in the OPERA PA-model, it is recommended to consider three different cases: a fast, a medium and a slow streamline, representative for the residence times established in Chapter 3.

Table 8.1 summarizes for each of these three cases the path length, average porosity, travel time, and ‘equivalent height’^e of the plume.

Table 8.1 Travel distances, averaged porosities, travel times and equivalent height at the interface *Host Rock - Overburden* for the three subcases of fast, medium and slow streamlines, for a moderate climate (DV)

Streamline	Path length x [km]	Porosity η_{aq} [-]	Travel time [yr]	Equivalent height H_{aq} [m]
Fast	23.3	0.38	30'700	2.84
Medium	14.0	0.28	164'000	3.86
Slow	28.2	0.30	853'000	2.67

8.2.2. Hydraulic conductivity Boom Clay

In Chapter 3, the hydraulic conductivity for the Boom Clay and the other geological layers, when not characterized in the national hydrogeological database REGIS, were based on relations between the lithology, depth, porosity and permeability provided by TNO. These relations are shortly described in paragraph 2.5.3 of OPERA-PU-TNO411^f and are valid for the non-mud samples for the Boom Clay and were also applied to the other geological formations. In OPERA-PU-TNO411 also permeability values for the mud sediments are reported, that are about 100 to 1000 times smaller than the permeability of the non-mud samples.

Unfortunately no spatial distribution of the permeability due to the variability of the texture (mud and non-mud) has been provided in OPERA-PU-TNO411, although some general trends were reported. More recent spatial analyses of this data in OPERA-PU-NRG6121, Section 4.2.2., showed that non-mud samples are mainly from the Dutch-German border region in Limburg (OPERA-PU-NRG6121, Fig. 4-3 and 4.4), or are located at the upper or lower boundaries of the Boom Clay layer (see OPERA-PU-NRG6121, Table 4.2). Some uncertainties with respect to the classification of some samples as ‘Boom Clay’ in light of the updated mapping of the Boom Clay layer in OPERA-PU-TNO411 is noted as well. It is suggested to exclude these samples from further analysis since it can be questioned whether locations with a high sand content are suitable for disposal of radioactive waste.

In Chapter 3, it was chosen to use the hydraulic conductivity values based on the non-mud samples as that choice is considered more conservative since these values are expected to lead to shorter travel times in the Overburden. In Figure 3.7, a comparison between the conservative residence times in the Boom Clay was given for the standard model and a model having a factor 100 lower hydraulic conductivity values in the Boom Clay. On average, the residence time in the Boom Clay clearly increases, but less than a factor 100. A comparison between the travel time between the Boom Clay interface and the biosphere for the reference run and a run with 100 times lower hydraulic conductivity of the Boom Clay, representing mud texture, is given in Figure 8.1.

^e The equivalent height of the plume is defined as the height of the plume in the aquifer with the highest flow velocity and for which the concentration reduction due the vertical transversal dispersion was translated into a thicker plume with uniform concentration.

^f OPERA-PU-TNO411 uses the definition Rupel Clay Member for Boom Clay

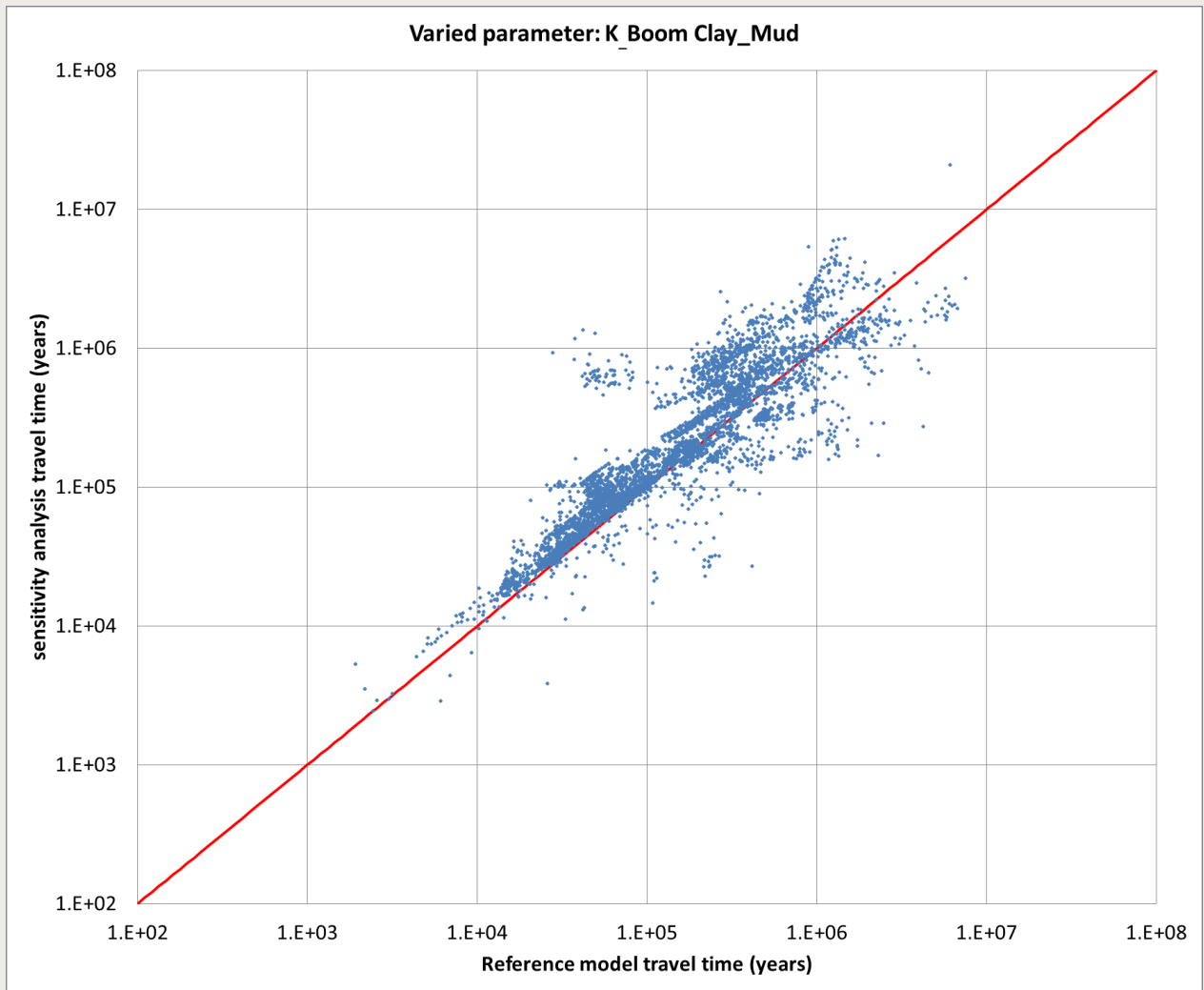


Figure 8.1 Comparison of the critical travel times for scenario with a 100 times lower hydraulic conductivity in the Boom Clay (representing mud texture) and the reference model.

In the figure, it is clearly visible that the majority of streamlines have a longer critical travel time in the model with the hydraulic conductivity based on mud texture, but the difference is much smaller than the factor of 100 with which the hydraulic conductivity in the Boom Clay was decreased. For some pathlines the critical travel time even decreased. The hydrological explanation for it is that on a larger scale the flow resistance for the deep groundwater flow (Boom Clay and below) is not only due to the flow resistance in the Boom Clay (very low conductivity but relatively small thickness and large horizontal extent) but also in the horizontal flow resistance in the layers below (larger hydraulic conductivity, but relatively large flow length and limited aquifer thickness). Increasing the resistance of the Boom Clay does not increase the total resistance of the deep groundwater flow system with the same magnitude. As an additional effect, the flow direction over the Boom Clay may change locally, and for some pathlines it can result in a much shorter critical travel time. However, the overall difference in travel times is comparable small with respect to the overall variability found.

In addition to the travel times already presented in Chapter 3, the residence time and travel distance per model layer computed for the lower permeabilities are shown in Table 8.2. The selection of the fast, median and slow pathlines are based on the 10, 50 and 90 percentiles of the critical travel time distribution using the model with the hydraulic conductivity for the mud-texture of the Boom Clay.

Table 8.2 Pathline characteristics for the fast, median and slow pathline in case the hydraulic conductivity in the Boom Clay is based on the mud texture

model layer	layer name	fast		median		slow		
		residence time (years)	distance (m)	residence time (years)	distance (m)	residence time (years)	distance (m)	
1	NHI_1	0	0	0	0	0	0	
	NHI_aquitard 1	0	0	0	0	0	0	
2	NHI_2	3.10E+01	1.00E+02	3.00E+01	1.30E+02	< 100 ^g	5.13E+02	
	NHI_aquitard 2	0	0	0	0	0	0	
3	NHI_3	1.00E+02	4.09E+02	1.00E+01	9.19E+01	1.00E+02	3.87E+02	
	NHI_aquitard 3	0	0	0	0	0	0	
4	NHI_4	4.00E+00	2.19E+00	2.00E+01	3.26E+01	1.00E+02	4.77E+02	
	NHI_aquitard 4	0	0	0	0	0	0	
5	NHI_5	2.91E+02	1.95E+02	5.00E+01	1.40E+02	1.00E+02	1.74E+02	
	NHI_aquitard 5	0	0	0	0	0	0	
6	NHI_6	2.24E+02	1.51E+02	1.70E+02	2.70E+02	5.00E+02	1.98E+02	
	NHI_aquitard 6	0	0	0	0	2.40E+02	2.66E+01	
7	NHI_7	2.29E+03	1.37E+03	2.80E+02	4.49E+02	0	0	
8	Maassluis	0	0	0	0	4.00E+02	1.95E+02	
9	Oosterhout	0	0	5.10E+03	2.00E+04	1.20E+03	7.63E+02	
10	Breda	3.41E+04	1.38E+04	8.66E+04		4.83E+04	8.14E+04	4.81E+03
11	Someren	0	0	1.48E+04		2.54E+03	0	0
12	Veldhoven	0	0	2.06E+04		5.36E+03	0	0
13	Voort	0	0	4.12E+04	1.25E+04	0	0	
14	Steensel	0	0	0	0	0	0	
15	Rupel Clay	0	0	0	0	0	0	
16	Vessem	0	0	0	0	3.04E+05	1.75E+04	
17	Lower North Sea Group	0	0	0	0	6.39E+05	4.32E+04	
	total	3.71E+04	1.60E+04	1.69E+05	8.98E+04	1.03E+06	6.82E+04	

Considering the rather small differences in travel times compared to the values given in Chapter 3 ($\leq 20\%$), and the limited influence of the travel time on the long-term safety, no adaptations of the data provided for the three identified streamlines in Chapter 3 are considered necessary for the PA-model.

^g Accuracy of the model output of travel times was given in 100 years; for this residence time a zero value was obtained, which is translated into “< 100 year”

8.2.3. Interfaces Boom Clay - Overburden - Biosphere - Local well

The connection for the different submodels for the compartment 'Host Rock', 'Overburden' and 'Biosphere' is not straightforward. After thorough evaluations, the PA model for radionuclide transport in the Boom Clay considers diffusion as the main transport process and does not include advection, whereas the PA model in the overburden translates the advection into a residence time in the various geological layers and does not include diffusion (OPERA-PU-GRS7222).

In the overburden model analyzed in Chapter 3, it was chosen to model advection through the Boom Clay as well, albeit with a lower hydraulic conductivity for the Boom Clay in comparison with the other geological formations. There are two specific reasons for this choice.

The first reason is the specific velocity interpolation in the model code MODPATH that calculates the pathlines. Local velocities within one model cell are based on a linear interpolation of the flow velocities at the six interfaces of the model cell. If neglecting advection out of the Boom Clay, for instance by giving the hydraulic conductivity value of 0, the vertical velocity at the interface with the Boom Clay will be zero and a pathline would remain at the interface of the Boom Clay until it reaches a location where the Boom Clay is absent. This would be an unrealistic outcome and unnecessarily complicate the conceptualization of the OPERA disposal concept.

The second reason is that the flux into and out of the Boom Clay over a large horizontal area is not negligible compared to the magnitude of the horizontal flux in the aquifers above and below the Boom Clay.

At the interface of the Boom Clay with the overburden, the mass flux of the nuclide in both models should be equal:

$$\int F(x,y,t) \, dy \, dx = \int v(x,y) \, c(x,y,t) \, dy \, dx$$

With: $F(x,y,t)$ = the nuclide mass flux at time t at location x,y in the Boom Clay model; $V(x,y)$ is the stationary vertical Darcy velocity at the interface between the Boom Clay and the overburden model at location x,y ; $c(x,y,t)$ represents is the concentration at time t at location x,y at the overburden model.

The first flux $F(x,y,t)$ is obtained from the Boom Clay diffusion model and the Darcy velocity $v(x,y)$ is obtained from the groundwater flow model of the overburden. The concentration must be set to fulfill the equation above assuming some area of influence at the interface and probably assuming a spatially constant concentration at the interface within this area.

Interface Boom Clay - Overburden

In the overburden model, there are two possibilities at the interface Boom Clay - Overburden:

- 1 Flux is inwards into Boom Clay
- 2 Flux is outwards out of Boom Clay

In the first case, the diffusive flux is assumed to overcome the small advection between the repository and the interface of the Boom Clay with the overburden. Downstream of the repository there is no diffusive flux out of the Boom Clay and the nuclide plume may reenter the Boom Clay, see Figure 8.2. In such a situation, diffusion of radionuclides from the repository through the Boom Clay in the downward direction may result in larger risk as it has a shorter travel time. In Chapter 3, the critical travel time of that x,y location is based on pathline starting at the bottom of the Boom Clay. This pathline will intersect

through the Boom Clay somewhere downstream of the repository, unless the Boom Clay is absent at that downstream location. The residence times within the Boom Clay reported at Table 3.1 are due to passing the Boom Clay at this downstream location.

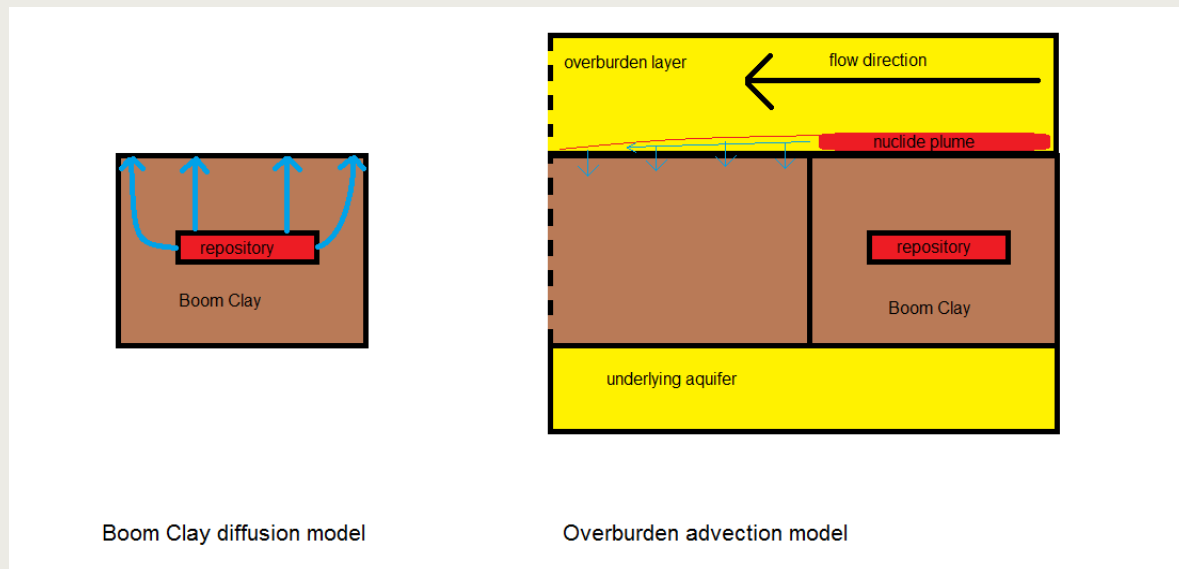


Figure 8.2 Schematic situation of the connection between the Boom Clay diffusion model and the overburden model when the groundwater flux at the interface is into the Boom Clay

In the second case, the nuclide plume will slowly move upward in the overburden aquifer when traveling downstream from the interface, see Figure 8.3. In Chapter 3, the critical travel time of that x,y location is based on pathline starting at the top of the Boom Clay. The initial thickness of the nuclide plume was obtained by starting two pathlines at the most outer edges of the interface at which a nuclide plume was expected to diffuse out of the Boom Clay. The distance between the outer edges was set equal to the maximum horizontal dimension of the repository, i.e. 3050 m reported in Figure 5.2 of OPERA-PG-COV008 (2011)^h. The thickness of the plume is proportional to the ratio of the vertical flow velocity at the interface and the horizontal flow velocity at the receiving aquifer. These velocities are obtained by the groundwater flow model of the Overburden.

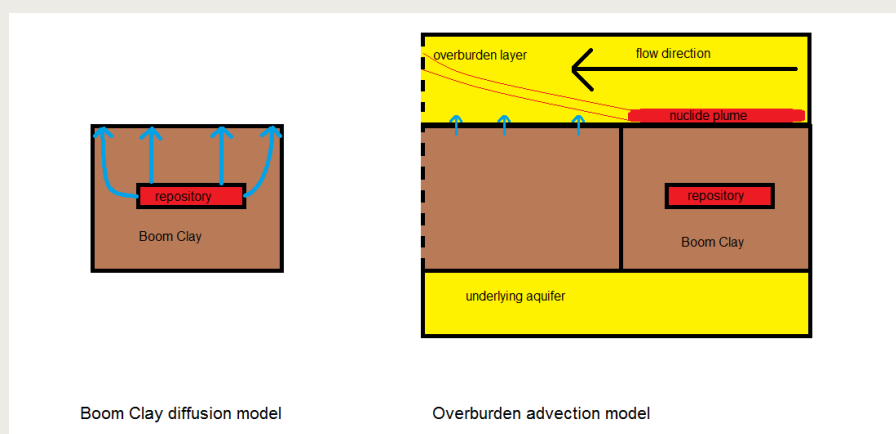


Figure 8.3 Schematic situation of the connection between the Boom Clay diffusion model and the overburden model when the groundwater flux at the interface is out of the Boom Clay

^h The maximum horizontal dimension is updated to 2450 m in the first update of the same report, OPERA-PG-COV008 (2014).

When flowing into another aquifer the thickness of the plume will change when the horizontal flow velocity of the aquifers is different. Moreover, the plume will get thicker due to vertical dispersion and the maximum concentration in the center will decrease. In paragraph 3.4, analytical calculations were performed in which rescaling was used to account for the different thicknesses of the plume in each aquifer.

The thickness that was reported was the 'initial' thickness in the aquifer with the highest flow velocity, which gives the smallest thickness of the plume. With 'initial' thickness the thickness of the plume without the vertical spreading by dispersion is meant. When taking the vertical spreading into account, the plume will become wider, but concentrations near the center of the plume will decrease.

Interface Overburden - Biosphere

In the case, that the interface between the geosphere and biosphere is a well, there are two possibilities for dilution:

- 1. the thickness of the plume near the well, including the effect of transversal dispersion, is smaller than the length of the well screen.*

In this case, the entire nuclide flux that passes the interface between the Boom Clay and the overburden reaches the well. The dilution takes place as the total abstraction rate of the well is larger the contaminated water flux. The water fluxes at the interface Boom Clay - overburden were not reported in Chapter 3, but they are obtained by multiplying the vertical Darcy velocity over the interface with the area that is assumed to be contaminated with nuclides. Here, it is assumed that this area is $3050^i \text{ m} \times 1300 \text{ m}$ (figure 5.2 in OPERA-PU-COV008 (2011)) = 3.965 km^2 . For the fast, median and slow pathline the vertical water flux over the interface Boom Clay -Geosphere equals $1.4 \text{ m}^3/\text{day}$ ($511 \text{ m}^3/\text{year}$) , $18 \text{ m}^3/\text{day}$ ($6570 \text{ m}^3/\text{year}$) and $1.5 \text{ m}^3/\text{day}$ ($548 \text{ m}^3/\text{year}$) respectively.

As the vertical water flux for the median pathline is higher than the water fluxes of the slow and fast pathline, it can be concluded that there is no clear relation between the water fluxes over the interface and the travel time through the overburden. Based on the values of the three pathlines only, it is impossible to conclude without further detailed calculations whether water fluxes at the other selected locations may be much larger. Therefore, the cumulative distribution of the water fluxes of all these locations were calculated and are shown in Figure 8.4. It is clear that the value of $18 \text{ m}^3/\text{day}$ for the median pathline is at the upper edge of the distribution.

ⁱ In an updated version, OPERA-PU-COV008 (2014), a length of 2450 m is reported and moreover an distinction between the different nuclear waste classes may result in a smaller length of the interface, but dimensions for the storage facilities of the various waste classes are not particularly quantified. The relation between flux and area of the repository is linear so a straightforward linear scaling applies when assuming a different area for the repository.

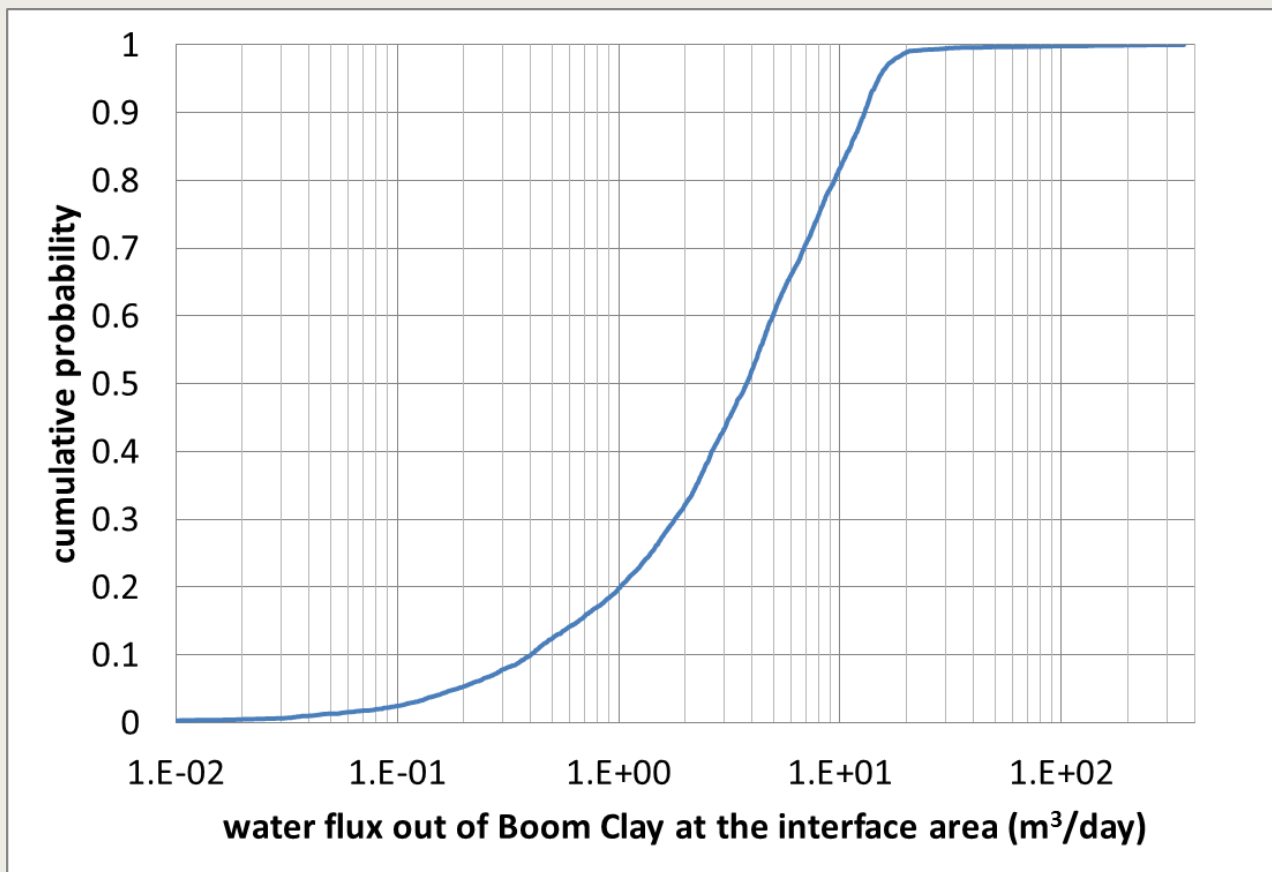


Figure 8.4 Cumulative distribution of the water flux over the interface Boom Clay - Overburden for all pathlines used in OPERA-PU-DLT621.

2. *the thickness of the plume near the well, including the effect of transversal dispersion, is larger than the length of the well screen.*

In this case, part of the nuclide plume will flow partly above or below the well screen and even a smaller flux than reported under option 1 will be abstracted by the well. In this situation the reduction of the maximum concentration, as reported in paragraph 3.4, is more relevant in case they give a larger reduction than the dilution when comparing the water fluxes over the Boom Clay - overburden interface with the abstraction rate of the well.

For the three pathlines, the reductions of the maximum concentration, reported in paragraph 3.4, were 98.7% (fast pathline), 78% (median pathline) and 99.1% (slow pathline).^j

One should avoid a misinterpretation of the water fluxes by simply multiplying the average flow velocity along the entire pathline with the assumed width (1100 m) and the initial or final 'equivalent height' of the plume. The 'equivalent height' was defined as the height of the plume in the aquifer with the highest flow velocity and for which the concentration reduction due the vertical transversal dispersion was translated into a thicker plume with uniform concentration.

^j For this option, the relation between the dilution factor and the length of the repository is not linear. For a decreasing length of the repository, the thickness of the initial plume decreases linearly as well, but the maximum concentration at the biosphere interface due to dispersion decreases faster than linearly.

The correct vertical water fluxes for the fast, median and slow pathline over the interface Boom Clay - Geosphere equal 1.4 m³/day, 18 m³/day and 1.5 m³/day respectively as reported under possibility 1 in this paragraph.

Here, for two example cases the dilution factors are analyzed:

- For a regional drinking water pumping station, a flux of 3.5 10⁵ m³/year is assumed. This flux is much higher than all the fluxes over the Boom Clay interface for the fast, median and slow pathlines and the thickness of the nuclide plume including the effect of transversal dispersion, will be smaller than the length of the well screen (possibility 1). The dilution factor F_d equals the ratio of the flux of the abstraction well and the flux over the Boom Clay interface. The reduction factors are 685, 53 and 639 for the fast, median and slow pathline.
- For a local drinking water well a flux of 10 m³/year is assumed. This flux is lower than all the fluxes over the Boom Clay interface for the fast, median and slow pathlines and the dilution factor F_d equals the decrease in maximum concentration (possibility 2). The dilution factors are 77 (1.0/(100%-98.7%) , 4.5 and 111 for the fast, median and slow pathline.

Note that setting the concentration at the Boom Clay interface using the equation in paragraph 8.2.3, the concentration for the median pathline will be significantly lower than the concentration of the other two pathlines, which compensates for the lower dilution factor.

The dilution factor has not a direct relation with the travel time. For the regional pumping station it is inversely related to the water flux over the Boom Clay interface. For the local well it is more complex as the dilution factor depends on the reduction of the maximum concentration due to vertical dispersion. In that case the dilution factor depends on the length of the flow path and the thickness of the plume; the latter linearly depends on the ratio of the flow velocity out of the Boom Clay and the horizontal flow velocity in the aquifers the water flows through. As the water flux for the median pathline of 18m³/day is at the upper end of the cumulative distribution shown in Figure 8.4, it is to be expected that the dilution factors as given for the median pathline are very low compared to values that would be obtained for other pathlines, for which the analysis here and in paragraph 3.3 was not performed. Based on this analysis, a dilution factor for small biosphere fluxes (such as the local well) in the range of 4.5 - 100 is recommended for the calculations in the PA model to account for the uncertainty in this dilution factor.

8.2.4. Climate scenarios

In chapter 4, scenario calculations were performed for different climate conditions. The results that were reported are the graphical relation between the travel time starting at the same x,y-location for the moderate climate (present conditions) and the specific climate condition under consideration. Moreover, the maximum reduction factor in the travel time was reported. Statistical values of the travel times for the climate scenarios were not reported. For some scenarios, these values strongly depend on the exact location of some of the added features to the model, such as the location of the ice cover or the exact position of the river systems during permafrost conditions.

The minimum and 10-percentile values of the travel times for the different scenarios have been calculated from the original data and are provided in Table 8.3.

Table 8.3 Maximum reduction factor of the total travel time and the estimated minimum and 10-percentile value for the total travel time for the different climate conditions of the Normal evolutions scenario

Climate scenario	Maximum reduction factor of the total travel time [-]	Estimated travel times	
		minimum value [year]	10-percentile [year]
Moderate climate (DV)	1	1941	30692
Cold climate without ice cover (permafrost) CB	11	1540	116980
Cold climate with ice cover (glaciation) CG	63	6089	73664
Warm Climate, climate change prediction WH of KNMI (CM2)	6.5	1990	29785
Warm climate, Mediterranean climate (CM)	7.3	1802	52780

8.3. Recommendations

From the analysis in this addendum, some additional recommendations for future research became clear that were not explicitly mentioned in Chapter 6. These additional recommendations are:

1. For the quantification of the hydraulic conductivity of the Boom Clay, the spatial distribution of the mud and non-mud texture is not explicitly characterized. Information about the horizontal spatial distribution of the mud and non-mud textures in the entire Netherlands, and if relevant the vertical variability at these locations will help to improve the overburden model. Moreover different values for the hydraulic conductivity of the Boom Clay were reported in the various OPERA documents. Additional quantification about the spatial distribution of the mud and non-mud texture and the corresponding hydraulic conductivity is highly recommended.
2. For the interfacial area at which nuclide fluxes will pass the Boom Clay - overburden interface, assumptions based on the repository dimensions are used. In OPERA-PU-DLT621 and OPERA-PU-NRG7251-NES different values for the width of the interfacial area were used. In addition no distinction in the nuclear waste classes and the spatial dimensions of the storage facilities of these classes are taken into account. Agreement between the different partners using these relevant dimensions is highly recommended.

8.4. Literature

OPERA-PU-COV008 (2011): Outline of a disposal concept in clay; Ewoud Verhoef, Erika Neeft, Jacques Grupa, Arjen Poley, 5 July 2011; COVRA N.V.

OPERA-PU-COV008 (2014): Outline of a disposal concept in clay; Ewoud Verhoef, Erika Neeft, Jacques Grupa, Arjen Poley, First update 13 November 2014; COVRA N.V.

OPERA-PU-TNO411: Geological and geohydrological characterization of the Boom Clay and its overburden; G.-J. Vis & J.M. Verweij; March 2014; COVRA N.V.

OPERA-PU-NRG6131: Model representation of radionuclide diffusion in Boom Clay; J.C.L. Meeussen, E. Rosca-Bocancea, T.J. Schröder, M. Koenen, F. Valega Mackenzie, N. Maes, C. Bruggeman; 7 February 2017; COVRA N.V.

OPERA-PU-NRG6121: Report on model representation of radionuclide sorption in Boom Clay; T.J. Schröder, J.C.L. Meeussen, J.J. Dijkstra, C. Bruggeman, N. Maes; 30 January 2017; COVRA N.V.

OPERA-PU-DLT621: Hydrological transport in the rock formations surrounding the host rock; J.R. Valstar & N. Goorden; June 2016; COVRA N.V.

OPERA-PU-GRS7222: Migration in the formation surrounding the host rock - PA model 'Aquifer'; J.B. Grupa, J.C.L. Meeussen, E. Rosca-Bocancea, A.F.B. Wildenborg, D. Buhmann, E. Laggiard; 25 January 2017; COVRA N.V.

Appendix 1: description of the geological formations near and below the base of the NHI model

The following information is a summary of the descriptions available on <http://www.dinoloket.nl/nomenclator> with additional information about the presence of a formation in the NHI model and the REGIS database.

1 *Maassluis Formation*

Description: Dominant: Sand, very fine to moderately coarse, grey, calcareous, contains marine shells, glimmers. Less dominant: clay grey to dark grey, often silty, often sandy, calcareous, both shell rich and shell poor

Distribution: Western, central and northern part of The Netherlands; Grid data available in DGM and for some parts of the country also a subdivision into 'Maassluis sand' and 'Maassluis complex' is available in REGIS.

This formation is modeled within the NHI model for a part of the country only. In other parts, it is underneath the base of the NHI model.

2 *Oosterhout Formation*

Description: Succession of sands, sandy clays, and grey and greenish clays. The glauconite content is moderate to low. In the southern and north-eastern parts of the Netherlands, the lower part of the formation consists of sands that are extremely rich in shells and bryozoans ('Crag facies'). In most areas the latter deposits are overlain by clays.

Distribution: The formation is present in the central and western Netherlands (with the exception of the extreme southwest), and the entire offshore area. Grid data are available in DGM and hydraulic property data is available without subdivisions in REGIS for part of its distribution only.

This formation is modeled within the NHI model for a part of the country only. In other parts, it is underneath the base of the NHI model.

3 *Scheemda Formation*

Description: Complex lithological unit consisting predominantly of sands. Locally, it comprises gravels, brown-coal beds and clay beds as well. The sands and gravels are extremely rich in translucent quartz. In fine-grained parts of the sands a minor amount of glauconite is often present.

Distribution: Restricted to the north-eastern Netherlands, notably in the provinces of Groningen, Drenthe and the northern part of Overijssel. In the eastern part of the province of Gelderland, the Scheemda Formation interdigitates with the Kieseloölite Formation. It intertongues with the uppermost part of the Breda Formation and with the Oosterhout Formation. Grid Data: this formation is part of the Peize formation that is available in DGM.

This formation, where present, is modeled within the NHI model. In the parts of the Netherlands where the Maassluis or Oosterhout Formations are below the base of the NHI model, the Scheemda Formation is not present.

4 *Kieselooite Formation*

Description: The lower half of the formation consists predominantly of coarse-grained clastics (sand and gravel), the upper part of clay and sand. In the central part of the Roer Valley Graben, a maximum thickness of over 200 m is reached.

Distribution: The formation occurs in the eastern part of the province of Noord-Brabant, the province of Limburg, and in parts of eastern Gelderland and Overijssel. Laterally, the coarse-grained lower part of the formation merges into marine beds of the Breda Formation, and the finer-grained upper part into the Oosterhout Formation. Grid data are available in DGM.

This formation, where present, is modeled within the NHI model. In the parts of the Netherlands where the Maassluis or Oosterhout Formations are below the base of the NHI model, the Kieselooite Formation is not present.

5 *Breda Formation*

Description: Sequence of marine, glauconitic sands, sandy clays and clays. In many places a glauconite-rich layer occurs at the base

Distribution: The formation is present in most of the Netherlands subsurface. Is it missing in small areas in the extreme east, southeast and southwest of the country, and on the Kijkduin High and a north-western extension into the offshore area.

This formation is modeled within the NHI model for a part of the country only. In other parts, it is underneath the base of the NHI model.

6 *Inden Formation*

Description: In the type area in Germany, the formation consists of a brown-coal bed of about 40m thick. In the Netherlands the formation consists mainly of coastal-plain and fluvial sand (locally with gravel) with a few intercalated brown-coal seams.

Distribution: In the south-eastern Netherlands the formation is restricted to the Roer Valley Graben, north of the Feldbiss fault and south of the Peel Boundary fault.

7 *Ville Formation*

Description: In the type area and the adjacent Erft Block in Germany, the formation consists of a continuous brown-coal seam, about 100 metres thick, called the Main Seam. To the west of the area of continuous coal formation, three major coal seams, intercalated with sand, can be traced. The major wedge-shaped sand body between the upper two seams, which increases in thickness to over 300 m in a westerly direction is called the Neurath Sand Member. It grades in westerly direction into the glauconiferous sands and silts of the Breda Formation.

Distribution: The Ville Formation occurs in the Lower Rhine Embayment and its north-western extensions (eastern Roer Valley Graben, Peel and Venlo fault blocks). Laterally, the formation interdigitates with the marine Breda Formation

8 *Ville Formation: Heksenberg Member*

Definition: Sands with intercalated brown-coal seams, in two stacked clusters of 15-20 m and about 30 m thick respectively. These are the lateral extensions of the lower two coal seams of the Ville Formation. The total thickness of the member amounts to 90-100 m.

Distribution: In the Roer Valley Graben in the south-eastern Netherlands extending to the south and north over adjoining fault blocks.

9 *Veldhoven Formation: Someren Member*

Definition: The member represents the sandy upper part of the Veldhoven Formation. It comprises of clayey sands grading upwards into very fine-grained sands. The colour of the sand is greenish-grey and the glauconite content is low. Shells occur locally. The member is only easily recognised in the Roer Valley Graben.

Distribution: Thought to be preserved only in the Roer Valley Graben and on the Peel and Venlo Blocks, i.e. in down-faulted parts of the basin, close to the input area of coarse-grained clastics.

10 *Veldhoven Formation: Veldhoven Clay Member*

Definition: It consists of grey to greenish grey clays, locally with brownish colours. The member becomes more silty and sandy towards the top. The Veldhoven Clay Member is most typically developed in the Roer Valley Graben. On the Peel and Venlo Blocks it is only a thin clay layer between the Voort and Someren Members.

Distribution: Present in the central and south-eastern Netherlands, in local fault-bounded depressions, and in the very north-eastern end of the Dutch part of the continental shelf

11 *Veldhoven Formation: Voort Member*

Definition: The member represents the predominantly sandy lower part of the Veldhoven Formation as it occurs in the southern Netherlands. The member is best described as a stacking of coarsening upwards sequences at the scale of decametres. The proportion of clays is highest in the lower upper

part of the member. The uppermost part stands out on logs as a relatively homogeneous and clean sand. The member is well-developed in the Roer Valley Graben. On the Peel and Venlo blocks the proportion of argillaceous sediments is very low.

Distribution: Restricted to the south eastern part of the Netherlands, to an area centred around the Roer Valley Graben. The member rapidly thins in a northerly direction.

12 *Rupel Formation: Steensel Member*

Definition: The member represents the sandy upper part of the Rupel Formation. It comprises an alternation of clays and silty clays with thin sand layers, grading upwards into fine-grained sands with a high glauconite content.

Distribution: Restricted to the south-eastern part of the Netherlands, notably to an area centred around the Roer Valley Graben and the south-eastern part of the Zuiderzee Low.

13 *Rupel Formation: Rupel Clay Member (Boom Clay)*

Definition: The member consists of clays that become more silty towards basis and top. It is rich in pyrite, contains hardly any glauconite and calcium carbonate tends to be concentrated in the septaria layers. The silt content does not only change towards the top and the bottom of the member. Detailed studies in the Boom Clay in Belgium have shown that silt and clay layers alternate at a decimetre to metre scale. Moreover, the organic-matter content is highly variable and distinct bituminous layers are present. Large intervals are practically devoid of calcareous microfossils. In areas relatively close to the basin margin, the clay can be subdivided into three parts. The lower part of the clay is silty and has a blue-grey colour. Higher in the succession a great number of bituminous bands is intercalated and the colour of the clay changes to dark green-grey, dark-brown or even black. The dark clays, which stand out on gamma-ray logs, are overlain by green-grey to green clays that are more marly and slightly more silty.

Distribution: The Rupel Clay Member is present over most of the Netherlands on- and offshore area. It is absent in the extreme south-western and south-eastern parts of the country and locally in the northeast, and in a small part of the western offshore.

14 *Rupel Formation: Vessem Member*

Definition: The member comprises the predominantly sandy deposits that constitute the lower part of the Rupel Formation. Over the major part of the Netherlands onshore area, the Vessem Member is developed as a simple transgressive unit consisting of silty to clayey sands with a low glauconite content; flint pebbles or phosphorite nodules commonly occur at the base. Autochthonous phosphorite nodules occur in some areas. The sands and the intercalated clays have a low carbonate content or are devoid of calcium carbonate.

Distribution: The member is present in the southern half of the Netherlands and adjacent offshore area. It is absent on the Kijkduin High and at the north-western flank of the Zuiderzee Low

15 *Tongeren Formation: Goudsberg member*

Definition: Grey, blue-grey to green-grey clays with thin intercalations of carbonaceous clays, lignites and clayey sands. Shells are generally common, in particular *Cerithium*.

Distribution: Restricted to southern Limburg

16 *Tongeren Formation: Klimmen Member*

Definition: Clayey sands, coarsening upward into very fine-grained, micaceous sands with a low glauconite content. Locally, a thin layer of flint pebbles is found at the base. Calcareous fossils are scarce and the sands are locally lithified. The top of the sands shows an orange or purple staining, interpreted as the result of emergence and soil development.

Distribution: Restricted to southern Limburg.

17 *Dongen Formation: Asse Member*

Definition: The member consists of dark greenish-grey and blue-grey, plastic clays. The unit locally shows indications of bioturbation, and may be glauconitic and somewhat micaceous. Generally, it is slightly calcareous. Notably the upper part of the member is sandy and free of calcium carbonate in a

proximal position. In eastern Netherlands, close to the palaeo-coastline, this part is very sandy, has a brownish colour and contains lignite fragments.

Distribution: The member is present in the south-western Netherlands and adjacent offshore area, and the northern to north-eastern Netherlands (with the exception of the northern- and easternmost parts) and adjacent offshore area.

18 Dongen Formation: Brussel Sand Member

Definition: Succession of green-grey, glauconitic, very fine-grained sand with, mainly in the upper part, a number of hard, calcareous sandstone layers of some decimetres thickness (leading to high-resistivity peaks). Towards the base of the unit the clay content increases, and the calcium carbonate content and amount of glauconite decreases. A minor amount of mica occurs. Farther from the palaeo-coastline the member becomes silty and marly.

Distribution: The Brussels Sand Member is present in the south-western Netherlands and adjacent offshore area, the northern to north-eastern Netherlands (with the exception of the northern- and easternmost parts). It is missing as a result of erosion on the 'Southern Early Tertiary High'. Towards the distal part of the basin, the Brussels Sand Member grades into the Brussels Marl Member.

19 Dongen Formation: Brussel Marl Member

Definition: Greenish to brownish grey, silty, calcareous clay to marl. The unit is the distal equivalent of the Brussels Sand Member.

Distribution: The unit occurs in the northern- to north-westernmost part of the Netherlands and the adjacent offshore area. Laterally, it grades into the Brussels Sand Member towards the proximal part of the basin. The boundary with the latter is rather arbitrary.

20 Dongen Formation: Ieper Member

Definition: Generally soft, tough and sticky to hardened and friable clay. A subdivision into two parts can be recognised regionally. The lower part is characterised by its brown-grey colour, tending to beige or red-brown locally. The unit contains pyrite, is non-calcareous, and coalified plant remains are locally present at the base (possibly reworked material). The upper two-thirds have a characteristic green-grey colour. It has a sandy upper part with a number of larger sandstone intercalations and it is somewhat calcareous and glauconitic. Along the palaeo-coastline the clays are silty with some sand stringers, which become less common distally.

Distribution: The member is present throughout most of the Netherlands on- and offshore area, with the exception of southern Limburg and a zone of erosion on the 'Southern Early Tertiary High'.

21 Dongen Formation: Dongen Clay Member

Definition: Formation of dark-grey, green and brown, slightly calcareous clays, with an intercalated, glauconitic sand to sandstone body, which grades distally into a marly unit. The lowermost part of the formation is characterised by tuffaceous clays and is sandy in a proximal position. In the south-westernmost part of the country, the formation probably comprises continentally influenced deposits at its base.

Distribution: The formation is present in most of the Netherlands on- and offshore area, with the exception of the south-eastern and easternmost parts of the country, and a zone of erosion on the 'Southern Early Tertiary High'

22 Dongen Formation: Basal Dongen Sand Member

Definition: Light green-grey, locally glauconitic, usually thin sand with a fining-upward character. It can be very argillaceous, and may locally contain some well-cemented layers. In the south-eastern part of the province of Noord-Brabant, the Basal Dongen Sand Member comprises several sand bodies separated by clay beds, the sand bodies can be up to 20 m thick.

Distribution: The member is present in the southern and central part of the Netherlands and the adjacent offshore area. It is absent in southern Limburg and the easternmost parts of the country, and a zone of erosion on the 'Southern Early Tertiary High'.

23 Dongen Formation: Basal Dongen Tuffite Member

Definition: Tuffaceous clays, blue to violet-grey in colour, alternating with dark-grey and red-brown clays.

Distribution: The member occurs throughout the central and northern Netherlands and the adjacent offshore area, and is an excellent marker horizon. The unit interfingers with and locally overlies the Basal Dongen Sand Member.

24 Landen Formation: Reusel Member

Definition: In the south-eastern Netherlands the unit consists of two to three coarsening-upward sequences. The basal one is a small-scale alternation of hard siltstone and shale layers, capped by a thin clean sand. The upper unit has a sandier character with again a relatively clean thin sand at the top. The calcium-carbonate content decreases upwards, whereas the glauconite content increases in that direction leading to a soft-green colouring. The overall colour is light grey.

Distribution: The unit is only present in the province of Noord-Brabant and in northern and central Limburg.

25 Landen Formation: Landen Clay member

Definition: Generally dark-green, hard, flaky clay, somewhat silty, containing glauconite, pyrite and mica. The basal part of the member can be marly and of a lighter colour. In the eastern Netherlands (closer to the palaeo-coastline) the clay is fine-sandy to silty and its colour greenish, also brown. The member contains very little glauconite and is strongly burrowed.

Distribution: The member is present all over the Netherlands on- and offshore, with the exception of the 'Southern Early Tertiary High' and the very eastern part of the Netherlands as a result of later erosion and/or non-deposition.

26 Landen Formation: Gelinden Member

Definition: Hard and soft, mainly grey-white to yellow-brown, argillaceous marl with many burrows and yellow concretions. The lowermost beds generally consist of dark green marly clay.

Distribution: The member is present in the provinces of Noord-Brabant and the northern part of Limburg, northern Flevoland and the northern part of Gelderland.

27 Landen Formation: Heers Member

Definition: Very fine-grained, light- to dark-green/grey, glauconitic, partly calcareous sands, with some intercalated clay beds. Contain shells locally. Locally, the unit comprises two coarsening-upward sequences.

Distribution: Generally, south of the 'Southern Early Tertiary High' and locally north of it i.e. northern Gelderland and the IJsselmeer area, northern Noord-Holland and the western parts of the Waddenzee and Friesland.

28 Landen Formation: Swalmen Member

Definition: The major part of the member consists of an alternation of thin sand layers and humic clay layers, containing small pieces of coalified plant remains and locally, in its upper reaches, thin brown-coal beds. The sands have a yellowish grey-brown colour. The clay is hard and flaky, light to dark grey-brown to black, and contains pyrite nodules. The lower sandy layers locally contain shells and/or glauconite. Locally, very characteristic, bright red and olive-green spots and flames occur in the clays.

Distribution: The member is known from the province of Limburg and the very eastern part of Noord-Brabant. It possibly occurs as well in south-eastern Flevoland and the northern part of Gelderland.

Appendix 2: Method to calculate the horizontal and vertical hydraulic conductivity

In this paragraph, the method to define the horizontal and vertical hydraulic conductivity for the different formations, which are not available in the database REGIS is described.

The following information, provided by TNO is available for the lithologies:

- Composition of the formation, see Table A2.1,
- The porosity of the formation as function of depth, see Table A2.2,
- Permeability of the formation [LogmD] as function of the porosity, see Table A2.4.

Based on these parameters, the horizontal and vertical hydraulic conductivity are calculated by the following procedure, described in the steps below. This procedure is automatically executed by a python script. As example to demonstrate this procedure, the Boom Clay is taken:

1. The composition of the Boom Clay is defined by using a lookup function, which searches for the lithology and its composition, see table below, which results in 25% siltstone and 75% shale.

Table A2.1 Composition of each lithology in percentage, delivered by TNO

Lithology	Sandstone (%)	Siltstone (%)	Shale (%)	Marl (%)
NOORDZEE	50	0	50	0
O.NOORDZEE	50	0	50	0
DONGEN	25	0	50	25
M.NOORDZEE	50	0	50	0
RUPEL Formation	25	0	75	0
Boom Clay	0	25	75	0
STEENSEL	25	0	75	0
VESSEM MEMBER	33	33	34	0
TONGEREN	50	0	50	0
VELDHOVEN	75	0	25	0
VELDHOVEN Clay	0	0	100	0
SOMEREN	75	0	25	0
BREDA	75	0	25	0
KIEZELOOLIET	75	0	25	0
MAASSLUIS	75	0	25	0
OOSTERHOUT	75	0	25	0
VOORT Sand	100	0	0	0

2. Subsequently the average depth is calculated for each grid cell where the Boom Clay is present, by calculating the mean of the bottom and top of the Boom Clay.
3. The porosities for each grid cell can now be found in table A2.2, thereby using the combination of the average depth and the compositions of the formation.

Table A2.2 Porosity as function of depth and lithology, delivered by TNO

Depth(m)	Sandstone	Siltstone	Shale	Marl
0	41	55	70	50
250	38.02	48.54	57.07	44.24
500	35.26	42.85	46.56	39.16
750	32.7	37.84	38.03	34.68
1000	30.34	33.43	31.09	30.72
1250	28.15	29.55	25.45	27.23
1500	26.13	26.13	20.87	24.15
1750	24.25	23.12	17.14	21.43
2000	22.52	20.47	14.12	19.03
2250	20.91	18.14	11.66	16.91
2500	19.43	16.09	9.66	15.04
2750	18.05	14.28	8.04	13.39
3000	16.78	12.69	6.72	11.93
3250	15.61	11.29	5.65	10.65
3500	14.52	10.06	4.78	9.51
3750	13.51	8.98	4.07	8.51
4000	12.58	8.02	3.49	7.63
4250	11.71	7.18	3.03	6.85
4500	10.91	6.44	2.65	6.16
4750	10.17	5.79	2.34	5.56
5000	9.49	5.22	2.09	5.02
5250	8.86	4.71	1.88	4.55
5500	8.27	4.27	1.72	4.13
5750	7.73	3.88	1.58	3.76
6000	7.23	3.53	1.47	3.44
6250	6.76	3.23	1.39	3.15
6500	6.33	2.96	1.31	2.9
6750	5.94	2.73	1.25	2.68
7000	5.57	2.52	1.21	2.48
7250	5.23	2.34	1.17	2.31
7500	4.91	2.18	1.14	2.15

4. The porosity is calculated by multiplying the percentage of each composition times the porosity of this composition at average depth (calculated in step 2). For the Boom Clay this means for each grid cell: $\text{Porosity} = 0.25 * (\text{Porosity siltstone at calculated average depth}) + 0.75 * (\text{Porosity shale at calculated average depth})$.
5. As the porosity is known, the porosity-permeability relation in Table A2.3 is used. The permeability is defined in $[\log(\text{mD})]$ and is transformed to $[\text{m}^2]$ in order to calculate the hydraulic conductivity, which is defined in $[\text{m}/\text{day}]$. Furthermore an interpolation is performed, to get the permeability at a given porosity.

Table A2.3 Permeability of typical sandstone, shale, Siltstone and Marl for

Porosity [-]	Permeability [m ²]							
	Typical Sandstone		Typical Siltstone		Typical Shale		Typical Marl	
	Horizontal	Vertical	Horizontal	Vertical	Horizontal	Vertical	Horizontal	Vertical
0.01	1.80E-15	1.63E-16	2.75E-17	1.85E-18	1.24E-18	2.18E-19	3.75E-17	6.33E-18
0.25	2.19E-13	1.98E-14	5.40E-15	3.63E-16	1.25E-15	2.20E-16	6.17E-16	1.04E-16
0.41	8.26E-13	7.50E-14	1.85E-14	1.24E-15	1.54E-15	2.71E-16	1.94E-15	3.27E-16
0.5	8.26E-13	7.50E-14	2.58E-14	1.73E-15	1.71E-15	3.00E-16	2.68E-15	4.52E-16
0.55	8.26E-13	7.50E-14	2.99E-14	2.01E-15	1.66E-15	2.92E-16	2.68E-15	4.52E-16
0.7	8.26E-13	7.50E-14	2.99E-14	2.01E-15	2.07E-15	3.63E-16	2.68E-15	4.52E-16

6. Subsequently the hydraulic conductivity is calculated using the following formula:

$$\kappa = K \frac{\mu}{\rho g}$$

Where:

- κ = the permeability [m²],
- K = the hydraulic conductivity [m/s],
- μ = the dynamic viscosity of the fluid [kg/(m·s)], which depends on the depth, according to table A2.4,
- ρ = the density of the fluid, kg/m³, assumed constant at 1000 kg/m³,
- g = the acceleration due to gravity and is 9.81 m/s².

Table A2.4 Depth-viscosity relation of water

Depth [m]	Viscosity [kg/(m.s)]	Temp [°C]
0	0.001306	10
333	0.001002	20
667	0.0007978	30
1000	0.0006531	40
1333	0.0005471	50
1667	0.0004658	60
2000	0.0004044	70
2333	0.000355	80
2667	0.000315	90
3000	0.0002822	100

The outcome of this procedure is for each formation a spatially distributed vertical and horizontal hydraulic conductivity. As example the vertical hydraulic conductivity for the Boom Clay is presented in Figure A2.1.

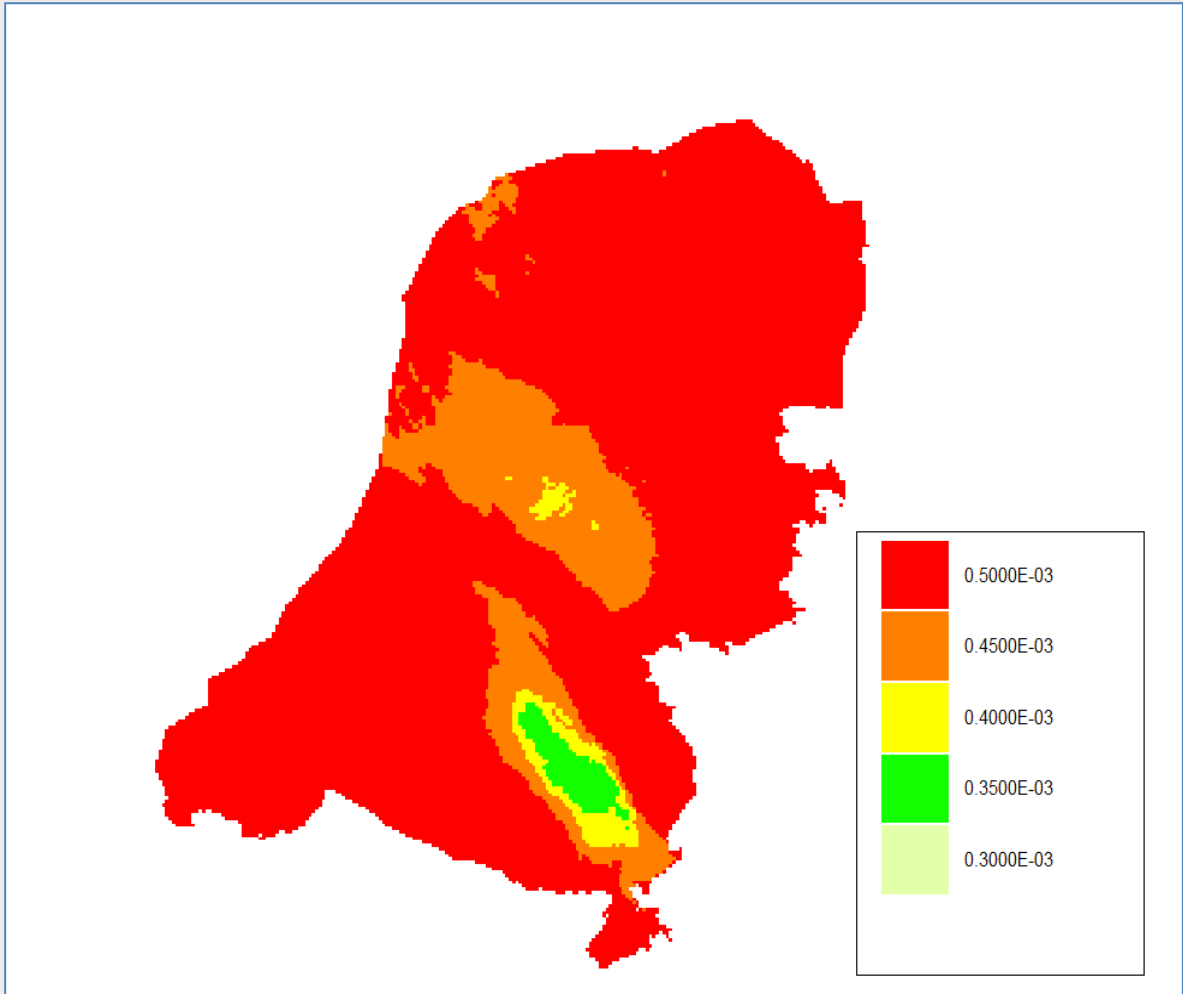


Figure A2.1 Vertical hydraulic conductivity [m/day] of the Boom Clay

Appendix 3: Conceptualization of the PA-model for the Overburden

J. Hart, T.J. Schröder, NRG

A3.1 Introduction

The PA-model of the Overburden compartment as described in (Grupa, 2017) is based on the Deltares report *OPERA-PU-DLT621* in a previous version (Valstar, 2016) and supplemental information separately provided by the authors to NRG. Discussion at the meeting of the OPERA Safety Case Group (OSCG) in April 2017 resulted in the viewpoint that the current implementation of the Overburden compartment might be improved with respect to the coupling to the biosphere. Furthermore, the Deltares report (Valstar, 2016) allows different interpretations about the degree of conservatism in the implementation of the information provided into the PA-model.

In the follow-up of the OSCG meeting a number of actions were agreed. One of the actions was related to the re-evaluation of the implementation of the Overburden model, which was performed by NRG and Deltares and is described in Chapter 8 and Appendix 3 of this document. The objective of this action is:

- a) to clarify potential misconceptions or -understandings in the interpretation of the results reported in (Valstar, 2016),
- b) to document the information provided by e-mail into a public accessible report, and
- c) to evaluate and eventually refine the current PA-model for overburden with emphasis on its coupling to the biosphere, in line with the assessment strategy discussed in the OSCG-meeting.

This Appendix addresses the third bullet, i.e. it translates the recommendations and conclusion of Deltares into an updated PA-model representation.

A3.2 Elaboration of refinements of the current PA-model for the Overburden

A3.2.1 Pathlines

In Section 8.2.1, an elaborated explanation of the Overburden pathlines as have been reported, and the consequences for the PA-model are shortly summarized below.

In Section 3.3, three pathlines were selected to be used in the OPERA performance assessment (PA) calculations in WP 7. The pathlines represent typical fast, median and slow flow paths of the Dutch subsurface through which aquifers and aquitards may carry along nuclides released from the Boom Clay.

The latter two pathlines, median and slow, have a part of their residence time (19 and 11%, respectively) in the Boom Clay (Table 3.1). They leave the Boom Clay at the lower boundary and re-enter the Boom Clay on their way to the surface. Consequently, any radionuclides carried along by aquifer water of the median and slow flow paths would again be susceptible to re-adsorption in the Boom Clay after they have diffused out of the Boom Clay and taken up by the aquifer water of the Overburden.

The strategy of the OPERA PA conservatively postulates that nuclides carried along by the aquifer system of the Overburden compartment are not susceptible to adsorption in that compartment. This implies that, irrespective the possibility of pathlines in the Overburden

traversing the Boom Clay, no additional adsorption of nuclides in Boom Clay is considered for this situation in the OPERA PA-model.

In Section 8.2.1, it is explained that the total travel times for the selected fast, median and slow pathlines are also realistic values in case one would exclude pathlines that intersect through the Boom Clay somewhere downstream of the repository.

In Section 2.2.4, rather high hydraulic conductivity values are assumed, based on relations between the lithology, depth, porosity and permeability provided by TNO (Vis & Verweij, 2012). Table 8.2 shows a selection of the fast, median and slow pathlines which are based on the 10, 50 and 90 percentiles of the travel time distribution using the Deltares model with 100 times lower hydraulic conductivity of the Boom Clay. Table 8.2 reveals relatively small differences ($\leq 20\%$) in travel times of pathlines intersecting the Boom Clay compared to the values given in Table 3.1, where the selected pathlines would traverse through the Boom Clay.

The conclusion of the evaluation in Section 8.2.2 is that no adaptations of the geometric data and travel times provided for the three identified pathlines in Table 3.1 are necessary for the PA-model of the Overburden.

A3.2.2 Dispersion in the Overburden

Section 8.2.3 provides an elaboration of Section 3.4 concerning the dispersion of a water plume in the Overburden contaminated with nuclides. When flowing into another aquifer the plume will get thicker due to vertical dispersion and the maximum concentration in the center will decrease.

The reduction in the nuclide concentration by dispersion has been reported for the three pathlines in Section 3.4, and amounts respectively 98.7% (fast pathline), 78% (median pathline) and 99.1% (slow pathline). Consequently, a dispersion related dilution factor ' F_{disp} ' can be defined that represents the dilution of radionuclide concentrations in the streamline between the point where it leaves the Boom Clay, and the end of the respective pathlines where they enter the biosphere. Example values for F_{disp} estimated in Section 8.2.3 are:

- $F_{disp} = 77$ for the fast pathline
- $F_{disp} = 4.5$ for the medium pathline
- $F_{disp} = 111$ for the slow pathline

These figures show that the dilution by dispersion F_{disp} is not one-to-one related to the travel time; it is therefore recommended not to directly apply the dilution factors of the three example streamlines that are derived in Table 3.1 on basis of their travel time, but to vary the dilution by dispersion independently from the travel time.

In Section 8.2.3, a dilution factor F_{disp} in the range of 4.5 - 100 is recommended for the calculations in the PA-model for small biosphere fluxes such as the local well. The above-mentioned values estimated for the three pathlines are approximately in that range (see also Table A.3.2 - "Dispersion dilution factor F_{disp} ").

In conclusion, for the *conservative* case of the OPERA PA ("DV") it is recommended to apply a dilution factor for the Overburden compartment of 4.5 for all three pathlines considered for the local well case (irrigation water pathway), representing the lower bound of the range of values recommended in Section 8.2.3. That value is also indicated in Table A.3.2.

Additionally, to account for the uncertainty range of the dilution factor in the Overburden compartment, additional other cases for the dilution factors may be defined, leading to a set of three cases:

- $F_{disp} = 4.5$; small dilution (“DV”, = default value in NES),
- $F_{disp} = 25$; intermediate dilution (“MD”),
- $F_{disp} = 100$; large dilution (“LD”).

Because the dilution factor F_{disp} is only related to the dilution in the Overburden compartment, it is recommended to apply the dilution in the last overburden cell that connects to the biosphere.

A3.2.3 Flow rates

Upon the release of radionuclides from the Boom Clay into the Overburden, a nuclide containing “plume” is formed which is carried along by the aquifer through the Overburden. The initial thickness of the plume is proportional to the ratio of the vertical flow velocity at the interface and the horizontal flow velocity at the receiving aquifer. In the previous version of this report, no water fluxes or velocities at the interface Boom Clay - overburden were reported. In Section 8.2.3, however, it is clarified that water fluxes were obtained by multiplying the vertical Darcy velocity over the interface with the area contaminated with nuclides. It is assumed that this area is 3050 m x 1300 m (3.965 km², see Figure 5.2 in Verhoef, 2011). Dilution by mixing of vertical and horizontal water flows is not accounted for.

For the three pathlines the following net vertical water fluxes at the interface Boom Clay - overburden are estimated in Section 8.2.3:

- Fast pathline: 1.4 m³/day (511 m³/year)
- Median pathline: 18 m³/day (6570 m³/year)
- Slow pathline: 1.5 m³/day (548 m³/year).

In Section 8.2.3 it is recognized that the water flux through the overburden has no relation with the travel time: the water flux for the median pathline (6570 m³/year) is larger than the water flows of the slow (548 m³/year) and fast (511 m³/year) pathlines. The water fluxes given are thus not ‘typical’ for the selected pathlines. Figure 8.4 shows the cumulative distribution of the vertical water fluxes out of the Boom Clay, ranging from ±150 m³/year (10-percentile) to about 4500 m³/year (90-percentile), with a mean value of slightly less than 1500 m³/year. The water flux of the median pathline therefore represents a value beyond the 95-percentile, and is also related to an ‘untypical’ low dilution (see previous section).

For the OPERA PA, it is proposed to use the dilution factor in the Overburden as leading parameter, and to assume initial fluxes at the bottom of the Overburden equal to 4500, 1500 and 150 m³/year for the small, intermediate and large dilution case, respectively. These values are consistent with the range given in Figure 8.4. Table A.3.1 summarizes the three suggested cases, including the total fluxes of the contaminated, dispersed flux at the top of the Overburden.

Table A.3.1 Recommended dispersion dilution factors and initial fluxes for three dilution cases

Dilution by dispersion	F_{disp} [-]	Initial flux [m ³ /yr]	Total dispersed flux [m ³ /yr]
Small dilution (DV)	4.5	4500	20 250
Intermediate dilution (MD)	25	1500	37 500
Large dilution (LD)	100	150	15 000

A3.2.4 Interface Boom Clay - Overburden

From the data provided in Table 3.1, the characteristics of the layers adjacent to the Boom Clay can be obtained. Hereby it is acknowledged that the fast pathline interfaces with the layer on top of the Boom Clay (“Veldhoven”), whereas the medium and slow pathlines interface with the layer at the bottom of the Boom Clay (“Vessem”). However, the vertical fluxes derived in Section 8.2 cannot be translated directly into cell heights of the interfacing cells: here, a conceptual discrepancy exists between the model that is used to determine travel times based on a vertical flux out of the Boom Clay, and the PA-model that assumed no advective flow in the Boom Clay at all.

Several assumptions evaluated (data not shown) do not lead to a consistent description that is more plausible than the currently used approach described in (Grupa, 2017) and parameterized in (Schröder, 2017). Reasons are that no horizontal fluxes on top of the Host Rock are provided, and that the flux rates are probably not too constant over a sub-layer of the Overburden. Therefore no change of the current model representation of the interface or its parameterization can be recommended.

A3.2.5 Interface Overburden - Biosphere

Section 8.2.3 provides also an elaboration of the interface Overburden to Biosphere. The evaluation is based on considerations about the transversal dispersion of a plume of contaminated Overburden water that has its origin at the interface Boom Clay - Overburden and that is carried along the three considered flow paths (fast, median, slow).

During the travel along these flow paths a plume of contaminated water in the Overburden will diverge as a result of lateral dispersion. This dilution by dispersion is accounted for by the dilution factor F_{disp} and is applied in the last Overburden cell that connects to the Biosphere (see also Section A3.2.2). Furthermore, due to mixing, a dilution applies in the Biosphere compartment, based on the ratio of the influx from the Overburden compartment and the flux in the Biosphere compartment, complementary to (Schröder, 2017). The dilution factors by mixing, F_d , for the *drinking water well* case are summarized in Table A.3.2.

In case the dispersed, contaminated plume will reach the Biosphere compartment, it depends on the (size of the) receptor how much dilution will occur. Two cases can be distinguished:

- The dispersed flow of the contaminated plume enters a Biosphere compartment with a larger flow rate (e.g. a regional pumping station) than the flow rate of the dispersed plume: In this case the dilution factor by mixing F_d equals the ratio of the overall flow rate in the target Biosphere compartment and the flow rate of the contaminated plume (see Table A.3.1).
- The dispersed flow of the contaminated plume enters a Biosphere compartment with a smaller flow rate (e.g. a local well) than the flow of the plume (150 - 4500 m³/year, see Table A.3.1): In this case the dilution factor by mixing F_d equals 1.

The overall dilution - from the first cell in the Overburden to the Biosphere compartment - is then obtained by multiplying F_{disp} and F_d .

Table A.3.2: Inflow to the *drinking water well* subcompartment and resulting mixing dilution factor in case of a typical regional pumping station for three dispersion dilution cases, and resulting overall net dilution between the inflow in the Overburden and the Biosphere compartment

Dilution case	Dispersion dilution factor F_{disp} [-]	Regional pumping station			Local well		
		Q_{flow} [m ³ /year]	Mixing dilution factor F_d [-]	Overall dilution [-]	Q_{flow} [m ³ /year]	Mixing dilution factor F_d [-]	Overall dilution [-]
Small dilution(DV)	4.5	3.5 10 ⁵	17.3	78.8	10	1	4.5
Intermediate dilution (MD)	25	3.5 10 ⁵	9.3	232	10	1	25
Large dilution (LD)	100	3.5 10 ⁵	23.3	2330	10	1	100

A3.2.6 Climate scenarios

In Chapter 4, scenario calculations were performed for different climate conditions. The results were reported as graphical relations between the travel time for the moderate climate (present conditions) and the specific alternative climate conditions. For each of these cases, the maximum reduction factor in the travel time was reported. Other statistical values for the travel times in the climate scenarios were however not reported.

The minimum and 10-percentile values of the travel times for the different scenarios have been calculated from the original data and are provided in Table 8.3 and Table A.3 below. These values are more accurate than the values visually derived in (Schröder, 2017).

Table A.3.3 Maximum reduction factor of the total travel time and the estimated minimum and 10-percentile value for the total travel time for the different climate conditions of the Normal evolutions scenario

Climate scenario	Maximum reduction factor of the total travel time [-]	Estimated travel times	
		minimum value [year]	10-percentile [year]
Moderate climate (DV)	1	1941	30692
Cold climate without ice cover (permafrost) CB	11	1540	116980
Cold climate with ice cover (glaciation) CG	63	6089	73664
Warm Climate, climate change prediction WH of KNMI (CM2)	6.5	1990	29785
Warm climate, Mediterranean climate (CM)	7.3	1802	52780

A3.3 Conclusions

The implications of the analyses discussed above on the OPERA PA-model are the following:

- Pathlines: no modifications of the PA-model are necessary for the following parameters (cf. Table 5-2 in Schröder, 2017):
 - Path length
 - Porosity
 - Travel time
 - Equivalent height of the first cell of the Overburden compartment
- Dispersion dilution factors F_{disp} and related initial flow rates: it is recommended to distinguish three dispersion dilution cases according to the data indicated in Table A.3.1 (see for example implementation also Table A.3.2), and to apply the dilution by dispersion to the last cell in the Overburden compartment that links to the overburden. This is additional to the cases distinguished in (Schröder, 2017).
- Mixing dilution factors F_d (cf. Section 6.3.1 of Schröder, 2017): it is recommended to apply mixing dilution factors based on the dispersed flow rates at the interface Overburden-Biosphere, and explicitly uncouple dilution by dispersion and dilution by mixing (see previous bullet).
- Climate scenarios: the visually estimated data in Table 5-3 of in (Schröder, 2017) should be replaced by the numerical exact data provided in Table A.3 above.

A3.4 Literature

- (Grupa, 2017) Grupa, JB JCL. Meeussen, E Rosca-Bocancea, AFB Wildenborg, D Buhmann, E Laggiard, *Migration in the formations surrounding the host rock - PA model 'Aquifer'*, OPERA-PU-GRS7222, January 2017.
- (Schröder, 2017) Schröder TJ, Hart J, J.C.L. Meeussen JCL, *Report on model parameterization - Normal evolution scenario*, OPERA-PU-NRG7251-NES, February 2017.
- (Valstar, 2016) Valstar JR, Goorden N, *Hydrological transport in the rock formations surrounding the host rock*, OPERA-PU-DLT621, April 2016 (previous report version).
- (Verhoef, 2011) (2011) Verhoef E, Neeft E, Grupa JB, Arjen Poley AD, *Outline of a disposal concept in clay*, OPERA-PU-COV008, 5 July 2011.
- (Vis & Verweij, 2014). Vis G-J, JM Verweij, *Geological and geohydrological characterization of the Boom Clay and its overburden*, OPERA-PU-TNO411, March 2014.

OPERA

Meer informatie:

Postadres
Postbus 202
4380 AE Vlissingen

T 0113-616 666
F 0113-616 650
E info@covra.nl

www.covra.nl

